Journal of Power Sources 482 (2021) 228872

Contents lists available at ScienceDirect

Journal of Power Sources

journal homepage: www.elsevier.com/locate/jpowsour

Challenges of today for Na-based batteries of the future: From materials to cell metrics

Ivana Hasa [a,b,c], Sathiya Mariyappan [d,e,f], Damien Saurel [g,f], Philipp Adelhelm [h,i], Alexey Y. Koposov [j], Christian Masquelier [k,e,f], Laurence Croguennec [l,e,f], Montse Casas-Cabanas [g,f,m,*]

[a] WMG, The University of Warwick, Coventry, CV4 7AL, United Kingdom
[b] Helmholtz Institute Ulm (HIU), Helmholtzstrasse 11, 89081, Ulm, Germany
[c] Karlsruhe Institute of Technology (KIT), P.O. Box 3640, 76021, Karlsruhe, Germany
[d] Chimie Du Solide-Energie, UMR 8260, Collège de France, 75231, Paris Cedex 05, France
[e] Réseau sur le Stockage Electrochimique de l'Energie (RS2E), FR CNRS 3459, Amiens, France
[f] ALISTORE-European Research Institute, 80039, Amiens, France
[g] Center for Cooperative Research on Alternative Energies (CIC EnergiGUNE), Basque Research and Technology Alliance (BRTA), Parque Tecnológico de Alava, Albert Einstein 48, 01510, Vitoria-Gasteiz, Spain
[h] Institute of Chemistry, Humboldt-University Berlin, Brook-Taylor-Str. 2, Berlin, Germany
[i] Helmholtz-Zentrum Berlin für Materialien und Energie, Hahn-Meitner-Platz 1, 14109 Berlin, Germany
[j] Department of Battery Technology, Institute for Energy Technology (IFE), Instituttveien 18, NO-2007 Kjeller, Norway
[k] Laboratoire de Réactivité et Chimie des Solides, UMR CNRS #7314, Université de Picardie Jules Verne, 80039, Amiens Cedex, France
[l] CNRS, Univ. Bordeaux, Bordeaux INP, ICMCB, UMR CNRS 5026, F-33600, Pessac, France
[m] Ikerbasque, Basque Foundation for Science, María Díaz de Haro 3, 48013, Bilbao, Spain

HIGHLIGHTS

- Assessment of Na-based battery technology: from materials to cell development.
- Realistic comparison of key performance indicators for Na-ion and Li-ion cells.
- Na-ion batteries can be considered as complementary alternatives to Li-ion batteries.
- Fundamental research is the key enabler for future development of the Na-based technology.

GRAPHICAL ABSTRACT

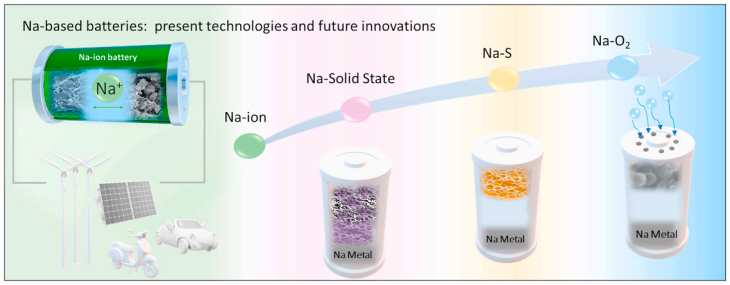

ARTICLE INFO

Keywords:
Na-based batteries
Na-ion
Na/O_2
Na/S
all solid-state Na batteries
Key performance indicators

ABSTRACT

Several emerging battery technologies are currently on endeavour to take a share of the dominant position taken by Li-ion batteries in the field of energy storage. Among them, sodium-based batteries offer a combination of attractive properties i.e., low cost, sustainable precursors and secure raw material supplies. Na-based batteries include related battery concepts, such as Na-ion, all solid-state Na batteries, Na/O_2 and Na/S, that differ in key components and in redox chemistry, and therefore result in separate challenges and metrics. Na-ion batteries represent an attractive solution which is almost ready to challenge Li-ion technology in certain applications; the

* Corresponding author. ALISTORE-European Research Institute, 80039, Amiens, France.
E-mail address: mcasas@cicenergigune.com (M. Casas-Cabanas).

https://doi.org/10.1016/j.jpowsour.2020.228872
Received 13 June 2020; Received in revised form 4 August 2020; Accepted 30 August 2020
Available online 17 September 2020
0378-7753/

other cell concepts represent a more disruptive innovation, with a higher performance gain, provided that major hurdles are overcome. The present review aims at highlighting the most promising materials in the field of Na-based batteries and challenges needed to be addressed to make this technology industrially appealing, by providing an in-depth analysis of performance metrics from recent literature. To this end, half-cell reported metrics have been extrapolated to full cell level for the more mature Na-ion technology to provide a fair comparison with existing technologies.

1. Introduction

Batteries are set to play a pivotal role in the coming decade as key enablers of a low-carbon economy. Today's global economic and environmental conditions have boosted the demand for energy storage systems, lifting the cost barriers for Li-ion batteries (LIBs) and allowing the applications of such batteries to progressively expand from mobility to the grid. Based on different growth scenarios, long-term market analyses estimate that in 2040 the number of electric vehicles (EVs) on the road will be from two to three orders of magnitude bigger than today. At the same time stationary storage installations will also increase exponentially, and may globally reach up to 1300 GWh [1]. With the further increase of production capabilities for LIBs around the world, the costs are expected to decline further, while the risks of demand-supply mismatch and supply constraints of the raw materials increase. In addition, the environmental and social challenges associated with the mass production of LIBs will become increasingly important as the market expands, since LIBs contain several critical (and/or toxic) raw materials, such as cobalt and natural graphite, whose suppliers concentrate in a number of third countries, including conflict zones [2,3]. Therefore, efficient reuse and recycling of LIBs become more critical as well as the search for alternative energy storage solutions based on materials that can be sourced in a sustainable and responsible way.

Among the available alternatives, Na-based batteries are on the rise as a potentially competing technology to Li-ion batteries within certain applications [4–7]. The umbrella term of Na-based technologies is often used to describe several related battery concepts that use Na^+ ions as charge carriers, and includes Na-ion, all solid-state Na batteries (Na-ASSBs), Na/S and Na/O_2 batteries, as shown on Fig. 1. These battery chemistries differ in key components and redox chemistry, resulting in separate challenges and performance metrics. Equivalent concepts and configurations are found for Li-based batteries. A Na-ion battery (NIB) combines a Na-containing positive electrode and a Na-free negative electrode, and, therefore, is assembled in the discharged state (Fig. 1a). In a common NIB, the positive electrode is an insertion-type material, the negative electrode varies between insertion, conversion and alloying types, and the electrolyte is typically used in a liquid form. Electrodes are porous films casted on current collectors and, in addition to active material, often contain carbon-based additives necessary for electronic conductivity and polymeric binding agents ensuring mechanical integrity and adhesion among particles and current collectors. Noteworthy, at low potential Na does not alloy with Al [8] - an appealing advantage of NIBs with respect to LIBs. Therefore, Al can be used as current collector material at the negative electrode instead of Cu (typically used in LIBs), enabling storage and transport at 0 V by short circuiting the cells [9]. Na-ASSBs use a solid electrolyte (an inorganic ionic conductor or a polymer matrix swollen with Na salts), which is intrinsically safer than flammable solvents typically used for electrolytes in NIBs. The use of Na metal as a negative electrode and a simple design of bipolar electrodes could also lead to higher energy densities compared to cells with liquid electrolyte. In Na-ASSBs the positive electrode material will be similar to that of NIBs, however, the pores in the electrode are filled with a solid electrolyte (catholyte), and both the composite positive electrode and the solid electrolyte must be dense (Fig. 1b). Na/O_2 batteries use a combination of a Na metal negative electrode and an external positive O_2 electrode with an aqueous or aprotic electrolyte. The cell casing has vent openings to allow for air to diffuse, and a porous carbon matrix is used in the positive electrode as a host for solid discharge products (Fig. 1c). Na/S cells are similar to Na/O_2 batteries, but such cells are sealed since the positive electrode electroactive material, sulphur, is

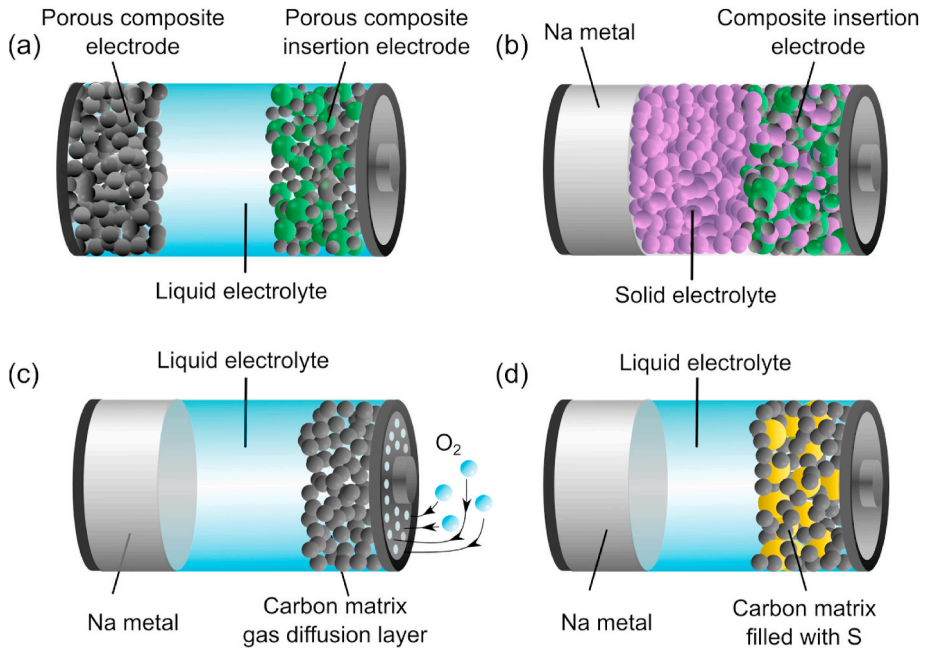

Fig. 1. Schematic cell configuration of the most common types of Na-based batteries. (a) Na-ion battery; (b) All solid-state sodium battery with Na metal negative electrode; (c) Na/O_2 battery and (d) Na/S battery. Note that also other versions exist including redox-flow types, for example.

hosted in a carbon porous matrix that provides electronic conductivity and accommodates the large volumetric changes that result upon discharging (Fig. 1d).

Most of these concepts are not new. Indeed, the research on NIBs was very active prior to LIB's commercialization [10]. Na/S and Na–$NiCl_2$ molten salt batteries using liquid Na metal at the negative electrode and a β-Al_2O_3 solid electrolyte have been manufactured since the mid-1990s (not considered here). Nevertheless, Na-based batteries have experienced a tremendous development during the past decade, emerging as a relevant addition to the pantheon of potential systems able to replace and/or supplement LIBs in specific applications. In this focus review we provide an in-depth preliminary assessment of emerging Na-based batteries, covering the most relevant aspects of materials and cell development.

2. Na-ion batteries

2.1. Positive electrode materials

The development of positive electrode materials for NIBs has experienced a rapid growth, due to the extensive knowledge gained from the chemistry developed for LIBs. Sodium analogues of various families of electrode materials known for LIBs are often found to show similar insertion properties for NIBs. As in LIBs, the most studied and highly successful candidates for positive electrodes can be parted between layered oxides and polyanionic compounds, although Prussian blue analogues (PBAs) with open cavities also show appealing sodium insertion properties [11–13]. Considering such variety, the enduring question now is whether there will be a single winning chemistry, or will different chemistries co-exist for a variety of market applications requiring specific performance metrics dictated by energy density, power, cyclability, safety and cost? To answer this question, we discuss herein the advantages and disadvantages for all three families of Na-ion positive electrodes (layered oxides, polyanionic structures and PBAs) in terms of energy density, rate capability, cyclability, cost and sustainability.

2.1.1. Sodium layered oxides

Layered sodium transition metal oxides ($Na_xMM'O_2$, M,M' = transition metal ion(s), Mg, Al, Sn, vacancies, etc.), simply termed as layered oxides, have two-dimensional layered structures for reversible sodium insertion (Fig. 2a and b). Layered oxides gained their superiority over other chemistries due to their low molecular weight and hence expected high theoretical specific capacity. With the proven success of lithium layered oxides (e.g. $LiNi_{0.8}Mn_{0.1}Co_{0.1}O_2$) in LIBs [14], the sodium analogues are extensively studied as well. Noteworthy, the sodium layered oxide chemistry is richer than that of their Li-analogues due to the ability of Na^+ to reside not only in octahedral (O) but also in prismatic (P) sites in comparison to solely octahedral site occupancy by Li^+ ions [15]. Additionally, redox processes such as Fe^{3+}/Fe^{4+}, that are rather unusual with Li-ion compounds, were found to be accessible with sodium layered oxides [16,17]. As a result, a large variety of compounds differing in oxygen stacking (P2, P3, O3 or P2–O3 intergrowths, against solely O3 for Li-analogues) with many different combinations of transition metal ion(s) have been studied, and numerous compounds with specific capacities as high as 200 $mAh.g^{-1}$ have been reported [18,19]. Demonstrations in prototype cells in pouch/cylindrical formats have also been performed by start-up companies such as Faradion (UK) and HiNa (China) using O3 or P2–O3 mixed phases of $Na_xNi_{1-x-y-z}Mg_xMn_yTi_zO_2$ and $Na_xCu_{1-y-z}Fe_yMn_zO_2$ as the positive electrode active material, respectively [20–22].

However, some scepticism prevails with the major question being, will layered oxides conquer the top position by competing with polyanionic compounds such as $Na_3V_2(PO_4)_2F_3$ (NVPF) and PBAs; and if so, which will be the winning chemical composition? A rather difficult question to answer, especially considering the possibility of evaluating different combinations of almost all 3d metals and also some of the non-transition metal ion(s). Additionally, non-uniformities in reports from different research groups exploring different compositions, often with little information provided regarding particular performance, lifetime and cost metrics, make it difficult to make fair and accurate comparisons (see Table S1). Hence, material design considerations based on crystal and electronic structure of layered oxides are required, also taking into account their structural stability upon long cycling in full cells.

Compounds with full sodium stoichiometry (1Na per transition metal ion) are reported to thermodynamically prefer the O3-type structure, while P-type phases are exclusively stabilized with sodium deficiency (less than 1 sodium in the pristine material), see Fig. 2a and b for two of the best performing examples. Though fully sodiated P-type compounds can be obtained by electrochemical insertion of sodium, the process is not viable in NIBs where there is no extra sodium available to compensate this non-stoichiometry. This drawback could be solved either by the addition of sacrificial salt(s) that oxidize/decompose irreversibly to provide extra sodium [23–25] or by using Na metal as the negative electrode [26]. Otherwise, uncompensated Na-deficiency in the P-type (P2 and P3) compounds leads to poor full cell capacity (Fig. 2b, Table S1), demanding the switch to O3-type materials for practical applications in spite of the reported better Na-diffusion property and, in some cases, moisture stability of P-type compounds [27].

Nevertheless, O3-type layered oxides undergo continuous phase transitions resulting from competing Coulombic and van der Waals forces, that induce slab gliding (O3 ⇔ P3 ⇔ O3/O1 etc.) as the Na^+ content changes upon cycling. Furthermore, in O3-type layered oxides the structural reversibility deteriorates, especially while cycling at high potentials aimed to utilize the full 1Na capacity [28–31]. To avoid this structural instability and to improve cycle life, the sodium layered oxides are used with c. a. 50% of their capacity (~120–140 $mAh.g^{-1}$) through electrochemical operation within a reduced voltage window. Such a low capacity, together with a lower average redox potential compared to Li analogues, leads to considerably lower specific energy than that of the phosphate-containing compound $Na_3V_2(PO_4)_2F_3$ (NVPF) [29]. Since high specific energy is a major criterion for practical applications, increasing the redox potential while utilizing the full available capacity are the main research hurdles for sodium layered oxides.

The sole strategy used to achieve these goals is based on selection of the adequate combination of transition metal ion(s) and fine-tune their stoichiometry. Hence, either redox centres that show high redox potential (e.g. Cu^{2+}/Cu^{3+}, Fe^{3+}/Fe^{4+} as in $Na_xCu_{1-y-z}Fe_yMn_zO_2$) [32] or non-redox centres that increase the ionicity of the associated redox centre (e.g. substitution of Ti^{4+}/Sn^{4+} in $NaNi_{0.5}Mn_{0.5}O_2$) [33,34] are used to increase the redox potential of the sodium layered oxides. These compounds have also been reported to show improved structural stability upon cycling. The underlying key point is to optimize the M−O bond ionicity which regulates the redox potential as well as the relative stability of O3 *vs* intermediate P3 phases [29,35]. A reversible capacity of >170 $mAh.g^{-1}$ with an average cell voltage of ~3.1 V stabilized for few hundred cycles (Fig. 3a), accounting to a specific energy of 500 $Wh.kg^{-1}$, was reported for $NaNi_{0.5-y}(Cu/Zn/Mg)_yMn_{0.5-z}Ti_zO_2$ materials [20,30,36]. As will be seen in section 5, these high figures allow this compound to be competitive compared to NVPF based on first cycles capacity. Note however that, as seen in Fig. 3, the capacity retention upon cycling is not as good for O3 as for NVPF.

Further research efforts to increase the specific energy are currently focused on developing Na-rich layered oxides with extra capacity derived from excess sodium and anionic redox activity, as reported with Li-rich phases. Na-analogues of all the known Li-rich phases do not exist, because Na^+ is bigger in size compared to Li^+ and hence difficult to stabilize in the transition metal layer together with smaller transition metal ions (e.g. 3*d* metals). Thus, the anionic redox activity in sodium layered oxides has been reported on either Na-deficient P2/P3 phases or in compounds based on 4*d* / 5*d* metals, resulting in unacceptably low

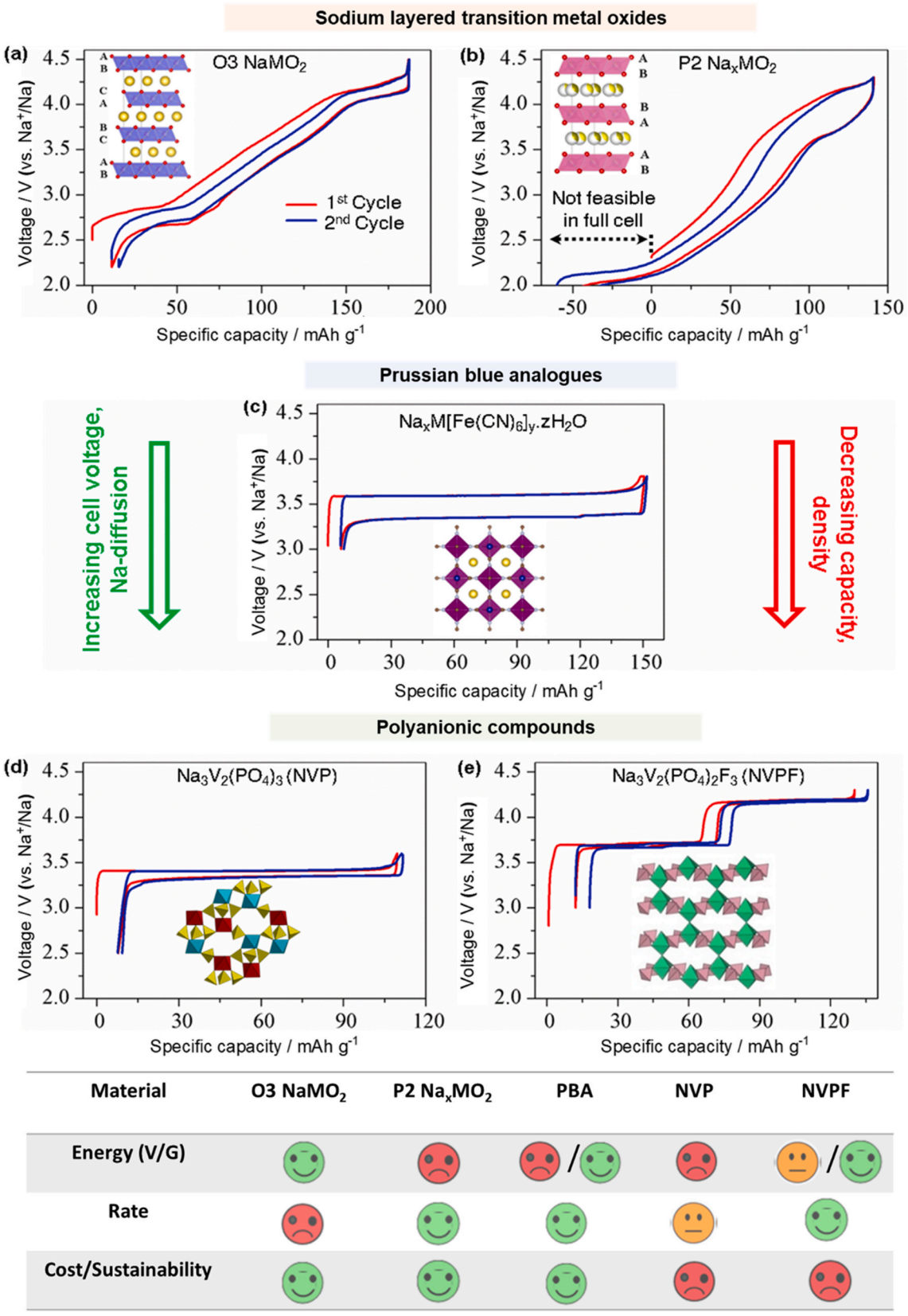

(caption on next page)

Fig. 2. Charge-discharge voltage profile of some representative compounds of the three different positive electrode families used in NIBs with their corresponding structure as inset. The compounds used as examples are O3–$NaNi_{0.45}Zn_{0.05}Mn_{0.4}Ti_{0.1}O_2$, P2–$Na_{0.67}Cu_{0.14}Fe_{0.2}Mn_{0.66}O_2$, Na_xM $[Fe(CN)_6]_y.zH_2O$, $Na_3V_2(PO_4)_3$ and $Na_3V_2(PO_4)_2F_3$. Half-cell data using metallic sodium as counter electrode are used to have a direct comparison of the redox potential and capacity of these compounds; the electrolyte used was 1 M $NaPF_6$ in organic carbonate(s) and the cells were cycled at C/10 rate (Capacity to remove 1 Na is used as 1C). All cycling data used here are derived from laboratory data where the electrode materials are either home-made or commercially bought for comparative studies; the structure of the compounds were drawn using VESTA software. Sodium layered oxides show electrochemical signatures with several sloping and plateau regions due to successive solid solution and biphasic type phase transitions in the voltage window of 2–4.5 V vs Na^+/Na, whereas a plateau-like behaviour is observed with polyanionic phases, with $Na_3V_2(PO_4)_2F_3$ showing the highest average cell voltage. On moving from layered oxides to PBAs or polyanionic phases, there is a decrease in capacity due to high molecular weight, while increasing redox voltage and Na-diffusion are observed. The extra capacity observed with P2 layered oxides down to 2 V is not feasible in Na-ion full cells using HC or any Na-free negative electrode. The table below the figure summarizes the advantageous and disadvantageous properties of each material in terms of volumetric (V) and gravimetric (G) energy, rate and cost/sustainability. Green, orange and red symbols are used to indicate high, average and poor performance of the material with the corresponding parameter respectively. (For interpretation of the references to colour in this figure legend, the reader is referred to the Web version of this article.)

capacity [37,38]. Noteworthy, the Li-rich layered oxides have also intrinsic disadvantages, such as oxygen release, voltage decay, etc., and have not reached the commercialization stage within the Li-ion technology either [39].

Besides the specific energy, another significant parameter to be considered is the rate performance of the electrode material, as NIBs are expected to find its market in high power applications such as stationary energy storage, where sudden frequency adjustments are required. Polyanionic NVPF and PBAs topped in this parameter as significant capacity (more than 80%) retention is achieved at rates as fast as 10C (1 Na removal in ~6 min, see insets of Fig. 3b and c) [20,40]. In sodium layered oxides the Na-diffusion kinetics of each phase needs to be considered as they undergo continuous structural transformations during cycling, and the slowest diffusion phase controls the whole cell reaction. Further, the existence of phase mixtures may also impede the Na^+-diffusion by grain boundary effects. As a result, sodium layered oxides are cycled mostly at 0.1C rate (1 Na removal in 10 h) and hardly ~80% capacity is retained even at 1C rate (see the inset in Fig. 3a). Interestingly, a buckling effect of the Jahn-Teller active Fe^{4+} ion is claimed by Ceder et al. to improve the rate capability of O3– $NaCu_{1/3}Fe_{1/3}Mn_{1/3}O_2$, whose cycle life is still debatable due to utilization of the less stable Fe^{3+}/Fe^{4+} redox pair upon long cycling [32]. Recent reports describing O3–P2 mixtures provide interesting rate capabilities, although a deeper understanding of the phase distribution at the atomic level is still required (intergrowth *vs* composite) [22,41,42].

In short, at the present moment, layered oxides can exhibit specific energies comparable or even slightly superior to those of polyanionic materials with the advantageous use of cheap and non-toxic transition metal elements. Additionally, layered oxides are denser materials compared to NVPF or PBA, and, therefore, allow higher volumetric energy density (e.g. achieved 250 Wh. L^{-1} with $NaNi_{0.4}Cu_{0.1}Mn_{0.4}Ti_{0.1}O_2$ *vs* 175 Wh. L^{-1} for NVPF in cell level) [30]. Further considerations on the influence of density on the full cell performance can be found in section 5. However, their disadvantage remains in the structural instability upon Na-insertion/de-insertion that impedes power rate capability and cycle life (Fig. 3). Recent studies by Song et al., reported stable cycling over 1000 cycles by using O3 $NaNi_{0.68}Mn_{0.22}Co_{0.10}O_2$ achieved through optimization of the electrolyte and the electrode's surface properties (See Table S1 for the details on reported data so far) [43]. The result provides a hope for the sodium layered oxides to reach commercial applications especially for high energy/low cost requirements if the synthesis, processing difficulties in reaching homogeneous materials and moisture sensitivity of layered oxides, that requires strictly controlled atmosphere for material storage and processing, could be solved [44]. Future development towards practical applications requires studies of the synthetic protocols to obtain homogeneous materials in bulk batches using industrially viable methods such as co-precipitation. Additionally, a deeper understanding of low and high temperature electrochemical cycling, and thermal stability at high potentials in the presence of an electrolyte is also required before reaching the commercialization.

2.1.2. Polyanionic compounds

Besides layered oxides, polyanionic compounds are attractive as positive electrode materials for NIBs due to their operating voltage, which can be widely tuned by changing the nature of the involved redox couple as well as the composition and the structure of the anionic framework (see Table S2) [45]. Indeed, the strength of the X–O (X = P, S, Si, C) bonding in the anionic framework has an influence on the covalency of the M − O bond (and, therefore, on the position of the antibonding energy levels) resulting in a larger operating voltage *vs* Na for a given redox couple than for the bare oxide. This allows to counterbalance the obvious penalty due to the higher molar mass of the polyanion (PO_4^{3-}, SO_4^{2-} and SiO_4^{4-}). Their frameworks and properties are quite diverse, depending on the nature of the anionic groups, the crystal structure type (NASICON, Tavorite, Olivine, Alluaudite, layered, etc.) and the dimension of the ionic diffusion paths (1D for olivine $NaFePO_4$, 2D for $Na_3V_2(PO_4)_2F_3$ and 3D for NASICON $Na_3V_2(PO_4)_3$ for instance) [46]. However, they typically present a better structural stability compared to layered oxides at deintercalated state, allowing reversible full extraction of up to 1 or 2 Na.

$NaFePO_4$ [47,48], $Na_2FeP_2O_7$, [49] $Na_4(Fe,Mn)_3(PO_4)_2(P_2O_7)$ [50,51], $Na_{2+2x}Fe_{2-x}(SO_4)_3$ [52] and Na_2MnSiO_4 [53] are interesting examples of low-cost polyanion-type materials built on environmentally friendly elements (Fe, Mn, P, S, Si, etc.). Nevertheless, their performances are still too limited for NIBs due to low capacities for the diphosphates and mixed phosphates (<100 mAh.g^{-1}), low voltages (<3 V *vs* Na^+/Na) and low rate capabilities for the silicates, high sensitivity to water for sulfates and difficulties to properly control most of their syntheses (see Table S2 in supplementary information for comparison of these different polyanionic materials). Among all the polyanion-type materials reported up to now, the two V^{3+}-containing compositions $Na_3V_2(PO_4)_3$ and $Na_3V_2(PO_4)_2F_3$ are the most promising phosphate-based materials in terms of performance. They both show the reversible extraction of 2 Na^+ ions per formula unit (ca. 100–120 mAh.g^{-1}, see Fig. 2d and e) at a voltage higher than 3.4 V *vs* Na^+/Na and in the stable electrochemical window of the currently available liquid electrolytes.

The structure of the NASICON $Na_3V_2(PO_4)_3$ can be described as a 3D framework, with a "lantern" basic repeating unit made of two VO_6 octahedra and three PO_4 tetrahedra linked to each other by corners sharing only, and with each lantern connected to six others to build 3D diffusion paths for Na^+ ions (Fig. 2d) [54]. Although often described by mistake as being also of NASICON-type, the structure of the fluorinated oxyphosphate $Na_3V_2(PO_4)_2F_3$ is built of $V_2O_8F_3$ bi-octahedral units (F–VO_4–F–VO_4–F) which are linked together by PO_4 tetrahedra to generate a 3D network with channels for the 2D diffusion of Na^+ ions (Fig. 2e) [55]. As for most of the polyanionic compounds, the electronic conductivities of $Na_3V_2(PO_4)_3$ and $Na_3V_2(PO_4)_2F_3$ are rather low due to the presence of highly covalent phosphate groups that isolate the transition metal centres from each other. Nanocomposites and surface-conducting modifications (e.g. with the formation of thin carbon coating) are hence prepared, not only to enhance the grain electronic conductivity, but also to prevent particle growth during the synthesis or

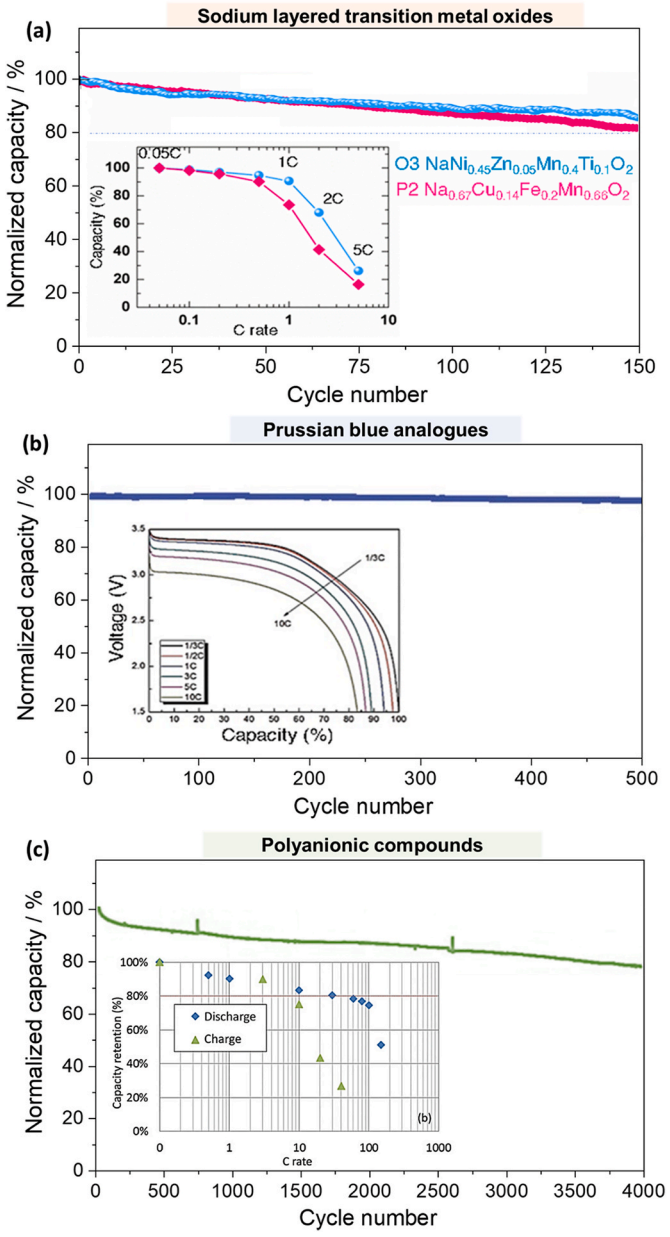

Fig. 3. Comparison of cycle life (capacity retention) and power rate capability of three different families of positive electrodes. (a) Sodium layered oxides O3 $NaNi_{0.45}Zn_{0.05}Mn_{0.4}Ti_{0.1}O_2$ (100% capacity = 145 mAh.g^{-1}) and P2 $Na_{0.67}Cu_{0.14}Fe_{0.2}Mn_{0.66}O_2$ (100% capacity = 103 mAh.g^{-1}) cycled in coin cell at C/10 rate using hard carbon as negative electrode and 1 M $NaPF_6$ in propylene carbonate as electrolyte. Inset shows the power rate capability of the materials tested in Na-half cells using sodium metal as counter and negative electrode. The capacity of 172 and 255 mAh.g^{-1} are taken as 100% capacity for O3 and P2 layered oxides respectively. (b) Prussian blue analogue $Na_xMnFe(CN)_6$ cycled vs hard carbon in a Novasis pouch cell. Inset reporting the associated voltage profiles upon cycling at different C rates; Reprinted (adapted) with permission from Ref. [20] Copyright (2020) John Wiley and Sons. (c) Polyanionic $Na_3V_2(PO_4)_2F_3$ in a 75 Wh. kg^{-1} 18 650 cell using hard carbon as negative electrode at 1C rate. Inset reporting rate capability test at 100% Depth of discharge (DOD) for a 55 Wh. kg^{-1} 18 650 cell prototype; Reprinted (adapted) with permission from Refs. [40] Copyright (2020) John Wiley and Sons. (For interpretation of the references to colour in this figure legend, the reader is referred to the Web version of this article.)

agglomeration during long-term electrochemical cycling at high rates [56].

Solid state and wet synthesis methods are the most traditional routes used to prepare $Na_3V^{III}{}_2(PO_4)_3$ and $Na_3V^{III}{}_2(PO_4)_2F_3$. Nevertheless, a careful control of the thermal treatment's temperature and atmosphere is required to obtain the material with optimized performance, i.e. without $Na_3V_2(PO_4)_3$ as an impurity or without partial substitution of oxygen for fluorine that leads to the formation of the mixed valence compositions $Na_3V^{III}{}_{2-y}(V^{IV}O)_y(PO_4)_2F_{3-y}$ ($0 \le y \le 2$). In both cases, the average operating voltage is driven to lower values, thus, resulting in lower energy densities. Nuclear Magnetic Resonance (NMR) and Infra-Red (IR) spectroscopies were shown to be the tools of choice to track the presence of oxygen defects and vanadyl bonds ($\{V^{4+}{=}O\}^{2+}$) in $Na_3V_2(PO_4)_2F_3$, allowing to control the synthesis of the optimized active material [57,58]. In fact, most of the reported work on $Na_3V_2(PO_4)_2F_3$ often deals with compositions that are highly oxygen-rich, i.e. less fluorinated than expected.

During Na-deintercalation from $Na_3V_2(PO_4)_3$, a flat composition-voltage "plateau" is observed at ca. 3.4 V *vs* Na^+/Na, which corresponds to the activation of the V^{3+}/V^{4+} redox couple and to the extraction of two Na^+ ions from the structure to form $NaV_2(PO_4)_3$ through a bi-phasic reaction (Fig. 2d) [59]. Due to the presence of fluorine, the highest electronegative element, in the first coordination sphere of V^{3+} in $Na_3V_2(PO_4)_2F_3$ the 3*d* orbitals are strongly polarized, giving rise to an increased operating voltage of 0.5 V for the V^{3+}/V^{4+} redox couple when compared to that observed for $Na_3V_2(PO_4)_3$. Two Na^+ ions can be extracted from $Na_3V_2(PO_4)_2F_3$ at ca. 3.70 and 4.20 V *vs*. Na^+/Na (Fig. 2e) [60] through successive bi-phasic and solid solution reactions with the stabilization of five intermediate compositions, mainly driven by the structural reorganization of the Na^+ ions in order to minimize the electrostatic repulsions within the diffusion channels [61]. For $Na_3V_2(PO_4)_2F_3$, pairs of V^{3+} and V^{5+} are stabilized within the bi-octahedral units at the end of the first charge for the composition $NaV_2(PO_4)_2F_3$ [62], whereas for $Na_3V_2(PO_4)_3$ only pairs of V^{4+} are stabilized in the lanterns (built on two non-corner sharing VO_6 octahedra) for the composition $NaV_2(PO_4)_3$.

First proofs of concept were reported in full cells *vs* hard carbon (HC) for optimized nanocomposites of both $Na_3V_2(PO_4)_3$ and $Na_3V_2(PO_4)_2F_3$, with a discharge capacity of ~100 mAh.g^{-1} and attractive capacity retention even at high rates [63,64]. Recently, optimized hard carbon//$Na_3V_2(PO_4)_2F_3$ 18650 full cells and cycled at 1*C* at ambient temperature could maintain more than 80% of their initial capacity after 4000 cycles (Fig. 3c, Table S1) [40]. Outstanding performances were also demonstrated for $Na_3(VO)_2(PO_4)_2F$ [65], the end-member of the $Na_3V^{3+}{}_{2-y}(V^{4+}O)_y(PO_4)_2F_{3-y}$ solid solution, but with a significant lowering of the average voltage of *ca.* 0.10 V, due to a larger amount of V^{4+} (or $\{V{=}O\}^{2+}$ vanadyle bond) in the initial structure. Only the two end-members of the $Na_3V^{III}{}_{2-y}(V^{IV}O)_y(PO_4)_2F_{3-y}$ ($0 \le y \le 2$) family show voltage-composition plateaus, while all other intermediate compositions show sloping electrochemical voltage-composition features associated to solid solution type reactions [66,67].

One of the challenges to further improve the performance of $Na_3V_2(PO_4)_2F_3$ still to be addressed is the structural stabilization of the highly de-intercalated composition needed to achieve a reversible electrochemical cycling over three Na^+ ions per formula unit [60]. The extraction of the third Na^+ ion from $Na_3V_2(PO_4)_3$ by chemical oxidation with the formation of the composition $V^{4+}V^{5+}(PO_4)_3$ was reported [68] but never reproduced. Recently, the extraction of the third Na^+ ion from $Na_3V_2(PO_4)_2F_3$ was achieved at an upper cut-off voltage of 4.75 V *vs* Na^+/Na followed by an extended floating at the end of charge [69]. Unfortunately, this three-electron reaction leads to an irreversible structural transformation leading to the formation of a highly disordered structure that allows the re-intercalation of only two Na^+ ions. Indeed, a third Na^+ ion could be re-intercalated but only after a sloping discharge down to a very low voltage of 1 V *vs* Na^+/Na, not practically acceptable for a positive electrode material. In $Na_3V^{3+}{}_{2-y}(V^{4+}O)_y(PO_4)_2F_{3-y}$, the

presence of oxygen defects prevents the de-intercalation of more than two Na^+ ions per formula unit, which can be used as a barrier *vs* overcharge and structural destabilization [67].

Cation substitution for vanadium with spectator ions (such as Al) or redox active ones (such as Fe and Mn) was explored as a possible strategy to activate the de-intercalation of the third Na^+ ion through the involvement of the V^{4+}/V^{5+} redox couple and to contribute to a substantial increase in the energy density of these polyanion-based compounds. This activation was first demonstrated to occur at 3.9 V *vs* Na^+/Na by introducing Al^{3+} in $Na_3V_{1.5}Al_{0.5}(PO_4)_3$, compared to 4.75 V for $Na_3V_2(PO_4)_2F_3$ [70]. New Na-rich NASICON compositions, such as $Na_4Mn^{2+}V^{3+}(PO_4)_3$, were also reported to be quite promising because of the activation of the V^{3+}/V^{4+}, Mn^{2+}/Mn^{3+} and V^{4+}/V^{5+} redox couples that results in the extraction of three Na^+ ions during the first charge at a higher average operating voltage (ca. 3.6 V *vs* 3.4 V for NVPF) [71–73]. Nevertheless, several puzzling questions remain considering this three Na^+ ions exchange per two transition metal cations: why is the presence of a foreign cation essential in the activation of V^{4+}/V^{5+} redox couple in the NASICON framework? Why irreversible structural modifications and significant capacity losses are observed for $Na_3V_{1.5}Al_{0.5}(PO_4)_3$ and $Na_4VMn(PO_4)_3$, but also for $Na_3V_2(PO_4)_2F_3$, as soon as more than 2 Na^+ ions are de-intercalated per formula unit upon the activation of the V^{4+}/V^{5+} redox couple at high voltage?

Interestingly, both V^{3+}-containing $Na_3V_2(PO_4)_3$ and $Na_3V_2(PO_4)_2F_3$ compounds, and especially the latter, remain highly competitive with the most promising layered oxides. They revealed robustness as positive electrode materials for power-type NIBs, with energy densities of ca. 400 and 500 Wh. kg^{-1} respectively, moisture stability when stored in air and thermal stability in the charged state of the battery [67]. However, both materials behave very differently: in the $Na_3V_2(PO_4)_3$ NASICON phase the redox activity of vanadium is fully independent from the nature of the second metal ion in the same lantern (the MO_6 octahedra do not share corners between each other), whereas in $Na_3V_2(PO_4)_2F_3$ the nature of the terminal bonds V-X (X = F, O) and of the transition metal ions in the bi-octahedral units tailors the redox properties of vanadium. A significant modification of the crystal field by partial substitution for vanadium or by altering the nature of the anions are the key tracks to prospect further in order to achieve a reversible extraction/re-insertion of three Na^+ ions. The worst penalty of these polyanion-type materials, beyond their rather low gravimetric capacity, remains their composition, as vanadium is a critical and highly toxic element, at least in its V^{5+} oxidation state. Its replacement by environmentally friendly elements (such as Fe, Mn) remains another challenge, as recent trials were demonstrated to be unsuccessful [67].

2.1.3. Prussian blue analogues (PBA)

PBAs are cyano-coordination compounds with general formula $A_xM[M'(CN)_6]_{1-y}.zH_2O$ where A = alkali metal; M, M' = transition metal ion and y is the fraction of vacancies present in the crystal structure [74,75]. They exhibit a three-dimensional framework with open channels for rapid alkali metal conduction (Fig. 2c), hence finding attractive applications as high power positive [20] and negative electrodes in NIBs. Through careful tuning of the transition metal ion, hence the redox potential, it is possible to use these compounds on either side [76]. For example, the US based company Natron energy proposes Na-ion cells made of a mixed metal hexacyanoferrate at the positive and a manganese hexacyanomanganate at the negative to achieve high power rate capabilities [77,78].

A maximum of $\sim 2e^-$ can be exchanged with PBAs using both M and M' as redox active transition metal ions, whose redox potential depends on their nature [79]. Hence, $2Na^+$ insertion was reported for the stoichiometric composition $Na_2FeFe(CN)_6$ leading to a competitive capacity of ~170 mAh.g^{-1} at an average cell voltage of ~2.7 V *vs* Na^+/Na [80]. The presence of vacancies was found to limit the sodium ion storage capacity.

With continuous research efforts and optimization strategies, the composition $Na_{2-\delta}MnFe(CN)_6.yH_2O$ developed by Sharp Laboratories of America, Inc. showed the most attractive capacity of ~140 mAh.g^{-1} at an average cell voltage of 3.4 V, thus providing a specific energy of ~520 Wh. kg^{-1}, a value close to that of $LiFePO_4$ in LIBs [20]. Prototype sodium ion cells using $Na_{2-\delta}MnFe(CN)_6.yH_2O$ were developed by the US based start-up Novasis, and high power rates with stable cycling (~85% capacity retention after 500 cycles at 0.1C rate) were achieved (Fig. 3b) [20]. The added advantage of PBAs is the simplicity of synthesis: for some attractive compositions a simple precipitation reaction conducted at low temperature is used for their preparation without the need for high temperature calcination [81]. PBAs are made of non-toxic and sustainable transition metal ions and show good stability in moist air, thus reducing the requirement of strict control of atmosphere during material storage and processing. The presence of cyanide group and the possible release of toxic (e.g. HCN) gases during decomposition can be problematic, but the studies showed that these compounds are thermally stable up to 200 °C [82].

Overall, PBAs with an achieved specific energy close to that of NVPFs and high-power rate capability exert attractive qualities for the fabrication of cheap NIB electrodes. However, PBAs have low density leading to poor volumetric energy density compared to sodium layered oxides [83], see section 5 for more details. The other impeding criterion is the presence of water molecules within the crystal structure and the poor knowledge about its effect on the electrochemistry. PBAs have 2 types of water molecules in their structure, i.e. zeolitic and coordinated water. Zeolitic water molecules, that occupy the alkali (Na^+) position, can be easily removed while the water molecules coordinated with the M-site ions generally undergo electrochemical decomposition at high potentials during cycling [84]. Complete removal of water molecules have been achieved by vacuum drying of PBAs at low temperatures (100 °C), however the resulting material is found to show pronounced structural distortions that reduce the cycle life [84]. Thus, by better understanding the role of water molecules and identifying a strategy to reduce/control its amount, one can hope that PBAs would reach commercial success in high power applications despite of their poor energy density.

2.2. Negative electrode materials

In this section a brief overview of the state-of-art negative electrode materials for NIBs will be presented. Negative electrode materials can be classified in five different types according to their reaction mechanism, namely: insertion-based negative electrodes, including carbon and Ti-based oxides, alloying compounds, conversion-type materials and mixed alloying-conversion systems. Their typical electrochemical properties in terms of delivered capacity, operating working voltage, and voltage-composition signature are shown on Fig. 4. Herein, electrochemistry, structure and morphology will be discussed in combination with their reaction mechanisms and performance. A more comprehensive literature survey describing these classes of negative electrode materials for NIBs has been already reported, and well summarized in previous reviews [85–90]. Therefore, the purpose of the present review is to highlight the most promising identified negative electrode materials for successful implementation in future commercial NIB prototypes with different energy and power requirements.

2.2.1. Carbonaceous materials

Throughout the development of the LIB technology, the active material for the negative electrode evolved from soft carbon (SC) used in the seminal Sony cell of 1991, later replaced by HC for enhanced energy density, to finally graphite when electrolyte optimization allowed to forbid the detrimental solvent co-intercalation [100].

Similar to the positive electrode materials, the search for negative electrode active materials for NIBs followed the steps of the Li-ion technology, although with some notable differences. Graphite has been soon discarded for its impossibility to form Na binary intercalation compounds, in favour of non-graphitic SC and HC. While both SC and

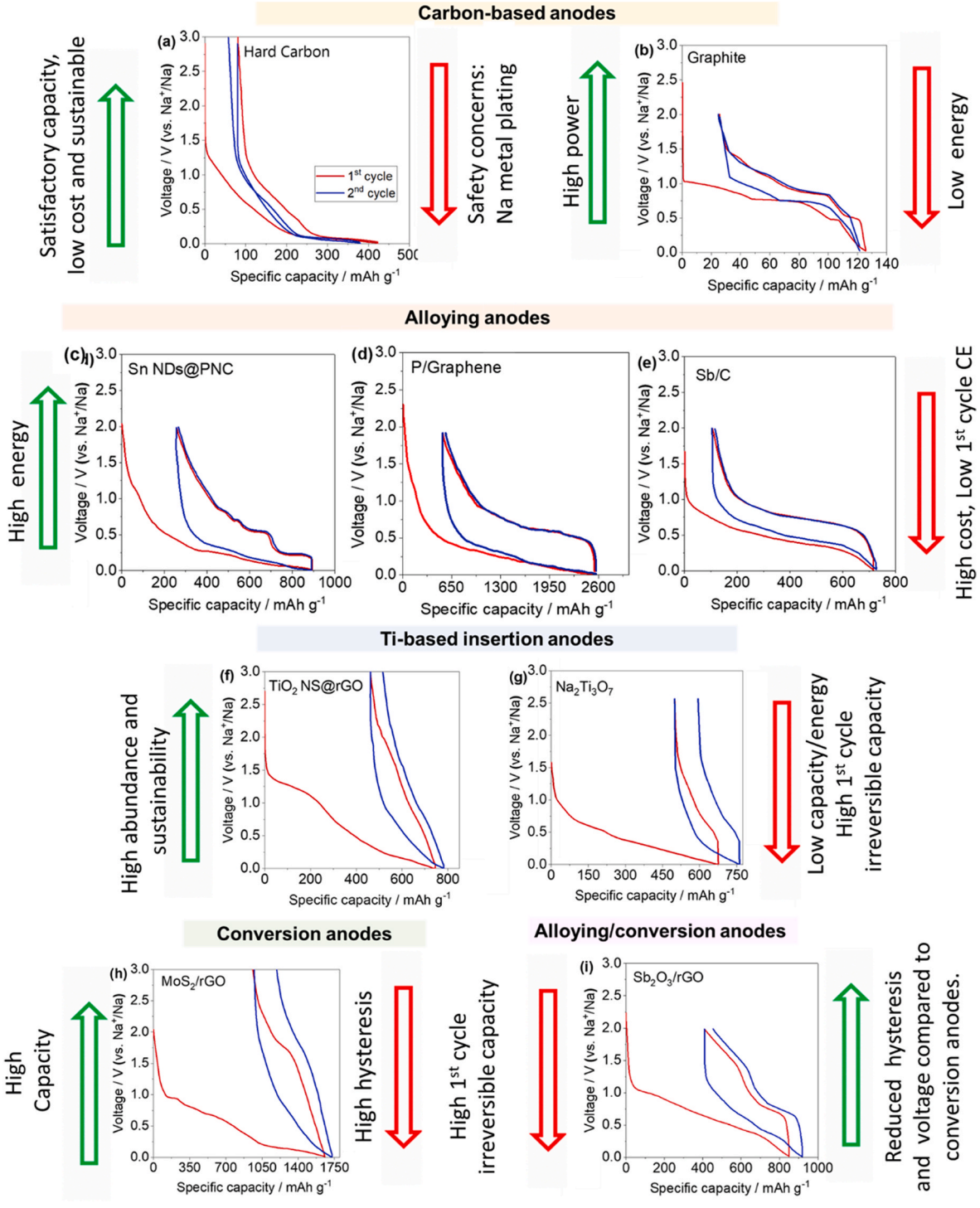

Material	Hard Carbon	Graphite	Sn/C	P/C	Sb/C	TiO_2	Na_2TiO_3	MoS_2/C	Sb_2O_3/C
Energy	🙂	☹	🙂	🙂	🙂	☹	☹	😐	😐
Rate	☹	🙂	🙂	🙂	🙂	😐	😐	☹	😐
Cost/Sustainability	🙂	😐	🙂	🙂	☹	🙂	🙂	☹	☹

(caption on next page)

Fig. 4. Selected carbon-based, Ti-based insertion, alloying, conversion, and alloying/conversion negative electrode materials reported for NIB application. (a) 1st and 2nd cycles voltage profiles for filter paper-derived micro-nano structure carbon (DPC-A) electrode (current density: 20 mA g^{-1}; electrolyte: 1 M $NaClO_4$ – EC:PC (1:1, v/v)) [91]; (b) graphite cycled in glyme based electrolyte (current density: 200 mA g^{-1}; electrolyte: 1 M $NaClO_4$ TEGDME) [92]; (c) Sn nanodots finely encapsulated in porous N-doped carbon (NDs@PNC fiber) (current density: 200 mA g^{-1}; electrolyte: 1 M $NaClO_4$ –PC (+5% vol FEC)) [93]; (d) phosphorous-graphene composite (P content of 52.2%, current density: 250 mA g^{-1}; electrolyte: 1 M $NaClO_4$ – EC:DEC+5%vol FEC) [94]; (e) Sb/C nanocomposite (current density: 100 mA g^{-1}; electrolyte: 1 M $NaPF_6$ –EC:DEC) [95]; (f) TiO_2 nanosheets/reduced graphene oxide composite (TiO_2 NSs@rGO) (current density: 1C; electrolyte: 1 M $NaClO_4$ – PC: FEC (95:5, v/v)) [96]; (g) Microspheric $Na_2Ti_3O_7$ (current density: 354 mA g^{-1}; electrolyte: 1 M $NaClO_4$ –PC) [97]; (h) MoS_2/reduced graphene oxide (RGO) nano-composite (current density: 20 mA g^{-1}; electrolyte: 1 M $NaClO_4$ –EC:PC (1:1, v/v)) [98]; (i) Sb_2O_3/reduced graphene oxide (RGO) composite (current density: 100 mA g^{-1}; electrolyte: 1 M $NaClO_4$ –EC:PC (1:1, w/w) + 5 wt% FEC)) [99]. The table below the figure summarizes the advantageous (green) and disadvantageous (red) properties of each material in terms of energy, rate and cost/sustainability. Capacity values of composites (c,d,e,f,h,i) are given as reported, that is normalized over the total mass of composites except for P/C (d) and Sb/C (e) for which it is normalized to the metal mass. (For interpretation of the references to colour in this figure legend, the reader is referred to the Web version of this article.)

HC present a sloping voltage-composition curve below 1 V, HCs exhibit an additional low voltage plateau below 100 mV (Figs. 4a and 5a). This boosts the capacity up to the range of 300–350 mAh.g^{-1} and lowers the working voltage down to 0.3–0.4 V, with best reports reaching initial Coulombic efficiencies above 80% [101,102]. Specific capacities are further improvable up to 400 mAh g^{-1} by high temperature treatment [103], allowing a significant improvement in terms of specific energy compared to the best SCs, which have demonstrated specific capacities in the range of 200–250 mAh.g^{-1} with working voltages around 0.5–0.6 V and best Coulombic efficiencies within the range of 70–80% [104]. Although it has been suggested that optimized SC exhibits superior rate capability, HC remains the present benchmark for negative electrodes of NIBs from the perspective of energy density.

Indeed, while a variety of chemistries and compounds were proposed at the positive electrode side, the implementation of HC at the negative electrode side is a constant feature among all the research efforts carried out worldwide to make NIBs a commercial reality. Examples include the first cylindrical "18650" NIB cell using HC negative electrodes *vs* NVPF as the positive electrode by the joint effort from the French National Centre for Scientific Research (CNRS) and the French Alternative Energies and Atomic Energy Commission (CEA) (Fig. 3c) [105]. Likewise, the work performed at Sharp Laboratories of America Inc. and later at Novasis Energies Inc. generated a sodium cell employing a Prussian blue positive electrode and a HC negative electrode [20]. Finally, the Faradion Limited's cell employs a layered oxide positive electrode and a HC based negative electrode [106], as well as the Hi-Na battery developed in China [107].

However, despite an important role of HC towards commercialization of NIBs, the gap in performance compared to graphite in LIBs motivates an intense effort to push it even further. Two main strategies are being followed [108]. On one side, some groups seek an increase of the capacity of HC while maintaining its characteristically low working voltage, see e.g. Refs. [101,109–111]. On the other side, the exploration of alternative forms of sp^2 carbon is explored to boost the (pseudo) ad/chemisorption contribution to the capacity. These forms include graphene-related materials and other doped (and undoped) carbon materials with a high specific surface area [111–113] This led, in certain cases, to a huge gain in capacity but at the cost of higher potentials and poorer Coulombic efficiencies [114], with a limited gain in terms of practical energy density at full cell level compared to best HCs [108]. The understanding of the mechanism of Na storage in HC currently appears to be a bottleneck in the further development, as it hampers the identification of design guidelines to circumvent the trade-off between high capacity, low working potential and high Coulombic efficiency [87,108,115].

SCs and HCs are sp^2-type carbon polymorphs which show a tendency to generate layered structures with various degrees of distortion and disorder, where graphene serves as a building block. Non-graphitic SC and HC are typically produced by the pyrolysis of organic precursors at temperatures between 500 and 1500 °C. Whether the final product after pyrolysis will be HC or SC mainly depends on the nature of the precursor. HC precursors are typically obtained by carbonization of oxygen-rich precursors including plant-derived biomasses, sucrose, glucose, cellulose, and lignin. Meanwhile SC is primarily derived from hydrogen-rich precursors such as hydrocarbon, and aromatic compounds. A detailed literature survey of precursors employed for SCs and HCs is given in other insightful review papers [87,108,116].

The designation "soft" and "hard carbon" derives from their mechanical strength, which, as well as their ability to graphitize, depends on the plasticity of their layered structure [87,108,117]. Indeed, graphitization involves the transformation of the fully turbostratic initial structure to an ABAB or ABCABC layer stacking arrangement, which requires the layers to glide and spin [117,118]. Similar to graphite, the structure of SCs exhibits such plasticity providing softness under stress and ability to graphitize above 2200 °C (graphitizable carbons). On the contrary, the fine structure of HC forbids this plasticity, inducing mechanical hardness and inability to graphitize even at temperatures higher than 3000 °C ("non-graphitizable carbon").

Despite the seminal publications by R. Franklin reported 70 years ago [117], the complex multiscale structure and microstructure of HC is still not fully understood [87,108]. Several questions about the internal structure of HC still remain open, particularly addressing the influence of the structure on its electrochemical behaviour. Will a full understanding of the HC's structure enable a rational design of advanced HC negative electrodes? Or will technological development and optimization of the material processing allow to overcome and essentially neglect the scientific question? Such dilemma behind the research efforts currently ongoing in academic and industrial centres still remains. However, despite these questions, a common reporting methodology and testing protocol should be adopted by the scientific community to enable a fair comparison among cell performance and elucidate the hidden structure-function correlations. Many aspects are in the control of such structure-property relationship, including the unit cell parameters and defects of the local layered structure, the microstructural features forbidding layers gliding and rotation, the presence of closed and open micropores, or the presence of H and heteroatoms such as O or N. Such complexity induces a multitude of potential redox active chemical, structural and microstructural features. It also makes the view of the structure and microstructure strongly dependent on the characterization technique used. This leads to many proposed potential mechanisms, such as interlayer intercalation, ad-/chemisorption at defect and heteroatom sites of the open micropores, Na^+ pseudo-adsorption or clustering in the closed microporosity [87,108,110,119,120]. The balance between these mechanisms is highly dependent on the precursor and the synthetic conditions, and, thus, its assignment to the various voltage regions of HC is often contradictive between reports [87,108,109,116,119–123].

Among the large number of scientific reports focused on the mechanisms of charge storage in HC, a few relevant elements offering design clues will be highlighted here. The use of intensity calibrated small-angle X-ray scattering (SAXS) has recently shown that HC having a low surface area as detected by gas adsorption (which is required to ensure high Coulombic efficiency) [87,108], can at the same time exhibit a high concentration of closed micropores (ca. 25% in volume) [124]. Such studies open the door for potential increase of the capacity by fine-tuning of the closed microporosity without affecting the

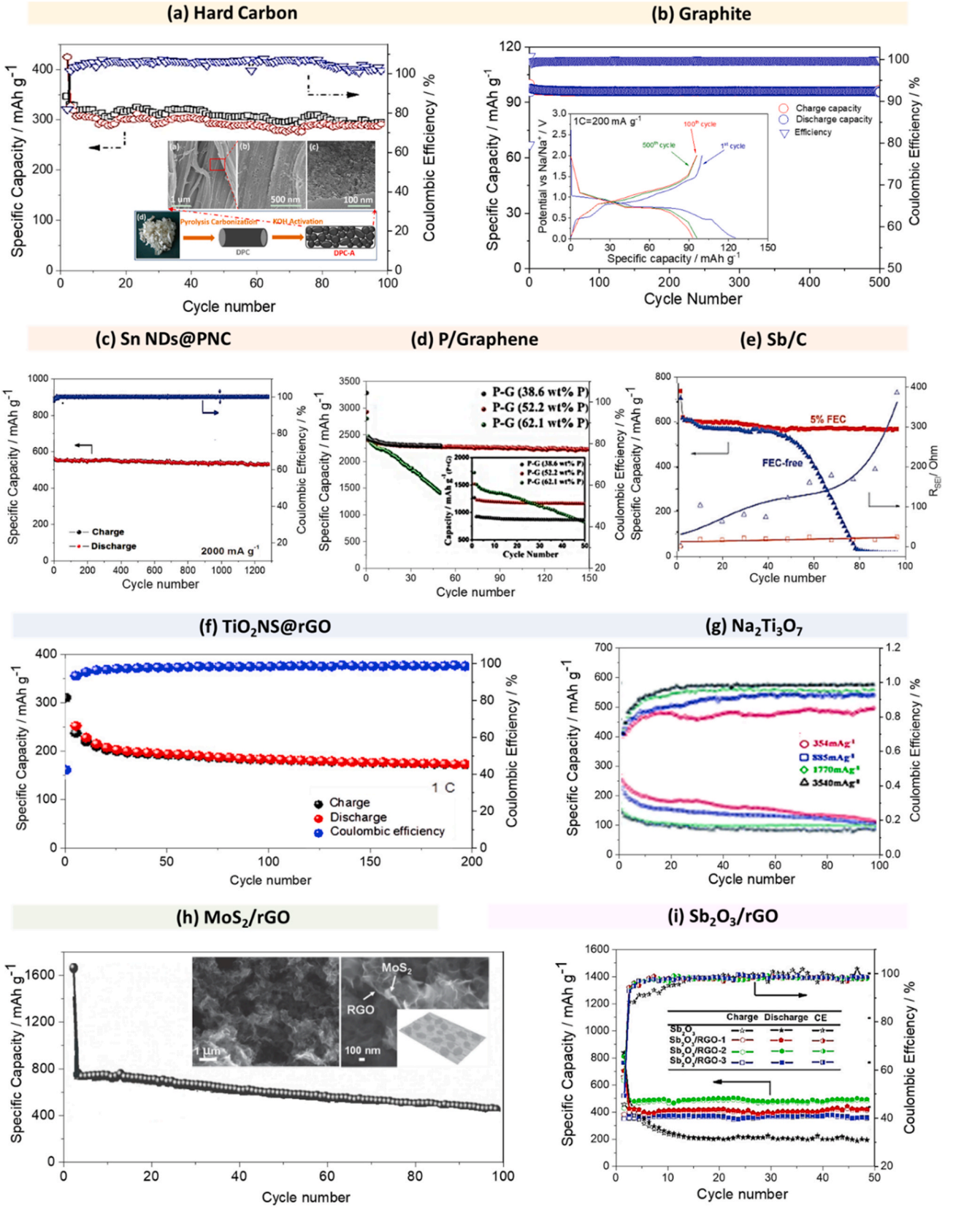

(caption on next page)

Fig. 5. Cycling performance of the selected carbon-based, Ti-based insertion, alloying, conversion, and alloying/conversion negative electrode materials. The corresponding 1st and 2nd voltage profiles are reported in Fig. 4. (a) Filter paper-derived micro-nano structure carbon (DPC-A) electrode (current density: 20 mA g^{-1}; electrolyte: 1 M $NaClO_4$ – EC:PC (1:1, v/v)). Inset reporting the schematic illustration of the synthesis procedure. Reprinted and adapted from Refs. [91] with permission from Springer Nature Copyright © (2016), distributed under the terms of the Creative Commons CC BY license; (b) graphite cycled in glyme based electrolyte (current density: 200 mA g^{-1}; electrolyte: 1 M $NaClO_4$ TEGDME); Inset reporting the corresponding voltage profile at the 1st, 100th and 500th cycles. Reprinted and adapted from Refs. [92] with permission from Elsevier B·V Copyright © (2016); (c) Sn nanodots finely encapsulated in porous N-doped carbon (NDs@PNC fiber) (current density: 2000 mA g^{-1}; electrolyte: 1 M $NaClO_4$ –PC (+5% vol FEC)). Reprinted and adapted from Ref. [93] with permission WILEY-VCH Verlag GmbH & Co Copyright © (2015); (d) phosphorous-graphene composite (P content of 52.2%), (current density: 250 mA g^{-1}; electrolyte: 1 M $NaClO_4$ – EC: DEC+5%vol FEC). Reprinted and adapted from Ref. [94] with permission from WILEY-VCH Verlag GmbH & Co Copyright © (2015); (e) Sb/C nanocomposite cycling (current density: 100 mA g^{-1}; electrolyte: 1 M $NaClO_4$ – EC:DEC vs. 1 M $NaClO_4$ – EC:DEC+5%FEC) with associated changes of the SEI film resistances. Reprinted and adapted from Ref. [95] with permission from The Royal Society of Chemistry Copyright © (2012); (f) TiO_2 nanosheets/reduced graphene oxide composite (TiO_2 NSs@rGO) (current density: 20C; electrolyte: 1 M $NaClO_4$ – PC:FEC (95:5, v/v)). Reprinted and adapted from Ref. [96] with permission from IOP Publishing Ltd Copyright © (2018); (g) Microspheric $Na_2Ti_3O_7$ (current densities: 354 mA g^{-1}, 885 mA g^{-1}, 1770 mA g^{-1}, 3540 mA g^{-1}; electrolyte: 1 M $NaClO_4$ –PC). Reprinted and adapted from Ref. [97] with permission from The Royal Society of Chemistry Copyright © (2013); (h) MoS_2/reduced graphene oxide (RGO) nano-composite (current density: 20 mA g^{-1}; electrolyte: 1 M $NaClO_4$ – EC:PC (1:1, v/v)). Inset reporting associated SEM images of the nanocomposite electrode. Reprinted and adapted from Ref. [98] with permission from WILEY-VCH Verlag GmbH & Co Copyright © (2015); (i) Sb_2O_3/reduced graphene oxide (RGO) composites with different carbon ratio (current density: 100 mA g^{-1}; electrolyte: 1 M $NaClO_4$ – EC:PC (1:1, w/w) +5 wt% FEC)). Reprinted and adapted from Refs. [99] with permission from Elsevier Ltd and Techna Group S. r.l. Copyright © (2016). Capacity values of composites (c,d,e,f,h,i) are given as reported, that is normalized over the total mass of composites except for P/C (d) and Sb/C (e) for which it is normalized to the metal mass.

Coulombic efficiency and identify SAXS as a tool capable of characterizing this essential feature. Another interesting approach is that of Li et al. [109], which demonstrates that S and P dopants can be used to fine-tune the structure and microstructure of the final carbon by modifying the carbonization process, although only trace amount of dopants are present in the final carbon. The wide range of precursors offered by vegetal biomass also represent a tremendous reservoir for unexpected discoveries [87,108]. As it will be discussed in section 2.3 of the present review, the amount of charge lost for the SEI formation is strongly affected by the chemistry and quality of the electrolyte [112], whose optimization could allow mitigating the poor Coulombic efficiency of otherwise highly performing carbons. The Na^+-solvent co-intercalation phenomena discovered in graphite with ether-based (glyme) electrolytes is also worth mentioning [92,125–127]. Although ca. 100 mAh.g^{-1} at about 1 V reached in co-intercalated graphite is too far to consider competition with HC (Figs. 4b and 5b), this is an interesting unexpected option to manipulate the mechanism of charge storage in carbonaceous materials [112].

Beyond improvements of the performance metrics, a great challenge for HC is represented by the safety concerns: most of its capacity is delivered in the low voltage plateau below 100 mV [87], i.e. slightly above Na metal plating. At elevated charge rates and/or low temperatures, this could lead to undesired dendrite formation and thermal runaway. In addition to the above-mentioned considerations, it is important to properly select the precursors for HC and follow the low-cost and sustainable philosophy of NIBs. The cost and abundancy of the precursor, the renewable nature of its production, the yield of its carbonization or the toxicity of the released gases are all critical parameters to be taken into account for a rational choice of the precursor [7,128].

2.2.2. *Alloy-forming materials*

Alloy-forming materials have been proposed to deliver a substantially improved capacity as negative electrodes compared to HCs while still operating at low potentials [129]. The possibility of delivering a large number of Na per each atom of the host negative electrode material has always been attractive and was the primary driving force for the development of the alloy-forming materials. In comparison with HCs, the substantially higher capacity of these materials leads to stability issues originating from the large volumetric changes associated with sodiation/de-sodiation. Those issues are often addressed by nanostructuring, core/shell structures and preparation of composite materials designed to mitigate pulverization of the active materials during cycling [130,131]. Despite their promising properties the main question still remains: could these materials be efficiently stabilized to provide long-term cycling stability without compromising energy density? The addition of the stabilizing components (often carbon) not only adds another processing step, but also affects practical capacity as well as energy density due to decrease of the electrode density and addition of "dead weight".

The alloy-forming materials are generally represented by individual elements and could be divided into two primary groups according to their position in the periodic table – representatives of group 14 and group 15. In addition, a number of examples of binary and tertiary alloys have also been reported [132–134]. The majority of the materials studied for this purpose are represented by rather benign and abundant elements, while potentially promising lead and arsenic were eliminated due to their toxicity [135,136].

Group 14. The group 14 is represented by 3 main contributors to the field – silicon (Si), germanium (Ge) and tin (Sn). Despite its attractiveness in LIBs, Si was not that successful in NIBs. The reported phase diagram of the Na/Si system illustrated the potential of forming a binary alloy with 1 Na atom per 1 atom of Si [137]. Due to poor Na diffusion kinetics, bulk Si is not attractive, whereas the potential of Si nanoparticles was demonstrated providing capacity retention of 248 mA g^{-1} after 100 cycles when cycled at 20 mA g^{-1} between 0.01 and 2.8 V [138,139]. Germanium, being substantially less abundant and therefore less attractive, has shown similar chemistry to silicon with possibility to alloy with 1 atom of Na per 1 atom of Ge [140,141].

Tin has been viewed as the most promising negative electrode material among the group 14 elements, due to its high theoretical capacity of 847 mAh.g^{-1} achieved by the formation of $Na_{15}Sn_4$ (Figs. 4c and 5c) [93,142]. Another benefit of tin is its high abundancy, non-toxicity and low cost. The alloying of Sn and Na is multi-step process progressing from Sn to $NaSn_5$ – NaSn – Na_9Sn_4 – $Na_{15}Sn_4$ [143]. Such high capacity of Sn ultimately results in high volumetric changes during its electrochemical operation as a negative electrode. The 420% volume expansion during sodiation and subsequent contraction during de-sodiation are the main obstacles for the use of Sn [144]. Such behaviour demonstrates a number of similarities between Sn in NIBs and Si in LIBs and therefore the majority of strategies for mitigation of Sn volume expansion upon cycling were adopted from Si-based negative electrodes. Such strategies allowed to demonstrate capacity retention of 483 mAh.g^{-1} over 1300 cycles when cycled at 2000 mA g^{-1} for ultra-small Sn nanodots (1–2 nm) embedded in N-doped carbon nanofibers as illustrated in Figs. 4c and 5c [93,95]. The most promising pathways are represented by nanosizing [145], electrolyte engineering [146], incorporation into various carbon-containing structures [147], doping and alloying with other elements such as Si, Sb and others [131].

Group 15. The elements from the group 15 (phosphorus, antimony, bismuth and even toxic arsenic) were found to be attractive candidates for the negative electrode materials in NIBs (Fig. 4e) [148]. Among them phosphorous represents an attractive candidate due to its low atomic weight and its ability to form Na_3P at low potential, with a theoretical

capacity of 2596 mAh.g^{-1} – the highest capacity among all potential negative electrode materials for NIBs [149]. Phosphorus exists in three main allotropes; however, white phosphorus is extremely flammable and therefore cannot be considered practical for batteries [150]. Red phosphorus is amorphous, while black phosphorus is crystalline, and both allotropes have been extensively studied. The majority of the published works report on the use of phosphorus/carbon composites because of the enormous volumetric changes (490%) [151], and because of the intrinsically poor electronic conductivity of P (1×10^{-14} S cm^{-1}). One of the best performances achieved for such a system was accomplished using phosphorus-graphene composites (Figs. 4d and 5d) [94,152]. Hierarchical micro/nanostructuration might lead to further improvements, as has been recently shown for P-based composites for LIBs [153]. Among the other elements of group 15, several studies have been reported on the use of antimony based negative electrodes [132,154,155]. In its carbon nanocomposite form, Sb/C can reversibly alloy up to 3 Na and deliver a specific capacity approaching 610 mAh.g^{-1} based on Sb mass, with satisfactory rate capability and a long-term cycling stability with 94% capacity retention over 100 cycles (Figs. 4e) and 5(e)) [95], however concerns about its toxicity, cost and sustainability hinder its applicability.

2.2.3. Oxides and chalcogenides

Metal oxides and chalcogenides have been widely explored for LIBs. Despite the chemical similarities between the two classes, different mechanisms describe their operation: intercalation, conversion and alloying/conversion materials [85,86,88–90]. The work conducted with oxides and chalcogenides is divided herein into two subsections: titanium-based oxide materials and conversion materials.

The first group is primarily represented by titanium oxide itself and its derivatives which operate through an insertion mechanism. Such titanium-based oxides, despite their relatively high operating voltage *vs* Na^+/Na and rather poor initial Coulombic efficiency (Figs. 4f and 5f) [96], have been considered as promising materials due to their low cost, low toxicity and availability. All the mechanisms involved upon electrochemical cycling of these compounds are similar and based on the $Ti^{4+/3+}$ redox couple [156,157]. Unlike the alloy-forming materials, oxides are generally characterized by less impressive capacity (comparable with that of HC though), which however represents an opportunity for longer cycle life due to minimized volumetric changes upon cycling. Several polymorphs have been identified and reported with the most promising one being anatase due to the lowest activation barrier for sodium insertion [158]. However, in general, titanium oxides suffer from relatively low conductivity and therefore various doping strategies have been deployed to improve the electronic conductivity of these material [159–161]. The sluggish sodium kinetics in titanium dioxide drives the development of nanostructures, chemical modifications and preparation of composites to enable fast charging in these materials. Such approach resulted in preparation of TiO_2 nanosheets/graphene oxide composites which are capable of delivering capacity of 175 mAh.g^{-1} even after 200 cycles when cycled at 1C (Fig. 5f) or the reversible capacity of 90 mAh.g^{-1} when cycled for 10 000 cycles at 20C [96].

Based on analogy with Li-ion batteries, Na titanates have also been developed for NIBs [97,162]. Among them, the most promising representative is $Na_2Ti_3O_7$ exhibiting the lowest operating voltage in the titanate family (~0.3 V *vs* Na^+/Na) [163], although with limited capacity, in the range of 200 mAh.g^{-1} (Figs. 4g and 5g) [97].

Conversion materials. Many conversion reactions can be generalized by $M_aX_b + (bc)\cdot Na \rightleftarrows aM + bNa_cX$ with M being a metal (Cu, Fe, Sn, …) and X being an anion (O, S, P, …) [164,165]. The reaction involves the formation of new phases during sodiation that are usually structurally very different from the starting material. In most cases, sodiation leads to the formation of an amorphous matrix of Na_cX in which nanoparticles of M are dispersed. In some cases, such as M = Sn, additional sodium can be stored through alloy formation. The number of possible conversion reactions and materials is quite large and in principle they all provide a very high theoretical capacity which makes them very appealing. Major challenges however relate to voltage hysteresis, unstable interfaces and poor first cycle Coulombic efficiencies as could be seen in Fig. 4h and 4i. The insulating properties of the Na_cX matrix and the volume changes upon cycling require the addition of larger amounts of carbon as well. Careful optimization of the electrode composition and the electrolyte are therefore necessary to enhance the electrochemical properties.

Transition metal oxides have been considered as potential negative electrode material due to their intrinsic stability and relative abundancy [166]. While iron, tin, cobalt and copper oxides represent the largest studied area, others such as antimony (Figs. 4i and 5i), nickel and molybdenum oxides have been also studied [99]. Transition metal sulfides are a promising alternative to the oxides due to better reversibility of the sodiation-de-sodiation process resulting in higher Coulombic efficiency and better stability [167]. Therefore, many transition metal sulfides have been studied in view of their performance as negative electrodes in NIBs [98]. Among them, two of the most popular candidates could be highlighted: iron-based sulfides and tin-based sulfides [142,166]. Although iron chalcogenides (such as FeS_2) show better rate performance and cycling stability than iron oxides, the high operating voltage (above 0.6 V *vs* Na^+/Na) of iron chalcogenides hinders their applications. Sulfides of tin (II) and tin (IV) rely on the conversion reaction followed by the alloying with tin and therefore, these materials are capable of delivering the sodiation capacities around 600 mAh.g^{-1} [168], however, similarly to iron oxides, their operating voltage is still quite high. The tremendous interest to the 2D materials gave rise to the whole subfamily of the layered chalcogenides as potential negative electrode materials not only for LIBs, but for NIBs as well. Among those, MoS_2 with S–Mo–S motifs stacked together by van der Waals forces is the most common representative, however, a variety of similar chalcogenides have been reported in the literature and covered in several reviews [169,170]. As a typical conversion-type material, MoS_2 allows to achieve a theoretical capacity of ~670 mAh.g^{-1} for complete sodiation [169]. However, its layered structure provides a variety of opportunities for material engineering aimed to mitigate the problems of volumetric changes, low electrical conductivity and improve ion diffusion. Those typically include preparation of different heterostructures and composites combining layers of MoS_2 with different carbon-containing species [171–174]. Despite a respectable electrochemical performance (Figs. 4h and 5h), the complexity of these materials in terms of their mass production in a controlled fashion raises a question of their applicability in the real batteries in the nearest future.

In addition to oxides and chalcogenides, metal phosphides represent one of the promising candidates in the present group [175]. They combine the conversion reaction resulting in the formation of phosphorus within the network of metal atoms which provide electronic conductivity. The formed phosphorus undergoes the alloying reaction described above delivering high capacity. Importantly, the pulverization problems associated with the use of phosphorus is partially mitigated in these compounds [176].

2.3. Liquid electrolytes and Solid Electrolyte Interphase (SEI)

Despite a number of studies which were devoted to the identification of the optimal electrolyte for NIBs, a standard well performing electrolyte has not been identified yet, as the performance of all the electrolyte formulations strongly depends on the specific chemistry of the electrode used in the tested cell. This highlights the crucial role of the electrode/electrolyte interfaces and the dependency of the overall behaviour on the specific surface reactivity of the employed electrode materials [177].

At the negative electrode side the understanding of the Solid Electrolyte Interphase (SEI) in NIBs may represent a key turning point for the development of the technology. It is well known that the formation of a stable SEI in NIBs is generally hindered by the higher solubility of the sodium salts and sodium-based SEI components when compared to the lithium parental compounds [146,178–181].

Most of the reported investigations of liquid electrolytes for NIBs have been focused on the use of sodium salts containing perchlorate (ClO_4^-), hexafluorophosphate (PF_6^-), trifluoromethanesulfonate ($CF_3SO_3^-$, OTf^-), bis(fluorosulfonyl)imide ($[N(SO_2F)_2]^-$, FSI^-), and bis (trifluoromethanesulfonyl)imide ($[N(CF_3SO_2)_2]^-$, $TFSI^-$) anions, combined with organic solvent mixtures of linear or cyclic carbonates and ethers [177,179]. Besides the conventional systems, ionic liquids (ILs) and aqueous-based systems have also been proposed. Table 1 collects the ionic conductivity values at room temperature for selected electrolyte systems described in literature [177,179].

While $NaClO_4$ was commonly used as a salt at the early stages of research for Na-based systems, the use of this salt is currently not recommended due to its potentially explosive character. Thus, $NaPF_6$ is the most widely employed salt in carbonate-based electrolytes. It is important to point out that the purity of $NaPF_6$ strongly affects the electrochemical performance of the investigated systems. Indeed, battery grade $NaPF_6$, when dissolved in carbonates, generally leads to colourless and transparent electrolyte solutions, with improved electrochemical response compared to chemistry grade [182], especially in terms of capacity retention and Coulombic efficiency. Alternatively, parasitic reactions are often observed when using non-battery grade $NaPF_6$ most likely attributable to impurities and secondary salt decomposition reactions [182].

Solvent systems utilizing propylene carbonate (PC) based electrolytes or mixtures of ethylene carbonate (EC) and dimethyl carbonate (DMC) are the most commonly used for electrolyte preparation [64,179]. However, more recently, it has been reported that linear carbonates might have a detrimental effect on cell performance (unstable SEI formation) [183], especially at high temperatures. That is attributed to the formation of parasitic reduction products at the negative electrode diffusing back into the electrolyte solution and depositing at the positive electrode side. This effect further highlights the difference between sodium and lithium systems, where linear carbonates are commonly employed without any limitations.

Additives represent another crucial component of electrolyte formulation, able to form compact, uniform and stable SEIs, thus substantially contributing to the cell's cycle life, rate capability and durability. For instance, Komaba et al. [184] reported the effect of fluoroethylene carbonate (FEC), *trans*-difluoroetyhene carbonate (DFEC), and vinylene carbonate (VC) on the electrochemical properties of Na/HC cells. It was found that by adding 2% in volume of FEC into the electrolyte the electrochemical response was greatly improved, while DFEC and VC had a negligible influence. The study was conducted employing a $NaClO_4$-based electrolyte. However, Delmas et al. [185] reported on the beneficial effect of both VC and FEC on the cycling stability of layered positive electrode materials when using a $NaPF_6$ containing electrolyte. Darwiche et al. [186] investigated the effect of FEC in sodium cells using a Sb-based negative electrode material. Outstanding performance in terms of capacity retention (100%) was reported for the electrolyte with added FEC, while only 2% of the initial capacity was retained in the FEC-free electrolyte after 100 cycles. It is important to point out that the studies were performed in half-cell configuration, employing a Na metal counter electrode, which has been shown to have a great impact on the observed performance [183,187–189]. Recent studies in NVPF/HC Na-ion full cells with $NaPF_6$ EC-PC electrolytes showed that optimum cell performance could be reached by using mixture of additives (including sodium difluoro (oxalato)borate (NaODFB), succinonitrile (SN), 1,3-propane sultone (PS) and VC) which work in synergy with each other [190].

Interestingly, ether-based electrolytes have shown excellent performances. They not only have been successfully employed to enable co-intercalation of solvated Na^+ ions into graphite [125,191], but they also present an ability to form a very stable SEI and enhance the Na stripping/plating efficiency. While for LIBs glyme-based electrolytes have been outperformed by ester-based ones, whether glymes will be a valid alternative electrolyte system for NIBs is still an open question. Will their limited anodic stability enable their use in the next generation high voltage NIB cells? More studies on their compatibility with positive electrode materials is required and an analysis on the impact of their toxicity should be taken into account. However, at the negative electrode side interesting and promising results have been reported. Cui et al. [192] demonstrated that a highly reversible plating/stripping process (dendritic-free) was achieved at room temperature by using $NaPF_6$-glyme systems. Such effect is most likely attributable to a uniform inorganic-rich SEI layer formation, impermeable to electrolyte solvent. The improved sodium storage behaviour with ether-based electrolytes has been reported for several materials including CuS nanosheets [193], bismuth [194], Sn [195,196], high specific surface area carbon [112] and TiO_2 [197]. In all cases and independently of the electrode chemistry, the enhanced performance was attributed to the formation of a thin, compact and uniform SEI enabling fast Na^+ ion transport. However, issues related to the use of glymes were also reported for HC [198] and Sb [199].

Besides optimal ionic conductivity, viscosity and satisfactory electrochemical performance, ester- and ether-based electrolytes suffer from high flammability and low anodic stability respectively. In search of safer high voltage electrolytes, ionic liquids (IL)-based electrolytes have been widely investigated as a promising alternative [200]. The research on ILs finds its primary motivation within the green chemistry approach. Indeed, the general use of non-volatile solvents such as ILs is a well-perceived strategy toward the reduction of waste, toxicity, and hazards at the industrial scale [201].

ILs generally present lower conductivity and higher viscosity than carbonate-based electrolytes, however they are generally successfully

Table 1
Ionic conductivity values reported in literature for different classes of Na-based electrolytes.

Electrolyte	Conductivity/ mS.cm^{-1}	Reference
1.0 M NPF_6 PC	7.98 at 20 °C	[223]
1.0 M $NaClO_4$ PC	6.4 at 20 °C	[223]
1.0 M NaTFSI PC	6.2 at 20 °C	[223]
1.0 M $NaClO_4$ EC:PC (50:50 wt%)	8.0 at 20 °C	[223]
1.0 M $NaClO_4$ EC:DMC (50:50 wt%)	10.2 at 20 °C	[223]
1.0 M $NaClO_4$ EC:DEC (50:50 wt%)	6.3 at 20 °C	[223]
1.0 M $NaClO_4$ TRIGLYME	3.8 at 20 °C	[223]
1.0 M $NaClO_4$ EC:TRIGLYME (50:50 wt%)	7.0 at 20 °C	[223]
1.0 M $NaClO_4$ EC:DME (50:50 wt%)	12.5 at 20 °C	[223]
0.8 M NaOTf EC:DMC (30:70 wt %)	3.7 at 40 °C	[224]
0.6 M $NaPF_6$ EC:DMC (30:70 wt %)	6.6 at 40 °C	[224]
1.0 M $NaClO_4$ EC:DMC (30:70 wt %)	5.0 at 40 °C	[224]
$F_{13}F$ NaFSI-PYR_{13}FSI (1:9 Molar ratio)	5.0 at 20 °C	[204]
$F_{14}F$ NaFSI-PYR_{14}FSI (1:9 Molar ratio)	3.0 at 20 °C	[204]
$F_{14}FT$ NaFSI-PYR_{14}FSI-PYR_{14}TFSI (1:4:5 Molar ratio)	2.0 at 20 °C	[204]
$F_{14}T$ NaFSI-PYR_{14}TFSI (1:9 Molar ratio)	1.0 at 20°	[204]
1.0 M $NaBF_4$ BMP-TFSI (Butylmethylpyrrolidinium-TFSI)	1.9 at 25°C	[225]
1.0 M $NaClO_4$ BMP-TFSI (Butylmethylpyrrolidinium-TFSI)	1.0 at 25°C	[225]
1.0 M NaTFSI BMP-TFSI (Butylmethylpyrrolidinium-TFSI)	0.5 at 25°C	[225]
1.0 M $NaPF_6$ BMP-TFSI (Butylmethylpyrrolidinium-TFSI)	0.4 at 25°C	[225]
1.0 M $NaPF_6$ in FEC/PC/1,1,2,2-tetrafluoroethyl 2,2,3,3-tetrafluoropropyl ether (HFE) + perfluoro-2-methyl-3-pentanone (PFMP)	5.8 at RT	[212]
1.0 M NaFSA/TMP (trimethyl phosphate)	7.9 at 30 °C	[213]
3.3 M NaFSA/TMP (trimethyl phosphate)	2.2 at 30 °C	[213]
2 M NaTFSI/TMP + FEC	6.0 at RT	[214]
0.05 M Na_2SO_4 H_2O	10 at 25°C	[226]
0.5 M Na_2SO_4 H_2O	65 at 25°C	[226]
2.0 M Na_2SO_4 H_2O	125 at 25°C	[226]
1.0 M $NaNO_3$ H_2O	80 at 25°C	[226]
5.0 M $NaNO_3$ H_2O	195 at 25°C	[226]
7.0 m NaOTF H_2O + 8.0 m NaOTf PC (1:1 wt%)	25 at 20 °C	[227]
15 m NaFSI H_2O	90 at 20 °C	[228]

employed when coupled with positive electrode materials. For instance, the electrochemical activity of the $Ni^{2+/3+}$redox couple of a $Na_4Ni_3(PO_4)_2(P_2O_7)$ positive electrode was firstly experimentally reported by using a NaTFSI:Py_{13}FSI (1:9 mol ratio) electrolyte [202]. Improved electrochemical behaviour of both layered oxides and polyanionic materials has been demonstrated, associated to the ability of ILs to hinder manganese dissolution and improve the properties of the positive electrode/electrolyte interface [203–206].

Nitta et al. [207] reported the electrochemical performance of a HC negative electrode in Na [FSA]-[C_3C_1pyrr][FSA] (FSA = bis(fluorosulfonyl)amide, C_3C_1pyrr = N-methyl-N-propylpyrrolidinium) IL over a wide temperature range of −10 °C to 90 °C. A stable cyclability was observed for the HC electrode at 90 °C, with a capacity retention ratio of 84% after 500 cycles. A full-cell voltage of 2.8 V with Coulombic efficiency higher than 99% was achieved by using $NaCrO_2$ as the positive electrode at 90 °C. Promising results have also been achieved by using alloying based negative electrode (Sb–C), as reported with a room temperature ionic IL-based NIB [208]. Moreover, it has been reported that IL-based electrolytes have a beneficial effect on the SEI stability when coupled with a TiO_2 based negative electrode attributed to an overall decrease of the cell resistance [209] as demonstrated by the excellent cycling stability and Coulombic efficiency. However, it is worth noting that the high cost of ILs-based electrolyte (mostly associated to their purification) still represents a serious obstacle for their successful implementation as electrolytes or additives [210].

In search of non-flammable electrolytes, substitution of H atoms in carbonate or ether solvents with F can dramatically increase their flash points. In 2001 Wang et al. reported on the fundamental properties of trimethyl phosphate (TMP) solvent-containing electrolytes for use in LIBs [211]. It is proposed that a F to H ratio exceeding 4 leads to the obtainment of totally non-flammable electrolytes. The property arises from the ability of fluorine to capture oxygen and hydrogen radicals when catching fire. Recently, organic phosphate-based electrolytes have attracted attention also for Na-metal [212], Na-ion [213] and Na/S [214] systems due to their intrinsic non-flammability, low viscosity and satisfactory ionic conductivity, wide thermal stability, and ability to dissolve high concentrations of sodium salts.

X. Zhen et al. [212] demonstrated that by successfully introducing a temperature-sensitive perfluoro-2-methyl-3-pentanone (PFMP) extinguishant into fluoroethylene carbonate (FEC)/propylene carbonate (PC)-based electrolytes via the bridging of non-polar highly fluorinated ethers, a complete non-flammability and an in situ heat-dissipating effect can be achieved. In addition, the NaF-based interphase formed on the Na metal surface and enabling a high plating/stripping stability and a dendrite-free morphology, allows the obtainment of a cell using Na metal at the negative electrode and high-voltage NVPF at the positive electrode and retaining over 87.1% of the original capacity after 1000 galvanostatic cycles. Indeed, one of the most interesting properties of this class of electrolytes is their ability to form highly fluorinated and thin passivating electrode/electrolyte interphases enabling suppression of deleterious side reactions at the interfaces. Thanks to the unique NaFSA-derived inorganic passivation film formed in the concentrated NaFSA/TMP electrolyte developed by Y. Wang et al. a HC/Na metal cell was cycled for over 1200 cycles at C/5, corresponding to a running time of over 15 months [213].

Another appealing class of electrolytes for NIBs is represented by aqueous systems [215,216]. Indeed, aqueous NIBs are, in principle, very attractive for large scale energy storage applications because of their inherent safety, environmental friendliness, and potential low cost. However, as for Li-based systems, the electrochemical reaction of Na^+ extraction/insertion in aqueous electrolytes is limited by the structural instability of the electrode materials in water, leading to a limited selection of electroactive materials, and by the side reactions occurring with H_2O or residual O_2, affecting their cycling stability [216–218]. In addition, it should be remembered that the working potential of electrode materials in aqueous electrolytes should be within the electrochemical stability window of water, beyond which the electrolysis of H_2O occurs. Y.-M. Chiang et al. [219] demonstrated the feasibility of an aqueous $NaTi_2(PO_4)_3/Na_{0.44}MnO_2$ cells with ultrafast rate capability (up to 70C) and superior high-rate cycling stability (for more than 1500 cycles). The system demonstrated a limited capacity of about 30 $mAh.g^{-1}$ based on the negative electrode mass which, however, does not represent a key performance metric for aqueous batteries. It is worth mentioning that at current rates lower than 1C the full cells experience severe capacity fading upon cycling which is most likely associated to the dissolution of the electrode materials.

Another interesting concept recently proposed are “water-in-salt” (WiS) electrolytes, constituted by concentrated aqueous solutions of salts in which the average number of water molecules available to solvate each ion is far below the “solvation numbers” that are well established for conventional electrolyte [216,220]. These systems present unique properties conferred by the formation of contact ion pairs (CIPs) and aggregated cation-anion pairs (ACAPs) leading to a reduced availability of solvent molecules and thus presenting high ionic conductivity and wider electrochemical stability window [221].

Recently a symmetric aqueous Na-ion cell employing NASICON electrodes and a sulfonate-containing WiS electrolyte exhibited extremely stable cycling performance over 1000 cycles at 20C without any capacity fading. It was suggested that the fluorine-rich interphases [222] formed in concentrated aqueous electrolytes facilitate the charge transfer and suppress electrode dissolution, as evidenced by the higher rate-performance and lower polarization offered by cells using fluorine-based electrolyte when compared to systems using $NaClO_4$ [222].

Promising results have been obtained in the recent years towards optimization and formulation of advanced electrolyte systems and stable electrode/electrolyte interfaces and well summarized in a recently published comprehensive overview [177]. A crucial aspect to consider for future development is to perform the investigation of developed electrolytes in full cell configuration, not only to avoid the detrimental effect of the Na metal negative electrode, but also to avoid electrolyte optimizations which are then not compatible with positive electrodes and *vice versa*. A systematic and rational design of electrolytes will be decisive for the future commercialization of NIBs, since stabilization of the interfaces governs the operation of these inherently complicated systems.

3. All solid-state sodium batteries

Safety issues related to flammable liquid electrolytes in standard NIBs remain, as for LIBs, a serious concern. In this regard, all solid-state batteries (ASSBs), which would use non-flammable sodium-conducting solid electrolytes, are considered as potential candidates for alternative energy storage devices, as reviewed in several recent papers [229–233]. As gathered in Ref. [233], a variety of Na-ASSBs have been designed and tested, including mainly Na, Na/Sn or $Na_2Ti_3O_7$ as negative electrodes and Na_x (Ni,Mn)O_2, $NaMnPO_4$ or $Na_3V_2(PO_4)_3$ as positive electrodes. Solid electrolytes may be of polymeric nature (PEO-, PAN- or PVA-based) or inorganic ion conductors (mainly oxides and sulfides). The first can be implemented in various geometries with high flexibility, enhanced mechanical stability, easier processability (especially when compared to sulfidic compounds) and improved interface compatibility (increased contact area due to higher flexibility). Some of the most recent advances for this class of electrolytes are described in detail in other comprehensive review papers [234,235] However, despite the significant progress which has been achieved since the first Na cell containing a polymer electrolyte was reported by West et al., in 1985. [236], polymers still suffer from poor electrochemical stability and conductivities at room temperature. Since Na-ASSBs are still at their infancy and far from demonstrated practical application, herein we'll focus our contribution on key materials and recent advances in inorganic Na^+ conductors research.

The seminal development of β-β"-Al_2O_3 (Na_2O–$11Al_2O_3$ and Na_2O–$5Al_2O_3$ respectively [237]) led to the industrial fabrication and operation of Na/S batteries (Ford motors and NGK-Japan) [238] that use molten Na at the negative electrode at elevated temperature [239], which may bring to safety concerns. Similar to lithium Li-ASSBs, the development of their sodium counterparts still requires great efforts on (i) mastering multiscale ion transport and the related interfaces, (ii) improving chemical and electrochemical stabilities of the solid electrolyte *vs* negative or positive electrodes and (iii) optimizing mechanical properties and advanced processing routes [240]. In such context, a myriad of interesting Na-containing inorganic ion conductors have already been identified, as recently reviewed by Ohno et el (Fig. 6a). [230].

In the middle of the 70's, NASICON – type sodium conductors $Na_xM_2(XO_4)_3$ of general formula $Na_{1+y}Zr_2Si_yP_{3-y}O_{12}$ ($0 \leq y \leq 3$) were proposed as solid electrolytes for Na batteries [241,242]. The content in Na^+ can be tuned by the substitution of Si^{IV} by P^V in the (XO_4) tetrahedra and by the substitution of Zr by a multitude of other elements on the (MO_6) octahedra. Hundreds of subsequent studies allowed to draw precise relationships between composition, structure (ordered monoclinic *vs* disordered rhombohedral) and mechanism (3-D correlated motion) for Na^+ transport, and to identify the best compromise for the content in Na (y close to 2–2.3) [243–245]. Recently, further improvements were achieved by adding NaF at the synthesis stage of NASICON materials, which resulted in composite electrolytes with modified grain boundaries that allow very fast ion transport overall: 4.10^{-3} S cm^{-1} at 25 °C for $Na_{3.2}Zr_2Si_{2.2}P_{0.8}O_{12}$-0.5NaF [246]. Interestingly, all-NASICON solid state batteries operating at temperatures up to 200 °C, have been built with $Na_3Zr_2(SiO_4)_2(PO_4)$ as electrolyte and $Na_3V_2(PO_4)_3$ at both negative and positive electrodes [247,248].

Sodium tetrathiophosphates derived from Na_3PS_4 [249] gained a lot of attention since the report of a record conductivity of 2.10^{-4} S cm^{-1} at RT for glass-ceramic cubic-Na_3PS_4 by Hayashi et al. [250]. Later a tetragonal form of Na_3PS_4 was obtained by rapid quenching from 700 °C [259] and, more recently, the orthorhombic (*Fddd*) high-temperature form γ-Na_3PS_4 was discovered [260]. The latter demonstrated a very

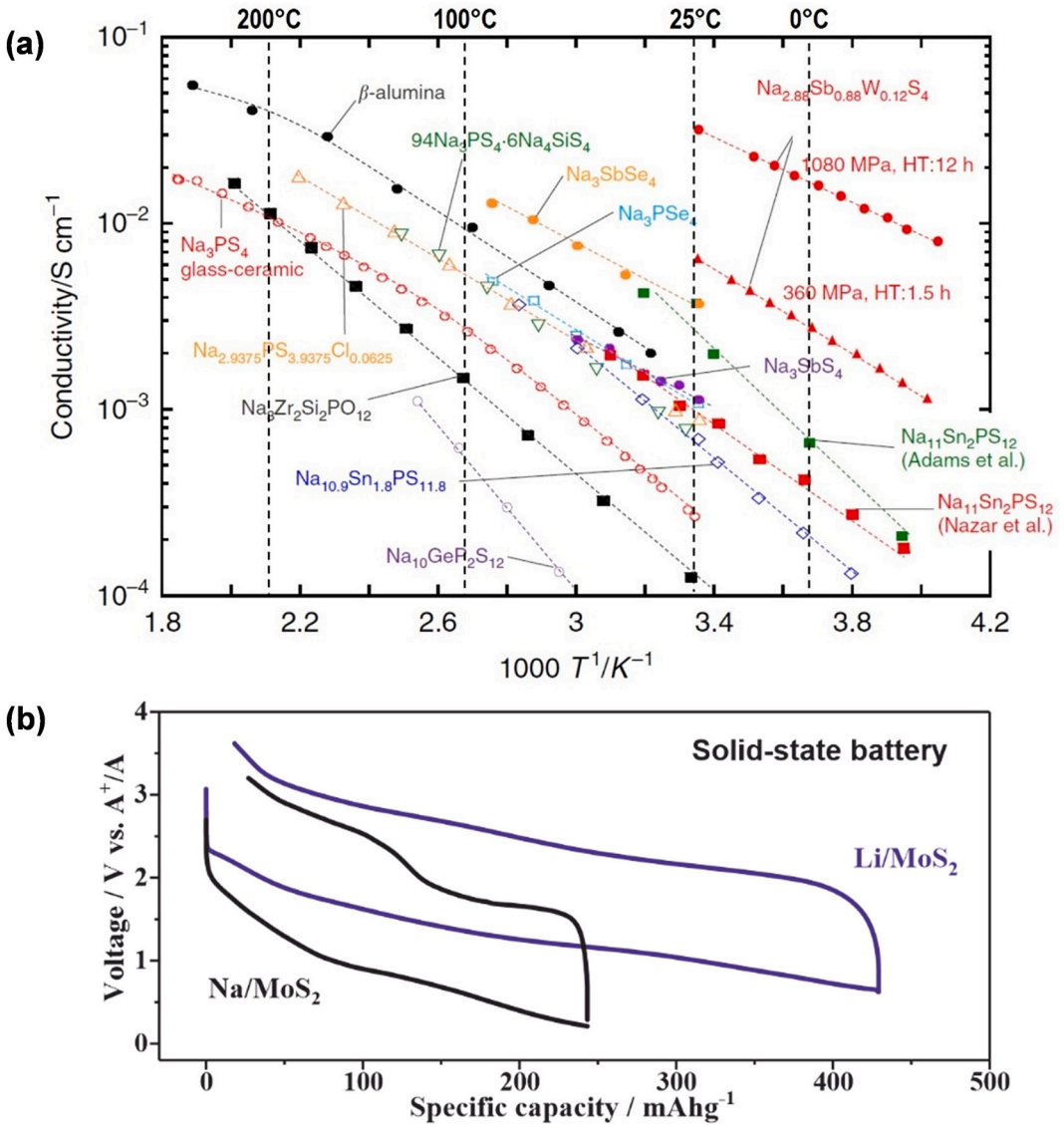

Fig. 6. Conductivity *vs* inverse of temperature for the most important classes of Na inorganic ionic conductors mentioned in this overview. Beta-alumina [237–239], Nasicon $Na_3Zr_2Si_2PO_{12}$ [241–245], Na_3PS_4 [249,250], Na_3SbS_4 [251,252], $Na_{10}SnP_2S_{12}$ and $Na_{11}Sn_2PS_{12}$ [253–256]. Reprinted and adapted from Ref. [257] under a Creative Commons Attribution 4.0 International License. (b) Comparison of voltage profiles for MoS_2 as electrode in sodium and lithium solid-state batteries with Na_3PS_4 and Li_3PS_4 as solid electrolytes and Sn–Na and as negative electrodes respectively (room temperature). Reprinted and adapted from Ref. [258] with permission from American Chemical Society Copyright © (2020).

fast Na^+-conduction (4.10^{-1} S cm^{-1} at 500 °C, $E_a = 0.1$ eV), associated with rotational motion of the thiophosphate polyanions, as in a plastic crystal. Attempts of doping or partial substitution of S (by Cl, Br, Se) [261–263] or P (by Si, Sb, Ge, Sn) [251,252] resulted in facilitating the ion transport as well as improving the moisture stability [257], opening the door for solution-based routes for the synthesis [264,265]. Importantly, it was recently argued that the high ionic conductivity of Na_3PS_4 was not related to the average crystal structure (tetragonal *vs* cubic) but rather to differences in defect concentrations induced by harsh ball-milling [266].

Na-containing materials that mimic the seminal Li-containing composition $Li_{10}GeP_2S_{12}$ [267] were recently computationally "designed" by the group of Ceder [253]. $Na_{10}SnP_2S_{12}$, with a RT ionic conductivity of 4.10^{-4} S cm^{-1} rivals the best sodium sulfide solid electrolytes and its stoichiometry can be varied by substituting Sn by Ge or Si. These findings were later on challenged by Nazar and Adams [254–256] who reported on the new sodium superionic conductor, $Na_{11}Sn_2PS_{12}$ ($1{,}4.10^{-3}$ S. cm^{-1} at RT, $E_a = 0.25$ eV). As for γ-Na_3PS_4, the dynamic response of the anion framework with facile $(PS_4)^{3-}$ anion rotation facilitates long-range cation mobility [268]. Depending on the sample preparation conditions (cooling rate), different degrees of disorder in the orientation of the PS_4 groups would alter the energy landscape for Na^+ ions [269,270].

In the same vein, complex Na-containing borohydrides such as $NaBH_4$, $Na_2(BH_4)NH_2$ and $Na_2B_{12}H_{12}$ possess high rotational mobility of their BH_4 groups [271–274] and have been identified as promising solid electrolytes [275] with ionic conductivities close to 10^{-2} S cm^{-1} at 450 K. The strategy to their optimization has been focused on decreasing their synthesis temperature to stabilize the fast-conducting phase by substitution (with carbon as in $NaCB_{11}H_{12}$ [276]) or through anion mixing between deca- and dodeca-boranes as in Na_2 $[B_{10}H_{10}]_{0.5}$ $[B_{12}H_{12}]_{0.5}$ [277–279]. These materials appear relatively stable against metallic Na, and 3 V batteries using $NaCrO_2$ at the positive electrode were successfully cycled [280,281]. The antiperovskite composition of Na_3OBH_4 has been reported to possess an ionic conductivity of 4.10^{-3} S cm^{-1} at room temperature [282], but to the present moment has not been reproduced [283]].

In conclusion, Na-ASSBs currently are far from being close to any commercialization as they did not demonstrate (yet) added value *vs*. their Li counterparts (see Fig. 6b for an example referring to the sodium storage behaviour of a MoS_2 electrode using a Na_3PS_4 solid state electrolyte and a Na–Sn alloy as negative electrode, compared to its Li counterpart cell using Li_3PS_4 electrolyte and In–Li negative electrode) [258]. However, significant progress is foreseen according to the variety of materials under development, i.e. interesting inorganic solid electrolytes to be combined with various electrode materials on the positive side. Importantly, Na-ASSBs would allow operation at temperatures (100–200 °C) not attainable with liquid electrolytes. As for Li-ASSBs though, huge efforts still need to be put on mastering the negative electrode (Na ? Na–Sn ? ….) interface with the solid electrolyte. More importantly, which processing technology will be implemented for the realization of real, viable, solid state batteries that could sustain high energy or power densities for extended cycle life?

4. Na/O_2 and Na/S batteries

$Na–O_2$ and Na-sulphur batteries are based on fundamentally different cell chemistries than NIBs or Na-ASSBs (which share intercalation positive electrode materials and have taken benefit from previous successful Li-ion development). Therefore, the research in this area is currently on a much more fundamental level. There are two main drivers to work on these cell concepts. Firstly, oxygen and sulphur are abundant elements and, combined with sodium, very cost-effective batteries could be achieved. Secondly, the specific capacities of oxygen and sulphur are very high and could lead to energy densities several times larger as compared to batteries based on insertion/intercalation mechanisms. While approaches using aqueous electrolytes are also being followed, most of the research in this field has been focused on Na/O_2 and Na/S batteries employing an aprotic electrolyte. The ideal reactions and energy densities are shown in Table 2 while the typical voltage profiles are reported in Fig. S1 in the supplementary information. Na metal is the intended negative electrode (although other materials could be used). Compared to the analogue Li-based cells, the cell voltage in case of sodium is lower by 390 mV (Na/S, Na_2S formation) and 630 mV (Na-oxygen, Na_2O_2 formation). The difference is due to a cathodic effect rather than the difference between the alkali metals [6,164]. However, there are notable differences between the lithium and sodium cell chemistries for both battery concepts. A comprehensive comparison is outside the scope of this review but can be found elsewhere [284].

4.1. Na/O_2 batteries

Reports on rechargeable Li/O_2 batteries date back to the 1980–90s [285,286], but greater interest developed in the late 2000s when the first reports on Na/O_2 batteries also appeared [287–289]. In contrast to conventional batteries that are enclosed systems, a metal/air battery exposes the positive electrode (oxygen electrode) to the environment. There is a conceptual similarity with fuel cells, which also use atmospheric oxygen as a reaction partner. During discharge, different sodium oxides (Na_2O, Na_2O_2, NaO_2) may be formed while gaseous oxygen is released during charging. The reaction takes place at a gas diffusion electrode layer which needs to ensure sufficiently fast O_2 transport and accommodate simultaneously the solid discharge products. Gas diffusion layers, often combined with high surface area carbon, are typically applied for this purpose. The concept of using atmospheric oxygen instead of enclosed intercalation materials allows to achieve very high

Table 2
Theoretical cell voltages, gravimetric and volumetric energy (Wh.kg^{-1}, Wh.l^{-1}) and charge (mAh.g^{-1}, mAh.cm^{-3}) densities for sodium/oxygen and sodium/sulphur batteries with metal negative electrode, based on active materials weight and density. Values for the gravimetric energy densities are given without and including the weight of oxygen. All other values given refer to the discharged state. Thermodynamic data derived from HSC Chemistry for all compounds being in their standard states at 25 °C.

Cell reaction	E°/V	w_{th}/Wh.kg^{-1}	Q_{th}/mAh.g^{-1}	w_{th}/Wh.l^{-1}	Q_{th}/mAh.cm^{-3}
$2\,Na + \frac{1}{2}O_2 \underset{Charge}{\overset{Discharge}{\rightleftharpoons}} Na_2O$	1.95	2273/1687	867	3828	1968
$2\,Na + O_2 \underset{Charge}{\overset{Discharge}{\rightleftharpoons}} Na_2O_2$	2.33	2717/1602	689	4493	1936
$Na + O_2 \underset{Charge}{\overset{Discharge}{\rightleftharpoons}} NaO_2$	2.27	2643/1105	488	2431	1074
$2\,Na + \frac{1}{8}S_8 \underset{Charge}{\overset{Discharge}{\rightleftharpoons}} Na_2S$	1.85	1273	687	2364/1580	1245
$2\,Na + \frac{1}{2}S_8 \underset{Charge}{\overset{Discharge}{\rightleftharpoons}} Na_2S_4$ (300 °C)	1.90	583	308	1124/845	653
Na-ion (average positive electrode vs Na^+/Na)	*~3.3*	*~560*	*~170*	*~2500*	*~760*

theoretical energy densities. However, such concept leads to many engineering complications: gas purification is required, solvent evaporation has to be minimized, and the electrode design (porosity) needs to be further optimized. Even assuming a perfectly working cell chemistry, these extra measures are detrimental to the energy density. Therefore, the practical energy densities of metal-air batteries are significantly lower than their theoretical ones [290–292]. After the initial enthusiasm on rechargeable metal-air batteries it became clear that the processes taking place at the oxygen electrode were poorly understood, and the primary electrochemical process in the cell was accompanied by side reactions caused by the decomposition of the electrolyte. Early approaches to decrease the large overpotential of around 1 V by using catalysts were not effective as they also catalysed the electrolyte decomposition. In case of Na/O_2 batteries, a surprising finding revealed that the discharge product are well-crystallized NaO_2 (sodium superoxide) particles in cells where ether electrolyte was used [289]. That product is formed at much lower overpotentials (~200 mV) and caused much less side reactions compared to analogue Li/O_2 cells, for which the main discharge product is Li_2O_2 [293]. This reaction is also very sensitive to water impurities, leading to the formation of $Na_2O_2{\cdot}H_2O$, which emphasizes the need for suitable membranes that allow the transfer between the cell and the environment of O_2 only [294,295]. The long term stability of NaO_2 in the cell also needs to be improved [296]. Although several key aspects of metal/air batteries are still not fully understood, it is now established that discharging and charging of such batteries involves complex dissolution and precipitation processes at the oxygen electrode [297]. Therefore, the electrode reaction can be influenced by numerous factors (current, type of solvent and electrolyte salt, impurities) [298–300]. Currently, the most important challenge to be solved for the oxygen electrode is to tame the role of singlet oxygen ($^1O_2$) that forms at all stages during cycling causing parasitic side reactions with the organic electrolyte and the carbon electrode [301,302]. The combined use of redox mediators that aim at decreasing the charging voltage (reducing overpotentials) and quenchers, which neutralize singlet oxygen seems currently to be the most effective strategy to run the cell in a more controlled manner [303]. On the negative electrode side, and common to Na/S batteries, sodium would be the preferred option in consideration of maximizing the cell energy density. Not surprisingly, the same challenges exist as for using lithium in LIBs which, despite many efforts, could still not be realized. The most important challenges relate to unfavorable SEI formation combined with dendrite formation requiring oversizing the electrode and leading to safety concerns. Numerous strategies are therefore being evaluated in order to make metal electrode a viable option [304]. As an example for sodium, fluorine-free electrolyte solutions have been recently suggested [305]. The practical use of sodium as negative electrode might be however limited due to its low melting point (98 °C).

4.2. Na/S batteries

The interest in Na/S batteries dates back to the late 1960s when the high temperature Na/S battery was patented by the Ford Motor Corp [238,306]. This development was enabled by the availability of the highly conductive ceramic electrolyte β-alumina. In such battery, at the typical operating temperature of around 300 °C, sodium and sulphur are molten and separated by the solid electrolyte. Although this technology has been developed over the years to yield a commercial product (NGK Insulators) for stationary storage, its market competitiveness is yet to be demonstrated. The high operating temperature leads to technological challenges and limits the discharge capacity (Table 1), which is why Na/S batteries operating at room temperature or intermediate temperatures are being reconsidered [239,307–309]. Further research in this field has been motivated by the potentially promising performance: the formal reduction of sulphur to form Na_2S corresponds to a capacity of 687 $mAh.g^{-1}$ (or 1672 $mAh.g^{-1}$ without accounting for the mass of sodium). Another motivation for Na/S batteries has been provided by the vibrant research on Li/S batteries which has experienced a significant progress over the last 10–15 years [310–313]. Li/S cells are also known for their chemical complexity because the reduction of sulphur during discharge leads to the formation of soluble polysulfides, which cause a series of detrimental effects such as the shuttle mechanism [314]. Moreover, sulphur and sulphides are insulators, which requires the use of a conductive carbon matrix as shown in Fig. 1d. This is similar to metal-air batteries and the cell reaction at the positive electrode involves dissolution and precipitation processes that complicate the cell chemistry and result in fast ageing. The same phenomena occur in Na/S batteries or any other metal-sulphur battery (with liquid electrolyte) which is why similar countermeasures could be taken in order to improve the rechargeability and utilization of the active material. Important strategies to improve the battery performance include nanostructuring of carbon/sulphur composites [315], implementation of membranes (inorganic, organic or mixed) [316–319] and optimization of the electrolyte composition [320–322]. Moreover, other cell concepts based on dissolved positive electrodes (solutions containing polysulfides) are explored, some of them being designed to operate at intermediate temperatures [323–325]. Very recently, solid-state configurations also became of interest [326–328]. General advantages and disadvantages of the different approaches are summarized in Ref. [308] A notable difference between the Li/S and Na/S chemistry is that many thermodynamically stable binary compounds exist at room temperature in case of sodium (Na_2S, Na_2S_2, Na_2S_4, Na_2S_5) while Li_2S is the only stable phase in case of lithium [329,330]. This leads to even more complexity in case of the Na/S cell which might be an advantage or a disadvantage, depending on what cell concept is applied. Overall, Na/S cells are much less explored compared to Li/S cells, and the cell chemistry of the Na/S system appears to be more complex. Therefore, the performance of Na/S batteries lacks behind the much more studied Li/S battery. However, quite some improvement was demonstrated in the last years and the feasibility to assemble multilayer pouch cells was recently shown [331]. Moreover, the variety of possible cell concepts and the low cost of elements make the Na/S technology a very attractive option for large scale energy storage.

5. From lab to market: evaluation of key performance indicators

While all Na-based systems are still at an early stage of development, NIBs are a step ahead compared to Na-ASSBs, Na/O_2 and Na/S systems, thanks to their similarities to LIBs. NIBs additionally offer a “drop in” approach, as they do not require a different cell design and, therefore, can be manufactured in similar production lines as those used for LIBs. Considering the massive investments required for setting up the manufacturing facilities, this “drop in” approach delivers substantial advantages towards NIBs commercialization provided that competitive metrics in terms of performances are achieved for cells and modules. Still, a recent comparative cost assessment of SIB and LIB technologies evaluated the cost reduction by replacing Na for Li within the range 10–30% at materials level [7,128], which goes down to 4.3% when including manufacturing costs [7]. This moderate figure is due to the fact that manufacturing processes as well as many components and materials involved in cell fabrication are identical or of similar cost for the two technologies. As a consequence, the performance metrics are of prime importance for the SIB technology to ensure a competitive cost per Wh, and finally find a place in the market.

It is, however, challenging to make fair and accurate comparisons of any newly developed cells with respect to commercial Li-ion cells. Specifically, little information is usually provided for Na-ion prototype cells regarding the full range of specifications (e.g. energy density, cycle life, €/kWh per cycle, etc.) under realistic conditions (full cell configuration, small amounts of electrolyte, high mass loadings, low current rates for cycling stability tests, etc.). Moreover, when comparing reports on Li-ion and Na-ion full cells, the comparison of performance metrics is usually performed between commercial-grade cylindrical or pouch-type

Li-ion cells, a mature technology based on 30+ years of both academic and technological research, with one-off Na-ion cells prepared using small batches of materials. As a result, the intrinsic properties of the two chemistries and those of the process and optimization of the cell prototypes cannot be decoupled. Finally, many design parameters having an impact in cell behaviour are manufacturer or application dependent, making it very difficult to find reports of a Li-ion and Na-ion cell fabricated following identical design parameters.

To avoid these shortcomings, half-cell performance metrics from the academic literature have been used here to extrapolate full cell performance indicators based on a common optimized design. This design assumes the same cell dimensions (as volume is usually the first design parameter to be established for a given application), and the same positive electrode coating thickness, electrode and electrolyte formulation and separator. All the other parameters have then been determined by the properties of the active materials involved (gravimetric capacity, voltage and density). This approach assumes the same level of process optimization for all cell components and manufacturing steps from active material preparation to cell assembly, for the two Li-ion and Na-ion battery technologies. This allows to evaluate the potential of the reviewed materials after the same technological development with respect to Li-ion commercial cells. Detailed information on the cell design as well as on the properties of the considered materials can be found in the supplementary information. The volume and weight of the cell envelope and contact tabs have not been taken into account as they are design dependent. However, since there is no reason to introduce design changes when switching to NIBs, these would not affect the differences in cell performance. As mentioned above, Na-ASSBs, Na/O_2 and Na/S systems are more disruptive battery technologies and therefore will not be evaluated in this section.

The calculated capacity and energy density at pouch cell level for different combinations of Li-ion and Na-ion active materials are presented in Table 3 and Fig. 7. Two sets of calculations have been performed based on the best positive and negative electrode materials identified in the previous sections and presented on Figs. 2 and 3. Positive electrode materials have been simulated against HC as the negative electrode, and negative electrode materials have been simulated against an O3-type layered oxide as the positive electrode material. The details of the materials and electrode properties used for the simulation are presented in Tables S3, S4 and S5 of Supplementary Information.

Table 3
Volumetric and gravimetric values of capacity and energy of the simulated pouch cells with 65 μm thick positive electrode coating based on the parameters of Tables S3–S5.

Active materials		Capacity (A h/L)	Capacity (A h/kg)	Energy (W h/L)	Energy (W h/kg)
+	–				
Li-ion cells					
NMC811	g	205.6	78.1	760.8	289.1
NMC111	g	179.7	66.7	656.1	243.4
LCO	g	167.7	60.8	628.9	227.9
LFP	g	155.2	63.3	520.0	212.0
LFP-C	g	148.0	61.1	495.8	204.5
LMO	g	134.9	51.4	526.1	200.5
Na-ion cells					
P2	HC	164.8	75.8	375.8	172.8
P2-CE	HC	137.0	60.9	350.6	156.0
NVP	HC	92.5	44.6	267.2	128.8
NVPF	HC	104.8	50.2	364.9	174.8
PBA	HC	89.8	51.1	262.3	149.2
O3	HC	160.5	71.2	462.3	205.1
O3	SC	133.2	60.0	360.9	162.7
O3	TiO_2/C	178.0	68.8	370.2	143.1
O3	NTO	153.8	57.7	359.8	134.9
O3	ci-g	91.2	41.7	210.7	96.4
O3	P/C	236.7	92.0	545.6	200.0
O3	Sb/C	217.4	79.7	588.4	215.6
O3	Sn/C	229.9	86.0	591.0	220.9
O3	MoS_2/C	224.4	83.5	397.1	147.7
O3	Sb_2O_3/C	221.6	81.2	478.6	175.5

The volumetric energy density of Na-ion positive electrode materials *vs.* HC is, in all cases, a step down compared to the NMC111-g Li-ion cell (Fig. 7a), which is taken here as reference for Li-ion technology. In terms of volumetric density, the O3-HC combination (462 Wh. L-1) is from far the best of the HC-based Na-ion cells, very close to the LFP-g Li-ion cell (496 Wh. L^{-1}) but reaches only 70% of the volumetric energy calculated for the NMC111-g cell. Interestingly, when HC is replaced by alloy-forming materials as negative electrode the volumetric energy density increases significantly, to reach 91% of the NMC111-g cell. This can be ascribed to their larger capacities combined with the fact that the density of some of these negative electrode materials is larger than that of graphite (Table S5), while that of HC is lower. However, this result needs to be handled with care as the calculations do not take into account the swelling of the electrode, which can be substantial for alloy-forming compounds (see section 2.2.2).

Some interesting differences could be found when analysing the gravimetric energy densities (Fig. 7b). The O3-HC gravimetric cell energy density is now slightly higher than that of LFP-g and LMO-g cells and reaches 84% of that for the NMC111-g cell. Replacing HC by higher capacity Sn/C and P/C composite negative electrode materials also allows to increase the energy density, to reach 95% of that of the NMC111-g reference. However, the gain from HC to alloys is less pronounced than for the volumetric energy densities. This can be ascribed to their higher capacity, resulting in thinner coatings and thus larger contribution to the weight from the separator (including electrolyte) and aluminium foil, as a consequence of the larger number of stacks (58 for O3-HC, 84 and 86 for Sn/C and P/rGO, respectively - see Table S6). NVPF appears to be the second-best performing Na-ion positive electrode material, but the overall gravimetric energy density is 15% lower than that with O3 when used with HC negative electrode material. The P2-HC cell reaches an energy density close to that of NVPF-HC, when considering the total available capacity (assuming a pre-sodiation process for the positive electrode material). If the initial Na deficiency is not compensated ("P2-CE" in Fig. 7), the performance of the cell with P2 material remains neatly lower than O3 and NVPF.

Despite the large capacity and voltage delivered by PBA in half cells, both gravimetric and volumetric energy densities are significantly lower compared to O3-HC and NVPF-HC cells. This is a result of the lower densities of PBA materials. The impact of the material density on the gravimetric energy is indirect, as it increases the relative contribution of the other elements of the cell, such as current collector, additives, electrolyte and separator, to the total weight. The same applies to the comparison between P/rGO and Sn/C, which exhibit very close energy densities in full cell despite having very different capacities, as a consequence of the strong difference of density between red phosphorous and tin.

Apart from alloy compounds, all other negative electrode materials, due to their lower capacity and higher voltage, result in significantly lower energy densities compared to HC, both volumetric and gravimetric. Moreover, the voltage is clearly more critical than capacity, as for instance MoS_2/rGO with 65% more capacity than HC, exhibits 28% lower gravimetric energy density.

The analysis of the contribution to the total weight by the various components of the O3-HC and NMC111-g cells, shown in Table S6, reveals that the lower cell voltage and capacity of O3 and HC compared to NMC111 and g, respectively, are partially compensated by the lower weight of the aluminium current collector. About 2.5 g cm^{-2} are saved by replacing Al for Cu on the negative electrode side, which corresponds to about 10–15% of the active material mass, and 6% (O3-HC) to 9% (NVPF-HC) of the total cell mass. This is further highlighted in Fig. 7c, which shows the areal weight of the various cell components for O3-HC and NVPF-HC Na-ion cells, compared to Li-ion NMC111-g and LMO-g cells, when the areal capacity is set to 3 mA g cm^{-2}. For example, the

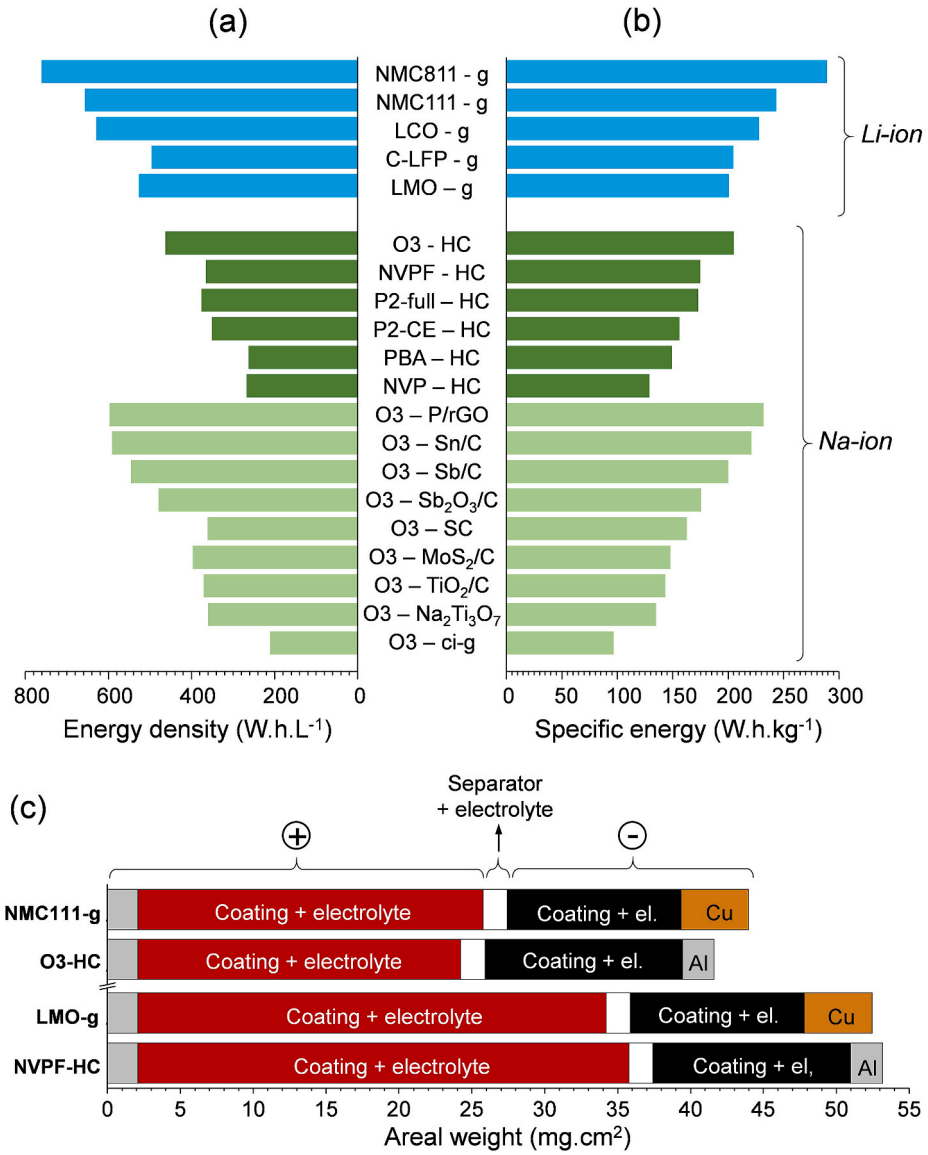

Fig. 7. Volumetric (a) and gravimetric (b) energy density of the simulated Li-ion (blue) and Na-ion pouch cells (dark green for positive electrode materials *vs* HC, and light green for negative electrode materials *vs* O3). (c) Weight of the various cell components, per cm^2, for a selection of Li-ion and Na-ion cells, calculated for an areal capacity of 3 mA h cm^{-2}. (For interpretation of the references to colour in this figure legend, the reader is referred to the Web version of this article.)

larger weight of the electrode coating of the NVPF-HC cell is almost completely compensated by the lighter current collector on the negative electrode side, resulting in lighter O3-HC cells compared to NMC111-g for the same areal capacity. This is a major advantage of the Na-ion chemistry, with relevant impact also on the total cost of the cells [7, 128].

The influence of the loading (areal capacity) on the difference of energy densities between Na-ion and Li-ion cells is shown in Fig. 8. Areal capacity in the range 2–3 mAh.cm^{-2} corresponds to the simulations shown in Fig. 7a and b for which the thickness of the positive electrode coating has been set to 65 μm. This represents a current standard for Li-ion cells with an intermediate balance between power and energy [332]. Li-ion cells optimized for maximum power use loadings closer to 1 mAh.cm^{-2}, while cells optimized for maximum energy are closer to 5 mAh.g^{-1} [332]. Interestingly, around 1 mAh.cm^{-2} and below, the energy densities of the Na cells are very close to that of the Li-ion cells. This is a direct consequence of the lighter aluminium current collector, as its relative contribution to the total weight of the cell increases when the mass loading is reduced. Therefore, the present simulations show that for a cell design oriented towards maximum energy density the best materials for Na-ion will hardly allow competing with the next generation of Li-ion cells. However, it also demonstrates that, for thinner coatings used for power-oriented cell designs, the benefit of aluminium current collector has more impact on the final weight and cost of the cell. Na-ion active materials allowing good rate performance, even if they do not allow the largest energy density, might thus be competitive in power-oriented cell designs.

The Na-ion chemistry presents some intrinsic drawbacks compared to Li-ion (heavier and larger alkali ion, 0.33 V larger standard potential) which tend to lower cell voltage and capacity. Nevertheless, from the present simulations it seems fair to consider that, with ongoing development, the present best materials available for Na-ion cells should allow approaching the energy density of the present generation of Li-ion commercial cells. Even the later is still far from matching the EU Integrated Strategic Energy Technology Plan (SET-Plan) Action 7 for 2020 and 2030 (a comparison of the current status of both technologies is given in Table S8, together with the performance targets set by the SET-Plan) [333]. NMC811, being implemented in the next generation commercial Li-ion cells [332,334], should allow to get closer to these goals. Nonetheless, the combination of attractive properties potentially offered

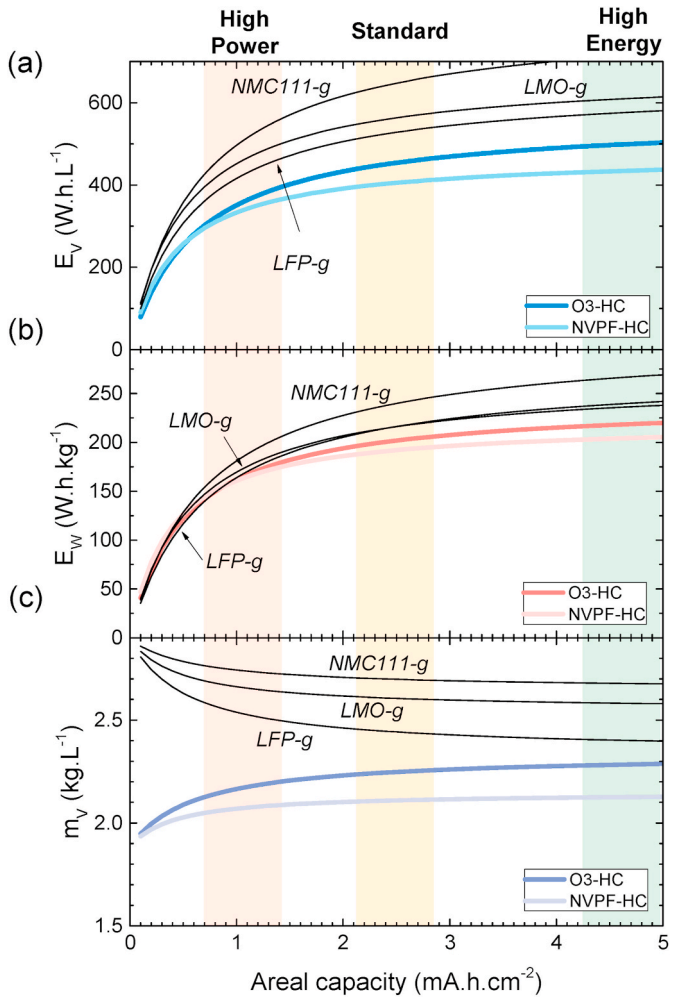

Fig. 8. Calculated full cell volumetric (a) and gravimetric (b) energy density, and volumetric weight (c), of O3-HC and NVPF-HC NIB cells (color lines), as a function of areal capacity; reference LIB cells NMC111-g, LMO-g and LFP-g LIB cells are shown as thin black lines. The shaded areas correspond to the typical areal capacity ranges of standard commercial cells (balanced between energy and power, yellow area), power-oriented design (orange area) and energy-oriented design (yellow area) [332,335].[332,335]. (For interpretation of the references to colour in this figure legend, the reader is referred to the Web version of this article.)

by NIBs (i.e., low cost, sustainable precursors and secure raw material supplies), fills a niche and could represent an important step towards beyond Li technologies in certain applications where energy density is less critical. We believe this work shows the benefit of full cell performance extrapolation of half-cell data in order to screen the most promising candidate materials.

6. Conclusion

While still a nascent technology, the impressive achievements realized to date indicate that Na-based batteries show a great promise as future energy storage solutions. The more disruptive Na/O_2, Na/S and Na-ASSBs may represent a significant game change, leading to an enormous gain in terms of performance, safety or cost. However, despite important advancements, their technological readiness level is still far from application. At the present moment, only NIBs can be considered as serious contenders to LIBs, with the potential to become the paradigm of green, safe, sustainable, and low-cost energy storage technologies of the future.

Performance-wise, several prototypes with different positive electrode chemistries (layered, polyanion or PBA type), coupled to a HC negative electrode, have demonstrated the potential of NIBs. These results strongly encourage further research on material development and cell assembly optimization. Indeed, considering the improvements which were achieved for LIBs since the initial deployment of this technology [336], the optimization of materials and processing should enable a similar achievement for the Na-based technology.

Preliminary assessments of the potential life-cycle of NIBs have proven that NIBs already provide an ecological benefit in terms of materials compared to LIBs [337]. Finally, several works estimate that NIBs can be cost-competitive when taking into account the bill of materials, as avoidance of aluminium leads to substantial cost savings (also for cobalt and lithium, although to a much lesser extent) [7,128,338]. It should however be noted that, both for LIBs and NIBs, specific energy has the highest impact in the cell cost, as less materials are required for electrode, current collector foils, electrolyte and separator. Thus, beside the low-cost, green, and sustainable philosophy of the Na-based technology, performance metrics such as high voltage and capacity are crucial for their deployment, not only for high energy density applications, in addition to lifetime and efficiency. Furthermore, costs strongly depend on market volume, and the average LIB prices are forecasted to continue dropping as they become mainstream after reaching the 100 $/KWh magic number. NIBs will thus be preferred in niche markets where a smaller scale of production is not a constraint. However, as LIB demand increases, raw materials supply shortfalls are to be expected for lithium and cobalt, while most NIBs are based in widespread cheaper materials.

In summary, extremely encouraging results have been achieved in a very short time when compared to the Li-ion technology. While it is envisioned that further technological improvement will be achieved by cell component fabrication/assembly optimization from an applied research point of view, the future research efforts should be devoted on fundamental research, materials discovery and understanding of the thermodynamic and kinetic processes governing the chemistry of these systems. In all cases, theoretical calculations can represent a powerful ally to understand electrochemical reaction mechanisms and to virtually screen of promising materials [333–336]. The driving force is strong and justified by the society's need of a more sustainable and greener future, where batteries can secure energy supply by bridging the gap between a clean energy production and utilization.

CRediT authorship contribution statement

Ivana Hasa: Writing - review & editing, Visualization. **Sathiya Mariyappan:** Writing - review & editing, Visualization, Investigation. **Damien Saurel:** Writing - review & editing, Methodology, Formal analysis, Visualization. **Philipp Adelhelm:** Writing - review & editing, Visualization. **Alexey Y. Koposov:** Writing - review & editing. **Christian Masquelier:** Writing - review & editing, Visualization. **Laurence Croguennec:** Writing - review & editing, Visualization. **Montse Casas-Cabanas:** Writing - review & editing, Supervision, Visualization.

Declaration of competing interest

The authors declare that they have no known competing financial interests or personal relationships that could have appeared to influence the work reported in this paper.

Acknowledgements

MCC and DS are grateful to the Basque Government through the Elkartek grants CICe2019 and CICe2020 (KK 2020/00078), to Ministerio de Economía y Competitividad through NIB-MOVE grant (PID2019-107468RB-C22) and to M. Galceran for helpful discussions. IH acknowledges the Bundesministerium für Bildung und Forschung (BMBF) for support through the TRANSITION project (03XP0186A). IH is also grateful for the financial support of the Helmholtz Association.

SM, LC and CM thank the RS2E Network for funding as well as the financial support of Région Nouvelle Aquitaine, of the French National Research Agency (STORE-EX Labex Project ANR-10-LABX-76-01) and of the European Union's Horizon 2020 research and innovation program under grant agreement No 875629. The authors are grateful to Argonne National Laboratory for providing the BatPac software.

Appendix A. Supplementary data

Supplementary data to this article can be found online at https://doi.org/10.1016/j.jpowsour.2020.228872.

References

[1] I. Tsiropoulos, D. Tarvydas, N. Lebedeva, Li-ion batteries for mobility and stationary storage applications Scenarios for costs and market growth. https://doi.org/10.2760/87175, 2018.
[2] Commission staff working document report on raw materials for battery applications, n.d. http://www.innoenergy.com/(accessed July 20, 2020).
[3] A. Verkehrswende, K. Meyer, M. Buchert, S. Degreif, P. Dolega, J. Franz, Ensuring a Sustainable Supply of Raw Materials for Electric Vehicles A Synthesis Paper on Raw Material Needs for Batteries and Fuel Cells about Ensuring a Sustainable Supply of Raw Materials for Electric Vehicles A Synthesis Paper on Raw Material Needs for Batteries and Fuel Cells PRODUCED on BEHALF of: Ensuring a Sustainable Supply of Raw Materials for Electric Vehicles: A Synthesis Paper on Raw Material Needs for Batteries and Fuel Cells, 2018. www.agora-verkehrswende.de. (Accessed 20 July 2020).
[4] V. Palomares, M. Casas-Cabanas, E. Castillo-Martínez, M.H. Han, T. Rojo, Update on Na-based battery materials. A growing research path, Energy Environ. Sci. 6 (2013) 2312–2337, https://doi.org/10.1039/c3ee41031e.
[5] H. Pan, Y.S. Hu, L. Chen, Room-temperature stationary sodium-ion batteries for large-scale electric energy storage, Energy Environ. Sci. 6 (2013) 2338–2360, https://doi.org/10.1039/c3ee40847g.
[6] P.K. Nayak, L. Yang, W. Brehm, P. Adelhelm, From lithium-ion to sodium-ion batteries: advantages, challenges, and surprises, Angew. Chem. Int. Ed. 57 (2018) 102–120, https://doi.org/10.1002/anie.201703772.
[7] C. Vaalma, D. Buchholz, M. Weil, S. Passerini, A cost and resource analysis of sodium-ion batteries, Nat. Rev. Mater. 3 (2018) 1–11, https://doi.org/10.1038/natrevmats.2018.13.
[8] J.L. Murray, The Al-Na (Aluminum-Sodium) system, Bull. Alloy Phase Diagrams 4 (1983) 407–410, https://doi.org/10.1007/BF02868094.
[9] Wo2016027082A1, Storage and/or transportation of sodium-ion cells - google Patents (n.d.), https://patents.google.com/patent/WO2016027082A1/en?oq=Barker++Wright+WO+%2F+2016%2F+027082. (Accessed 26 May 2020).
[10] C. Delmas, Sodium and sodium-ion batteries: 50 Years of research, Adv. Energy Mater. 8 (2018) 1703137, https://doi.org/10.1002/aenm.201703137.
[11] N. Yabuuchi, K. Kubota, M. Dahbi, S. Komaba, Research development on sodium-ion batteries, Chem. Rev. 114 (2014) 11636–11682, https://doi.org/10.1021/cr500192f.
[12] Y. Liu, X. Liu, T. Wang, L.Z. Fan, L. Jiao, Research and application progress on key materials for sodium-ion batteries, Sustain. Energy Fuels. 1 (2017) 986–1006, https://doi.org/10.1039/c7se00120g.
[13] K. Hurlbutt, S. Wheeler, I. Capone, M. Pasta, Prussian blue analogs as battery materials, Joule 2 (2018) 1950–1960, https://doi.org/10.1016/j.joule.2018.07.017.
[14] Y. Ding, Z.P. Cano, A. Yu, J. Lu, Z. Chen, Automotive Li-ion batteries: current status and future perspectives, Electrochem. Energy Rev. 2 (2019) 1–28, https://doi.org/10.1007/s41918-018-0022-z.
[15] C. Delmas, C. Fouassier, P. Hagenmuller, Structural classification and properties of the layered oxides, Phys. B+C 99 (1980) 81–85, https://doi.org/10.1016/0378-4363(80)90214-4.
[16] N. Yabuuchi, M. Kajiyama, J. Iwatate, H. Nishikawa, S. Hitomi, R. Okuyama, R. Usui, Y. Yamada, S. Komaba, P2-type Nax[Fe1/2Mn1/2]O2 made from earth-abundant elements for rechargeable Na batteries, Nat. Mater. 11 (2012) 512–517, https://doi.org/10.1038/nmat3309.
[17] N. Yabuuchi, M. Yano, H. Yoshida, S. Kuze, S. Komaba, Synthesis and electrode performance of O3-type NaFeO2-NaNi1/2Mn1/2O2Solid solution for rechargeable sodium batteries, J. Electrochem. Soc. 160 (2013) A3131–A3137, https://doi.org/10.1149/2.018305jes.
[18] K. Kubota, S. Kumakura, Y. Yoda, K. Kuroki, S. Komaba, Electrochemistry and solid-state chemistry of NaMeO2 (me = 3d transition metals), Adv. Energy Mater. 8 (2018) 1–30, https://doi.org/10.1002/aenm.201703415.
[19] I. Hasa, D. Buchholz, S. Passerini, J. Hassoun, A comparative study of layered transition metal oxide cathodes for application in sodium-ion battery, ACS Appl. Mater. Interfaces 7 (2015) 5206–5212, https://doi.org/10.1021/am5080437.
[20] A. Bauer, J. Song, S. Vail, W. Pan, J. Barker, Y. Lu, The scale-up and commercialization of nonaqueous Na-ion battery technologies, Adv. Energy Mater. 8 (2018) 1–13, https://doi.org/10.1002/aenm.201702869.
[21] Sodium-ion battery, (n.d.). https://en.wikipedia.org/wiki/Sodium-ion_battery#cite_note-31 (accessed April 20, 2020).
[22] J. Barker, The performance and commercialization of Faradion's non-aqueous Na-ion battery technologyitle, in: Int. Conf. Sodium Batter. (ICNaB-2019) vols. 4–7, Naperville, 2019. Novemb.
[23] G. Singh, B. Acebedo, M.C. Cabanas, D. Shanmukaraj, M. Armand, T. Rojo, An approach to overcome first cycle irreversible capacity in P2-Na 2/3[Fe1/2Mn1/2]O2, Electrochem. Commun. 37 (2013) 61–63, https://doi.org/10.1016/j.elecom.2013.10.008.
[24] M. Sathiya, J. Thomas, D. Batuk, V. Pimenta, R. Gopalan, J.-M. Tarascon, Dual stabilization and sacrificial effect of Na2CO3 for increasing capacities of Na-ion cells based on P2-NaxMO2 electrodes, Chem. Mater. 29 (2017) 5948–5956, https://doi.org/10.1021/acs.chemmater.7b01542.
[25] D. Shanmukaraj, K. Kretschmer, T. Sahu, W. Bao, T. Rojo, G. Wang, M. Armand, Highly efficient, cost effective, and safe sodiation agent for high-performance sodium-ion batteries, ChemSusChem 11 (2018) 3286–3291, https://doi.org/10.1002/cssc.201801099.
[26] B. Lee, E. Paek, D. Mitlin, S.W. Lee, Sodium metal anodes: emerging solutions to dendrite growth, Chem. Rev. 119 (2019) 5416–5460, https://doi.org/10.1021/acs.chemrev.8b00642.
[27] Y.-K. Sun, Direction for commercialization of O3-type layered cathodes for sodium-ion batteries, ACS Energy Lett 5 (2020) 1278–1280, https://doi.org/10.1021/acsenergylett.0c00597.
[28] S. Komaba, N. Yabuuchi, T. Nakayama, A. Ogata, T. Ishikawa, I. Nakai, Study on the reversible electrode reaction of Na1–xNi0.5Mn0.5O2 for a rechargeable sodium-ion battery, Inorg. Chem. 51 (2012) 6211–6220, https://doi.org/10.1021/ic300357d.
[29] S. Mariyappan, Q. Wang, J.M. Tarascon, Will sodium layered oxides ever Be competitive for sodium ion battery applications? J. Electrochem. Soc. 165 (2018) A3714–A3722, https://doi.org/10.1149/2.0201816jes.
[30] Q. Wang, S. Mariyappan, J. Vergnet, A.M. Abakumov, G. Rousse, F. Rabuel, M. Chakir, J.-M. Tarascon, Reaching the energy density limit of layered O3-NaNi0.5Mn0.5O2 electrodes via dual Cu and Ti substitution, Adv. Energy Mater. 9 (2019) 1901785, https://doi.org/10.1002/aenm.201901785.
[31] B. Silván, E. Gonzalo, L. Djuandhi, N. Sharma, F. Fauth, D. Saurel, On the dynamics of transition metal migration and its impact on the performance of layered oxides for sodium-ion batteries: NaFeO2 as a case study, J. Mater. Chem. A. 6 (2018) 15132–15146, https://doi.org/10.1039/c8ta02473a.
[32] X. Li, Y. Wang, D. Wu, L. Liu, S.-H. Bo, G. Ceder, Jahn–teller assisted Na diffusion for high performance Na ion batteries, Chem. Mater. 28 (2016) 6575–6583, https://doi.org/10.1021/acs.chemmater.6b02440.
[33] X. Qi, Y. Wang, L. Jiang, L. Mu, C. Zhao, L. Liu, Y.-S. Hu, L. Chen, X. Huang, Sodium-deficient O3-Na0.9[Ni0.4Mn xTi 0.6−x]O2 layered-oxide cathode materials for sodium-ion batteries, Part. Part. Syst. Char. 33 (2016) 538–544, https://doi.org/10.1002/ppsc.201500129.
[34] M. Sathiya, Q. Jacquet, M.-L. Doublet, O.M. Karakulina, J. Hadermann, J.-M. Tarascon, A chemical approach to raise cell voltage and suppress phase transition in O3 sodium layered oxide electrodes, Adv. Energy Mater 8 (2018) 1702599, https://doi.org/10.1002/aenm.201702599.
[35] X. Li, D. Wu, Y.-N. Zhou, L. Liu, X.-Q. Yang, G. Ceder, O3-type Na (Mn0.25Fe0.25Co0.25Ni0.25)O2: a quaternary layered cathode compound for rechargeable Na ion batteries, Electrochem. Commun. 49 (2014) 51–54, https://doi.org/10.1016/j.elecom.2014.10.003.
[36] S. Mariyappan, T. Marchandier, F. Rabuel, A. Iadecola, G. Rousse, A. V Morozov, A.M. Abakumov, J.-M. Tarascon, The role of divalent (Zn2+/Mg2+/Cu2+) substituents in achieving full capacity of sodium layered oxides for Na-ion battery applications, Chem. Mater. 32 (2020) 1657–1666, https://doi.org/10.1021/acs.chemmater.9b05205.
[37] A.J. Perez, D. Batuk, M. Saubanère, G. Rousse, D. Foix, E. McCalla, E.J. Berg, R. Dugas, K.H.W. van den Bos, M.-L. Doublet, D. Gonbeau, A.M. Abakumov, G. Van Tendeloo, J.-M. Tarascon, Strong oxygen participation in the redox governing the structural and electrochemical properties of Na-rich layered oxide Na2IrO3, Chem. Mater. 28 (2016) 8278–8288, https://doi.org/10.1021/acs.chemmater.6b03338.
[38] X. Rong, J. Liu, E. Hu, Y. Liu, Y. Wang, J. Wu, X. Yu, K. Page, Y.-S. Hu, W. Yang, H. Li, X.-Q. Yang, L. Chen, X. Huang, Structure-induced reversible anionic redox activity in Na layered oxide cathode, Joule 2 (2018) 125–140, https://doi.org/10.1016/j.joule.2017.10.008.
[39] G. Assat, J.-M. Tarascon, Fundamental understanding and practical challenges of anionic redox activity in Li-ion batteries, Nat. Energy. 3 (2018) 373–386, https://doi.org/10.1038/s41560-018-0097-0.
[40] T. Broux, F. Fauth, N. Hall, Y. Chatillon, M. Bianchini, T. Bamine, J.B. Leriche, E. Suard, D. Carlier, Y. Reynier, L. Simonin, C. Masquelier, L. Croguennec, High rate performance for carbon-coated Na3V2(PO4)2F3 in Na-ion batteries, Small Methods 3 (2019), https://doi.org/10.1002/smtd.201800215.
[41] G.-L. Xu, R. Amine, Y.-F. Xu, J. Liu, J. Gim, T. Ma, Y. Ren, C.-J. Sun, Y. Liu, X. Zhang, S.M. Heald, A. Solhy, I. Saadoune, W.L. Mattis, S.-G. Sun, Z. Chen, K. Amine, Insights into the structural effects of layered cathode materials for high voltage sodium-ion batteries, Energy Environ. Sci. 10 (2017) 1677–1693, https://doi.org/10.1039/C7EE00827A.
[42] M. Keller, D. Buchholz, S. Passerini, Layered Na-ion cathodes with outstanding performance resulting from the synergetic effect of mixed P- and O-type phases, Adv. Energy Mater. 6 (2016) 1501555, https://doi.org/10.1002/aenm.201501555.
[43] J. Song, K. Wang, J. Zheng, M.H. Engelhard, B. Xiao, E. Hu, Z. Zhu, C. Wang, M. Sui, Y. Lin, D. Reed, V.L. Sprenkle, P. Yan, X. Li, Controlling surface phase transition and chemical reactivity of O3-layered metal oxide cathodes for high-

performance Na-ion batteries, ACS Energy Lett (2020) 1718–1725, https://doi.org/10.1021/acsenergylett.0c00700.
[44] S. Roberts, E. Kendrick, The re-emergence of sodium ion batteries: testing, processing, and manufacturability, Nanotechnol. Sci. Appl. 11 (2018) 23–33, https://doi.org/10.2147/NSA.S146365.
[45] T. Jin, H. Li, K. Zhu, P.-F. Wang, P. Liu, L. Jiao, Polyanion-type cathode materials for sodium-ion batteries, Chem. Soc. Rev. 49 (2020) 2342–2377, https://doi.org/10.1039/c9cs00846b.
[46] C. Masquelier, L. Croguennec, Polyanionic (phosphates, silicates, sulfates) frameworks as electrode materials for rechargeable Li (or Na) batteries, Chem. Rev. 113 (2013) 6552–6591, https://doi.org/10.1021/cr3001862.
[47] P. Moreau, D. Guyomard, J. Gaubicher, F. Boucher, Structure and stability of sodium intercalated phases in olivine FePO 4, Chem. Mater. 22 (2010) 4126–4128, https://doi.org/10.1021/cm101377h.
[48] D. Saurel, M. Galceran, M. Reynaud, H. Anne, M. Casas-Cabanas, Rate dependence of the reaction mechanism in olivine NaFePO $_4$ Na-ion cathode material, Int. J. Energy Res. 42 (2018) 3258–3265, https://doi.org/10.1002/er.4078.
[49] J.M. Clark, P. Barpanda, A. Yamada, M.S. Islam, Sodium-ion battery cathodes Na2FeP2O7 and Na2MnP2O7: diffusion behaviour for high rate performance, J. Mater. Chem. A. 2 (2014) 11807–11812, https://doi.org/10.1039/c4ta02383h.
[50] K.H. Ha, S.H. Woo, D. Mok, N.S. Choi, Y. Park, S.M. Oh, Y. Kim, J. Kim, J. Lee, L. F. Nazar, K.T. Lee, Na4-αM2+α/2(P2O 7)2 ($2/3 \leq \alpha \leq 7/8$, M = Fe, Fe 0.5Mn0.5, Mn): a promising sodium ion cathode for na-ion batteries, Adv. Energy Mater. 3 (2013) 770–776, https://doi.org/10.1002/aenm.201200825.
[51] A.J. Fernández-Ropero, M. Zarrabeitia, M. Reynaud, T. Rojo, M. Casas-Cabanas, Toward safe and sustainable batteries: Na4Fe3(PO4)2P2O7 as a low-cost cathode for rechargeable aqueous Na-ion batteries, J. Phys. Chem. C 122 (2018) 133–142, https://doi.org/10.1021/acs.jpcc.7b09803.
[52] S.C. Chung, J. Ming, L. Lander, J. Lu, A. Yamada, Rhombohedral NASICON-type Na: XFe 2(SO4)3 for sodium ion batteries: comparison with phosphate and alluaudite phases, J. Mater. Chem. A. 6 (2018) 3919–3925, https://doi.org/10.1039/c7ta08606g.
[53] N. Kuganathan, A. Chroneos, Defects, dopants and sodium mobility in Na2MnSiO4, Sci. Rep. 8 (2018), https://doi.org/10.1038/s41598-018-32856-7.
[54] C.G. Delmas, R. Olazcuaga, F. Cherkaoui, R. Brochu, G. Le Flem, A new family of phosphates with the formula Na3M2(PO4)3 (M = Ti, V, Cr, Fe), C. R. Seances Acad. Sci. Série C (1978) 169–174.
[55] M. Bianchini, N. Brisset, F. Fauth, F. Weill, E. Elkaim, E. Suard, C. Masquelier, L. Croguennec, Na3V2(PO4)2F3 revisited: a high-resolution diffraction study, Chem. Mater. 26 (2014) 4238–4247, https://doi.org/10.1021/cm501644g.
[56] T. Jin, H. Li, K. Zhu, P.-F. Wang, P. Liu, L. Jiao, Polyanion-type cathode materials for sodium-ion batteries, Chem. Soc. Rev. 49 (2020) 2342–2377, https://doi.org/10.1039/c9cs00846b.
[57] T. Broux, T. Bamine, F. Fauth, L. Simonelli, W. Olszewski, C. Marini, M. Ménétrier, D. Carlier, C. Masquelier, L. Croguennec, Strong impact of the oxygen content in Na3V2(PO4)2F3-yOy ($0 \leq y \leq 2$) on its structural and electrochemical properties, Chem. Mater. 28 (2016) 7683–7692, https://doi.org/10.1021/acs.chemmater.6b02659.
[58] L.H.B. Nguyen, P. Sanz Camacho, T. Broux, J. Olchowka, C. Masquelier, L. Croguennec, D. Carlier, Density functional theory-assisted 31P and 23Na magic-angle spinning nuclear magnetic resonance study of the Na3V2(PO4)2F3-Na3V2(PO4)2FO2 solid solution: unraveling its local and electronic structures, Chem. Mater. 31 (2019) 9759–9768, https://doi.org/10.1021/acs.chemmater.9b03546.
[59] Z. Jian, L. Zhao, H. Pan, Y.S. Hu, H. Li, W. Chen, L. Chen, Carbon coated Na3V2(PO4)3 as novel electrode material for sodium ion batteries, Electrochem. Commun. 14 (2012) 86–89, https://doi.org/10.1016/j.elecom.2011.11.009.
[60] S.T. Dacek, W.D. Richards, D.A. Kitchaev, G. Ceder, Structure and dynamics of fluorophosphate Na-ion battery cathodes, Chem. Mater. 28 (2016) 5450–5460, https://doi.org/10.1021/acs.chemmater.6b01989.
[61] M. Bianchini, F. Fauth, N. Brisset, F. Weill, E. Suard, C. Masquelier, L. Croguennec, Comprehensive investigation of the Na3V2(PO4)2F3-NaV2(PO4)2F3 system by operando high resolution synchrotron X-ray diffraction, Chem. Mater. 27 (2015) 3009–3020, https://doi.org/10.1021/acs.chemmater.5b00361.
[62] T. Broux, T. Bamine, L. Simonelli, L. Stievano, F. Fauth, M. Ménétrier, D. Carlier, C. Masquelier, L. Croguennec, VIV disproportionation upon sodium extraction from Na3V2(PO4)2F3 observed by operando X-ray absorption spectroscopy and solid-state NMR, J. Phys. Chem. C 121 (2017) 4103–4111, https://doi.org/10.1021/acs.jpcc.6b11413.
[63] Z. Jian, W. Han, X. Lu, H. Yang, Y.S. Hu, J. Zhou, Z. Zhou, J. Li, W. Chen, D. Chen, L. Chen, Superior electrochemical performance and storage mechanism of Na 3 V 2 (PO 4) 3 cathode for room-temperature sodium-ion batteries, Adv. Energy Mater. 3 (2013) 156–160, https://doi.org/10.1002/aenm.201200558.
[64] A. Ponrouch, R. Dedryvere, D. Monti, A.E. Demet, J.M. Ateba Mba, L. Croguennec, C. Masquelier, P. Johansson, M.R. Palacin, R. Dedryvère, D. Monti, A.E. Demet, J.M. Ateba Mba, L. Croguennec, C. Masquelier, P. Johansson, M.R. Palacín, Towards high energy density sodium ion batteries through electrolyte optimization, Energy Environ. Sci. 6 (2013) 2361–2369, https://doi.org/10.1039/c3ee41379a.
[65] P. Serras, V. Palomares, P. Kubiak, L. Lezama, T. Rojo, Enhanced electrochemical performance of vanadyl (IV) Na3(VO)2(PO4)2F by ex-situ carbon coating, Electrochem. Commun. 34 (2013) 344–347, https://doi.org/10.1016/J.ELECOM.2013.07.010.
[66] N. Sharma, P. Serras, V. Palomares, H.E.A. Brand, J. Alonso, P. Kubiak, M. Luisa Fdez-Gubieda, T. Rojo, Sodium distribution and reaction mechanisms of a Na3V2O2(PO4)2F electrode during use in a sodium-ion battery, Chem. Mater. 26 (2014) 3391–3402, https://doi.org/10.1021/cm5005104.
[67] L.H.B. Nguyen, T. Broux, P.S. Camacho, D. Denux, L. Bourgeois, S. Belin, A. Iadecola, F. Fauth, D. Carlier, J. Olchowka, C. Masquelier, L. Croguennec, Stability in water and electrochemical properties of the Na3V2(PO4)2F3 – Na3(VO)2(PO4)2F solid solution, Energy Storage Mater 20 (2019) 324–334, https://doi.org/10.1016/j.ensm.2019.04.010.
[68] J. Gopalakrishnan, K.K. Rangan, V2(PO4)3: a novel NASICON-type vanadium phosphate synthesized by oxidative deintercalation of sodium from Na3V2(PO4)3, Chem. Mater. 4 (1992) 745–747, https://doi.org/10.1021/cm00022a001.
[69] G. Yan, S. Mariyappan, G. Rousse, Q. Jacquet, M. Deschamps, R. David, B. Mirvaux, J.W. Freeland, J.M. Tarascon, Higher energy and safer sodium ion batteries via an electrochemically made disordered Na 3 V 2 (PO 4) 2 F 3 material, Nat. Commun. 10 (2019), https://doi.org/10.1038/s41467-019-08359-y.
[70] F. Lalère, V. Seznec, M. Courty, R. David, J.N. Chotard, C. Masquelier, Improving the energy density of Na3V2(PO4)3-based positive electrodes through V/Al substitution, J. Mater. Chem. A. 3 (2015) 16198–16205, https://doi.org/10.1039/c5ta03528g.
[71] M.V. Zakharkin, O.A. Drozhzhin, I.V. Tereshchenko, D. Chernyshov, A. M. Abakumov, E.V. Antipov, K.J. Stevenson, Enhancing Na+ extraction limit through high voltage activation of the NASICON-type Na4MnV(PO4)3 cathode, ACS Appl. Energy Mater. 1 (2018) 5842–5846, https://doi.org/10.1021/acsaem.8b01269.
[72] F. Chen, V.M. Kovrugin, R. David, O. Mentré, F. Fauth, J.N. Chotard, C. Masquelier, A NASICON-type positive electrode for Na batteries with high energy density: Na4MnV(PO4)3, Small Methods 3 (2019), https://doi.org/10.1002/smtd.201800218.
[73] W. Zhou, L. Xue, X. Lü, H. Gao, Y. Li, S. Xin, G. Fu, Z. Cui, Y. Zhu, J. B. Goodenough, NaxMV(PO4)3 (M = Mn, Fe, Ni) structure and properties for sodium extraction, Nano Lett. 16 (2016) 7836–7841, https://doi.org/10.1021/acs.nanolett.6b04044.
[74] W.-J. Li, C. Han, G. Cheng, S.-L. Chou, H.-K. Liu, S.-X. Dou, Chemical properties, structural properties, and energy storage applications of prussian blue analogues, Small 15 (2019) 1900470, https://doi.org/10.1002/smll.201900470.
[75] Q. Liu, Z. Hu, M. Chen, C. Zou, H. Jin, S. Wang, S.-L. Chou, Y. Liu, S.-X. Dou, The cathode choice for commercialization of sodium-ion batteries: layered transition metal oxides versus prussian blue analogs, Adv. Funct. Mater. 30 (2020) 1909530, https://doi.org/10.1002/adfm.201909530.
[76] A. Firouzi, R. Qiao, S. Motallebi, C.W. Valencia, H.S. Israel, M. Fujimoto, L. A. Wray, Y.-D. Chuang, W. Yang, C.D. Wessells, Monovalent manganese based anodes and co-solvent electrolyte for stable low-cost high-rate sodium-ion batteries, Nat. Commun. 9 (2018) 861, https://doi.org/10.1038/s41467-018-03257-1.
[77] Chevron invests in prussian blue battery tech company Natron energy; Stationary Storage for EV Charging Stations, ((n.d.)).
[78] P. Judge, H5 adds sodium-ion batteries to Forced Physics test (2020).
[79] X. Bie, K. Kubota, T. Hosaka, K. Chihara, S. Komaba, Synthesis and electrochemical properties of Na-rich Prussian blue analogues containing Mn, Fe, Co, and Fe for Na-ion batteries, J. Power Sources 378 (2018) 322–330, https://doi.org/10.1016/j.jpowsour.2017.12.052.
[80] Y. You, X.-L. Wu, Y.-X. Yin, Y.-G. Guo, High-quality Prussian blue crystals as superior cathode materials for room-temperature sodium-ion batteries, Energy Environ. Sci. 7 (2014) 1643–1647, https://doi.org/10.1039/C3EE44004D.
[81] M. Pasta, R.Y. Wang, R. Ruffo, R. Qiao, H.-W. Lee, B. Shyam, M. Guo, Y. Wang, L. A. Wray, W. Yang, M.F. Toney, Y. Cui, Manganese–cobalt hexacyanoferrate cathodes for sodium-ion batteries, J. Mater. Chem. A. 4 (2016) 4211–4223, https://doi.org/10.1039/C5TA10571D.
[82] C. Aparicio, L. Machala, Z. Marusak, Thermal decomposition of Prussian blue under inert atmosphere, J. Therm. Anal. Calorim. 110 (2012) 661–669, https://doi.org/10.1007/s10973-011-1890-1.
[83] H.J. Buser, D. Schwarzenbach, W. Petter, A. Ludi, The crystal structure of Prussian Blue: Fe4[Fe(CN)6]3.xH2O, Inorg. Chem. 16 (1977) 2704–2710, https://doi.org/10.1021/ic50177a008.
[84] J. Song, L. Wang, Y. Lu, J. Liu, B. Guo, P. Xiao, J.-J. Lee, X.-Q. Yang, G. Henkelman, J.B. Goodenough, Removal of interstitial H2O in hexacyanometallates for a superior cathode of a sodium-ion battery, J. Am. Chem. Soc. 137 (2015) 2658–2664, https://doi.org/10.1021/ja512383b.
[85] I. Hasa, J. Hassoun, S. Passerini, Nanostructured Na-ion and Li-ion anodes for battery application: a comparative overview, Nano Res 10 (2017) 3942–3969, https://doi.org/10.1007/s12274-017-1513-7.
[86] H. Zhang, I. Hasa, S. Passerini, Beyond insertion for Na-ion batteries: nanostructured alloying and conversion anode materials, Adv. Energy Mater. (2018) 1702582.
[87] X. Dou, I. Hasa, D. Saurel, C. Vaalma, L. Wu, D. Buchholz, D. Bresser, S. Komaba, S. Passerini, Hard carbons for sodium-ion batteries : structure , analysis , sustainability , and electrochemistry, Mater. Today xxx (2019), https://doi.org/10.1016/j.mattod.2018.12.040.
[88] W. Luo, F. Shen, C. Bommier, H. Zhu, X. Ji, L. Hu, Na-ion battery anodes: materials and electrochemistry, Acc. Chem. Res. (2016), https://doi.org/10.1021/acs.accounts.5b00482 acs.accounts.5b00482.
[89] C. Bommier, X. Ji, Recent development on anodes for Na-ion batteries, Isr. J. Chem. 55 (2015) 486–507.
[90] M.M. Ángel, S. Damien, G.J. Luis, C. Montse, C. Elizabeth, R. Teófilo, Na-Ion batteries for large scale Applications: a review on anode materials and solid electrolyte interphase formation, Adv. Energy Mater. 7 (2017) 1700463.

[91] P. Zheng, T. Liu, S. Guo, Micro-nano structure hard carbon as a high performance anode material for sodium-ion batteries, Sci. Rep. 6 (2016) 1–7, https://doi.org/10.1038/srep35620.

[92] I. Hasa, X. Dou, D. Buchholz, Y. Shao-Horn, J. Hassoun, S. Passerini, B. Scrosati, A sodium-ion battery exploiting layered oxide cathode, graphite anode and glyme-based electrolyte, J. Power Sources 310 (2016) 26–31, https://doi.org/10.1016/j.jpowsour.2016.01.082.

[93] Y. Liu, N. Zhang, L. Jiao, J. Chen, Tin nanodots encapsulated in porous nitrogen-doped carbon nanofibers as a free-standing anode for advanced sodium-ion batteries, Adv. Mater. 27 (2015) 6702–6707, https://doi.org/10.1002/adma.201503015.

[94] L. Pei, Q. Zhao, C. Chen, J. Liang, J. Chen, Phosphorus nanoparticles encapsulated in graphene scrolls as a high-performance anode for sodium-ion batteries, ChemElectroChem 2 (2015) 1652–1655, https://doi.org/10.1002/celc.201500251.

[95] J. Qian, Y. Chen, L. Wu, Y. Cao, X. Ai, H. Yang, High capacity Na-storage and superior cyclability of nanocomposite Sb/C anode for Na-ion batteries, Chem. Commun. 48 (2012) 7070, https://doi.org/10.1039/c2cc32730a.

[96] R. Zhang, Y. Wang, H. Zhou, J. Lang, J. Xu, Y. Xiang, S. Ding, Mesoporous TiO2 nanosheets anchored on graphene for ultra long life Na-ion batteries, Nanotechnology 29 (2018), https://doi.org/10.1088/1361-6528/aab562.

[97] W. Wang, C. Yu, Z. Lin, J. Hou, H. Zhu, S. Jiao, Microspheric Na2Ti3O7 consisting of tiny nanotubes: an anode material for sodium-ion batteries with ultrafast charge–discharge rates, Nanoscale 5 (2013) 594–599.

[98] X. Xie, Z. Ao, D. Su, J. Zhang, G. Wang, MoS2/graphene composite anodes with enhanced performance for sodium-ion batteries: the role of the two-dimensional heterointerface, Adv. Funct. Mater. 25 (2015) 1393–1403, https://doi.org/10.1002/adfm.201404078.

[99] D. Li, D. Yan, J. Ma, W. Qin, X. Zhang, T. Lu, L. Pan, One-step microwave-assisted synthesis of Sb2O3/reduced graphene oxide composites as advanced anode materials for sodium-ion batteries, Ceram. Int. 42 (2016) 15634–15642, https://doi.org/10.1016/j.ceramint.2016.07.017.

[100] Y. Nishi, The development of lithium ion secondary batteries, Chem. Rec. 1 (2001) 406–413, https://doi.org/10.1002/tcr.1024.

[101] H. Yamamoto, S. Muratsubaki, K. Kubota, M. Fukunishi, H. Watanabe, J. Kim, S. Komaba, Synthesizing higher-capacity hard-carbons from cellulose for Na- and K-ion batteries, J. Mater. Chem. A. 6 (2018) 16844–16848, https://doi.org/10.1039/c8ta05203d.

[102] B. Xiao, T. Rojo, X. Li, Hard carbon as sodium-ion battery anodes: progress and challenges, ChemSusChem 12 (2019) 133–144, https://doi.org/10.1002/cssc.201801879.

[103] C. Zhao, Q. Wang, Y. Lu, B. Li, L. Chen, Y.S. Hu, High-temperature treatment induced carbon anode with ultrahigh Na storage capacity at low-voltage plateau, Sci. Bull. 63 (2018) 1125–1129, https://doi.org/10.1016/j.scib.2018.07.018.

[104] W. Luo, Z. Jian, Z. Xing, W. Wang, C. Bommier, M.M. Lerner, X. Ji, Electrochemically expandable soft carbon as anodes for Na-ion batteries, ACS Cent. Sci. 1 (2015) 516–522, https://doi.org/10.1021/acscentsci.5b00329.

[105] https://news.cnrs.fr/articles/a-battery-revolution-in-motion, (n.d.).

[106] FARADION, http://www.faradion.co.uk, ((n.d.)).

[107] http://www.hinabattery.com/en/index.php?catid=12, ((n.d.)).

[108] D. Saurel, B. Orayech, B. Xiao, D. Carriazo, X. Li, T. Rojo, From charge storage mechanism to performance: a roadmap toward high specific energy sodium-ion batteries through carbon anode optimization, Adv. Energy Mater. 8 (2018) 1–33, https://doi.org/10.1002/aenm.201703268.

[109] Z. Li, C. Bommier, Z. Sen Chong, Z. Jian, T.W. Surta, X. Wang, Z. Xing, J. C. Neuefeind, W.F. Stickle, M. Dolgos, P.A. Greaney, X. Ji, Mechanism of Na-ion storage in hard carbon anodes revealed by heteroatom doping, Adv. Energy Mater. 7 (2017) 1602894, https://doi.org/10.1002/aenm.201602894.

[110] S. Qiu, L. Xiao, M.L. Sushko, K.S. Han, Y. Shao, M. Yan, X. Liang, L. Mai, J. Feng, Y. Cao, X. Ai, H. Yang, J. Liu, Manipulating adsorption-insertion mechanisms in nanostructured carbon materials for high-efficiency sodium ion storage, Adv. Energy Mater. 7 (2017) 1700403, https://doi.org/10.1002/aenm.201700403.

[111] R. Raccichini, A. Varzi, S. Passerini, B. Scrosati, The role of graphene for electrochemical energy storage, Nat. Mater. 14 (2015) 271–279.

[112] J. Zhang, D.W. Wang, W. Lv, S. Zhang, Q. Liang, D. Zheng, F. Kang, Q.H. Yang, Achieving superb sodium storage performance on carbon anodes through an ether-derived solid electrolyte interphase, Energy Environ. Sci. 10 (2017) 370–376, https://doi.org/10.1039/c6ee03367a.

[113] Z. Lin, X. Xiong, J. Zheng, G. Wang, C. Yang, Three-dimensional N-doped graphene as anode material with superior cycle stability for sodium ion batteries, Mater. Lett. 202 (2017) 123–126, https://doi.org/10.1016/j.matlet.2017.05.046.

[114] I. Hasa, J. Hassoun, S. Passerini, Nanostructured Na -ion and Li- ion anodes for battery application: a comparative overview, Nano Res 3 (2017) 12274.

[115] C. Bommier, D. Mitlin, X. Ji, Internal structure – Na storage mechanisms – electrochemical performance relations in carbons, Prog. Mater. Sci. 97 (2018) 170–203, https://doi.org/10.1016/j.pmatsci.2018.04.006.

[116] H. Hou, X. Qiu, W. Wei, Y. Zhang, X. Ji, Carbon anode materials for advanced sodium-ion batteries, Adv. Energy Mater. 7 (2017), https://doi.org/10.1002/aenm.201602898.

[117] R.E. Franklin, Crystallite growth in graphitizing and non-graphitizing carbons, Proc. R. Soc. A Math. Phys. Eng. Sci. 209 (1951) 196–218, https://doi.org/10.1098/rspa.1951.0197.

[118] R.E. Franklin, The structure of graphitic carbons, Acta Crystallogr. 4 (1951) 253–261, https://doi.org/10.1107/S0365110X51000842.

[119] C. Bommier, T.W. Surta, M. Dolgos, X. Ji, New mechanistic insights on Na-ion storage in nongraphitizable carbon, Nano Lett. 15 (2015) 5888–5892, https://doi.org/10.1021/acs.nanolett.5b01969.

[120] J.M. Stratford, P.K. Allan, O. Pecher, P.A. Chater, C.P. Grey, Mechanistic insights into sodium storage in hard carbon anodes using local structure probes, Chem. Commun. 52 (2016) 12430–12433, https://doi.org/10.1039/c6cc06990h.

[121] M. Anji Reddy, M. Helen, A. Groß, M. Fichtner, H. Euchner, Insight into sodium insertion and the storage mechanism in hard carbon, ACS Energy Lett 3 (2018) 2851–2857, https://doi.org/10.1021/acsenergylett.8b01761.

[122] J.R. Dahn, T. Zheng, Y. Liu, J.S. Xue, Mechanisms for lithium insertion in carbonaceous materials, Science 270 (1995) 590–593, https://doi.org/10.1126/science.270.5236.590.

[123] P. Thomas, D. Billaud, Electrochemical insertion of sodium into hard carbons, Electrochim. Acta 47 (2002) 3303–3307, https://doi.org/10.1016/S0013-4686(02)00250-5.

[124] D. Saurel, J. Segalini, M. Jauregui, A. Pendashteh, B. Daffos, P. Simon, M. Casas-Cabanas, A SAXS outlook on disordered carbonaceous materials for electrochemical energy storage, Energy Storage Mater 21 (2019) 162–173, https://doi.org/10.1016/j.ensm.2019.05.007.

[125] B. Jache, P. Adelhelm, Use of graphite as a highly reversible electrode with superior cycle life for sodium-ion batteries by making use of co-intercalation phenomena, Angew. Chem. Int. Ed. 53 (2014) 10169–10173.

[126] Y. Li, Y. Lu, P. Adelhelm, M.M. Titirici, Y.S. Hu, Intercalation chemistry of graphite: alkali metal ions and beyond, Chem. Soc. Rev. 48 (2019) 4655–4687, https://doi.org/10.1039/c9cs00162j.

[127] H.H. Kim, J. Hong, G. Yoon, H.H. Kim, K.-Y. Park, M.-S. Park, W.-S. Yoon, K. Kang, Sodium intercalation chemistry in graphite, Energy Environ. Sci. 8 (2015) 2963–2969, https://doi.org/10.1039/c5ee02051d.

[128] J.F. Peters, A.P. Cruz, M. Weil, Exploring the economic potential of sodium-ion batteries, Batteries 5 (2019), https://doi.org/10.3390/batteries5010010.

[129] K. Song, C. Liu, L. Mi, S. Chou, W. Chen, C. Shen, Recent Progress on the Alloy-Based Anode for Sodium-Ion Batteries and Potassium-Ion Batteries, Small. n/a, 2019, e1903194, https://doi.org/10.1002/smll.201903194.

[130] M. Lao, Y. Zhang, W. Luo, Q. Yan, W. Sun, S.X. Dou, Alloy-based anode materials toward advanced sodium-ion batteries, Adv. Mater. 29 (2017) 1700622, https://doi.org/10.1002/adma.201700622.

[131] W.T. Jing, C.C. Yang, Q. Jiang, Recent progress on metallic Sn- and Sb-based anodes for sodium-ion batteries, J. Mater. Chem. A. 8 (2020) 2913–2933, https://doi.org/10.1039/C9TA11782B.

[132] H. Xie, W.P. Kalisvaart, B.C. Olsen, E.J. Luber, D. Mitlin, J.M. Buriak, Sn–Bi–Sb alloys as anode materials for sodium ion batteries, J. Mater. Chem. A. 5 (2017) 9661–9670, https://doi.org/10.1039/C7TA01443K.

[133] B. Farbod, K. Cui, W.P. Kalisvaart, M. Kupsta, B. Zahiri, A. Kohandehghan, E. M. Lotfabad, Z. Li, E.J. Luber, D. Mitlin, Anodes for sodium ion batteries based on tin–germanium–antimony alloys, ACS Nano 8 (2014) 4415–4429, https://doi.org/10.1021/nn4063598.

[134] W.P. Kalisvaart, B.C. Olsen, E.J. Luber, J.M. Buriak, Sb–Si alloys and multilayers for sodium-ion battery anodes, ACS Appl. Energy Mater. 2 (2019) 2205–2213, https://doi.org/10.1021/acsaem.8b02231.

[135] A. Darwiche, R. Dugas, B. Fraisse, L. Monconduit, Reinstating lead for high-loaded efficient negative electrode for rechargeable sodium-ion battery, J. Power Sources 304 (2016) 1–8, https://doi.org/10.1016/j.jpowsour.2015.10.087.

[136] Y.R. Lim, F. Shojaei, K. Park, C.S. Jung, J. Park, W. Il Cho, H.S. Kang, Arsenic for high-capacity lithium- and sodium-ion batteries, Nanoscale 10 (2018) 7047–7057, https://doi.org/10.1039/C8NR00276B.

[137] H. Morito, T. Yamada, T. Ikeda, H. Yamane, Na–Si binary phase diagram and solution growth of silicon crystals, J. Alloys Compd. 480 (2009) 723–726, https://doi.org/10.1016/j.jallcom.2009.02.036.

[138] Y. Xu, E. Swaans, S. Basak, H.W. Zandbergen, D.M. Borsa, F.M. Mulder, Reversible Na-ion uptake in Si nanoparticles, Adv. Energy Mater. 6 (2016) 1501436, https://doi.org/10.1002/aenm.201501436.

[139] L. Zeng, R. Liu, L. Han, F. Luo, X. Chen, J. Wang, Q. Qian, Q. Chen, M. Wei, Preparation of a Si/SiO2–ordered-mesoporous-carbon nanocomposite as an anode for high-performance lithium-ion and sodium-ion batteries, Chem. Eur J. 24 (2018) 4841–4848, https://doi.org/10.1002/chem.201704780.

[140] Z. Hu, S. Zhang, C. Zhang, G. Cui, High performance germanium-based anode materials, Coord. Chem. Rev. 326 (2016) 34–85, https://doi.org/10.1016/j.ccr.2016.08.002.

[141] L. Baggetto, J.K. Keum, J.F. Browning, G.M. Veith, Germanium as negative electrode material for sodium-ion batteries, Electrochem. Commun. 34 (2013) 41–44, https://doi.org/10.1016/j.elecom.2013.05.025.

[142] Z. Li, J. Ding, D. Mitlin, Tin and tin compounds for sodium ion battery anodes: phase transformations and performance, Acc. Chem. Res. 48 (2015) 1657–1665, https://doi.org/10.1021/acs.accounts.5b00114.

[143] S. Komaba, Y. Matsuura, T. Ishikawa, N. Yabuuchi, W. Murata, S. Kuze, Redox reaction of Sn-polyacrylate electrodes in aprotic Na cell, Electrochem. Commun. 21 (2012) 65–68, https://doi.org/10.1016/j.elecom.2012.05.017.

[144] H. Ying, W.-Q. Han, Metallic Sn-based anode materials: application in high-performance lithium-ion and sodium-ion batteries, Adv. Sci. 4 (2017) 1700298, https://doi.org/10.1002/advs.201700298.

[145] B. Luo, T. Qiu, D. Ye, L. Wang, L. Zhi, Tin nanoparticles encapsulated in graphene backboned carbonaceous foams as high-performance anodes for lithium-ion and sodium-ion storage, Nanomater. Energy 22 (2016) 232–240, https://doi.org/10.1016/j.nanoen.2016.02.024.

[146] R. Mogensen, D. Brandell, R. Younesi, Solubility of the solid electrolyte interphase (SEI) in sodium ion batteries, ACS Energy Lett 1 (2016) 1173–1178.

[147] Y. Xu, Y. Zhu, Y. Liu, C. Wang, Electrochemical performance of porous carbon/tin composite anodes for sodium-ion and lithium-ion batteries, Adv. Energy Mater. 3 (2013) 128–133, https://doi.org/10.1002/aenm.201200346.
[148] M. Mortazavi, Q. Ye, N. Birbilis, N. V Medhekar, High capacity group-15 alloy anodes for Na-ion batteries: electrochemical and mechanical insights, J. Power Sources 285 (2015) 29–36, https://doi.org/10.1016/j.jpowsour.2015.03.051.
[149] W.-J. Li, S.-L. Chou, J.-Z. Wang, H.-K. Liu, S.-X. Dou, Simply mixed commercial red phosphorus and carbon nanotube composite with exceptionally reversible sodium-ion storage, Nano Lett. 13 (2013) 5480–5484, https://doi.org/10.1021/nl403053v.
[150] J. Ni, L. Li, J. Lu, Phosphorus: an anode of choice for sodium-ion batteries, ACS Energy Lett 3 (2018) 1137–1144, https://doi.org/10.1021/acsenergylett.8b00312.
[151] J. Sun, H.-W. Lee, M. Pasta, H. Yuan, G. Zheng, Y. Sun, Y. Li, Y. Cui, A phosphorene–graphene hybrid material as a high-capacity anode for sodium-ion batteries, Nat. Nanotechnol. 10 (2015) 980–985, https://doi.org/10.1038/nnano.2015.194.
[152] Y. Zhang, X. Xia, B. Liu, S. Deng, D. Xie, Q. Liu, Y. Wang, J. Wu, X. Wang, J. Tu, Multiscale graphene-based materials for applications in sodium ion batteries, Adv. Energy Mater. 9 (2019) 1803342, https://doi.org/10.1002/aenm.201803342.
[153] R. Amine, A. Daali, X. Zhou, X. Liu, Y. Liu, Y. Ren, X. Zhang, L. Zhu, S. Al-Hallaj, Z. Chen, G.-L. Xu, K. Amine, A practical phosphorus-based anode material for high-energy lithium-ion batteries, Nanomater. Energy 74 (2020) 104849, https://doi.org/10.1016/j.nanoen.2020.104849.
[154] D. Su, S. Dou, G. Wang, Bismuth: a new anode for the Na-ion battery, Nanomater. Energy 12 (2015) 88–95, https://doi.org/10.1016/j.nanoen.2014.12.012.
[155] S. Liu, J. Feng, X. Bian, J. Liu, H. Xu, The morphology-controlled synthesis of a nanoporous-antimony anode for high-performance sodium-ion batteries, Energy Environ. Sci. 9 (2016) 1229–1236, https://doi.org/10.1039/C5EE03699B.
[156] S. Guo, J. Yi, Y. Sun, H. Zhou, Recent advances in titanium-based electrode materials for stationary sodium-ion batteries, Energy Environ. Sci. 9 (2016) 2978–3006, https://doi.org/10.1039/C6EE01807F.
[157] S. Fang, D. Bresser, S. Passerini, Transition metal oxide anodes for electrochemical energy storage in lithium- and sodium-ion batteries, Adv. Energy Mater. 10 (2020) 1902485, https://doi.org/10.1002/aenm.201902485.
[158] L. Ling, Y. Bai, Y. Li, Q. Ni, Z. Wang, F. Wu, C. Wu, Quick activation of nanoporous anatase TiO2 as high-rate and durable anode materials for sodium-ion batteries, ACS Appl. Mater. Interfaces 9 (2017) 39432–39440, https://doi.org/10.1021/acsami.7b13927.
[159] B. Wang, F. Zhao, G. Du, S. Porter, Y. Liu, P. Zhang, Z. Cheng, H.K. Liu, Z. Huang, Boron-doped anatase TiO2 as a high-performance anode material for sodium-ion batteries, ACS Appl. Mater. Interfaces 8 (2016) 16009–16015, https://doi.org/10.1021/acsami.6b03270.
[160] S. Liu, Z. Cai, J. Zhou, A. Pan, S. Liang, Nitrogen-doped TiO2 nanospheres for advanced sodium-ion battery and sodium-ion capacitor applications, J. Mater. Chem. A. 4 (2016) 18278–18283, https://doi.org/10.1039/C6TA08472A.
[161] M.N. Tahir, B. Oschmann, D. Buchholz, X. Dou, I. Lieberwirth, M. Panthöfer, W. Tremel, R. Zentel, S. Passerini, Extraordinary performance of carbon-coated anatase TiO2 as sodium-ion anode, Adv. Energy Mater. 6 (2016) 1501489, https://doi.org/10.1002/aenm.201501489.
[162] M.M. Doeff, J. Cabana, M. Shirpour, Titanate anodes for sodium ion batteries, J. Inorg. Organomet. Polym. Mater. 24 (2014) 5–14, https://doi.org/10.1007/s10904-013-9977-8.
[163] P. Senguttuvan, G. Rousse, V. Seznec, J.M. Tarascon, M.R. Palacín, Na2Ti3O7: lowest voltage ever reported oxide insertion electrode for sodium ion batteries, Chem. Mater. 23 (2011) 4109–4111, https://doi.org/10.1021/cm202076g.
[164] F. Klein, B. Jache, A. Bhide, P. Adelhelm, Conversion reactions for sodium-ion batteries, Phys. Chem. Chem. Phys. 15 (2013) 15876–15887, https://doi.org/10.1039/c3cp52125g.
[165] M. Zarrabeitia, F. Nobili, M.Á. Muñoz-Márquez, T. Rojo, M. Casas-Cabanas, Direct observation of electronic conductivity transitions and solid electrolyte interphase stability of $Na_2Ti_3O_7$ electrodes for Na-ion batteries, J. Power Sources 330 (2016), https://doi.org/10.1016/j.jpowsour.2016.08.112.
[166] S. Qi, B. Xu, V.T. Tiong, J. Hu, J. Ma, Progress on iron oxides and chalcogenides as anodes for sodium-ion batteries, Chem. Eng. J. 379 (2020) 122261, https://doi.org/10.1016/j.cej.2019.122261.
[167] Q. Zhou, L. Liu, Z. Huang, L. Yi, X. Wang, G. Cao, Co3S4@polyaniline nanotubes as high-performance anode materials for sodium ion batteries, J. Mater. Chem. A. 4 (2016) 5505–5516, https://doi.org/10.1039/C6TA01497F.
[168] Y. Liu, H. Kang, L. Jiao, C. Chen, K. Cao, Y. Wang, H. Yuan, Exfoliated-SnS2 restacked on graphene as a high-capacity, high-rate, and long-cycle life anode for sodium ion batteries, Nanoscale 7 (2015) 1325–1332, https://doi.org/10.1039/C4NR05106H.
[169] Z. Hu, Q. Liu, S.L. Chou, S.X. Dou, Advances and challenges in metal sulfides/selenides for next-generation rechargeable sodium-ion batteries, Adv. Mater. 29 (2017), https://doi.org/10.1002/adma.201700606.
[170] J. Wu, F. Ciucci, J. Kim, Molybdenum disulfide based nanomaterials for rechargeable batteries, Chem. Eur J. 26 (2020) 6296–6319, https://doi.org/10.1002/chem.201905524.
[171] X. Xie, Z. Ao, D. Su, J. Zhang, G. Wang, MoS2/graphene composite anodes with enhanced performance for sodium-ion batteries: the role of the two-dimensional heterointerface, Adv. Funct. Mater. 25 (2015) 1393–1403, https://doi.org/10.1002/adfm.201404078.
[172] C. Zhu, X. Mu, P.A. Vanaken, Y. Yu, J. Maier, Single-layered ultrasmall nanoplates of MoS2 embedded in carbon nanofibers with excellent electrochemical performance for lithium and sodium storage, Angew. Chem. Int. Ed. 53 (2014) 2152–2156, https://doi.org/10.1002/anie.201308354.
[173] W. Qin, T. Chen, L. Pan, L. Niu, B. Hu, D. Li, J. Li, Z. Sun, MoS2-reduced graphene oxide composites via microwave assisted synthesis for sodium ion battery anode with improved capacity and cycling performance, Electrochim. Acta 153 (2015) 55–61, https://doi.org/10.1016/j.electacta.2014.11.034.
[174] Y. Li, Y. Liang, F.C. Robles Hernandez, H. Deog Yoo, Q. An, Y. Yao, Enhancing sodium-ion battery performance with interlayer-expanded MoS2-PEO nanocomposites, Nanomater. Energy 15 (2015) 453–461, https://doi.org/10.1016/j.nanoen.2015.05.012.
[175] Q. Xia, W. Li, Z. Miao, S. Chou, H. Liu, Phosphorus and phosphide nanomaterials for sodium-ion batteries, Nano Res 10 (2017) 4055–4081, https://doi.org/10.1007/s12274-017-1671-7.
[176] Y. Kim, Y. Kim, A. Choi, S. Woo, D. Mok, N.-S. Choi, Y.S. Jung, J.H. Ryu, S.M. Oh, K.T. Lee, Tin phosphide as a promising anode material for Na-ion batteries, Adv. Mater. 26 (2014) 4139–4144, https://doi.org/10.1002/adma.201305638.
[177] G.G. Eshetu, G.A. Elia, M. Armand, M. Forsyth, S. Komaba, T. Rojo, S. Passerini, Electrolytes and interphases in sodium-based rechargeable batteries: recent advances and perspectives, Adv. Energy Mater. 2000093 (2020) 2000093, https://doi.org/10.1002/aenm.202000093.
[178] M.A. Muñoz-Márquez, M. Zarrabeitia, E. Castillo-Martínez, A. Eguía-Barrio, T. Rojo, M. Casas-Cabanas, Composition and evolution of the solid-electrolyte interphase in Na2Ti3O7 electrodes for Na-Ion batteries: XPS and auger parameter analysis, ACS Appl. Mater. Interfaces 7 (2015) 7801–7808, https://doi.org/10.1021/acsami.5b01375.
[179] a. Ponrouch, D. Monti, a. Boschin, B. Steen, P. Johansson, M.R. Palacín, Non-aqueous electrolytes for sodium-ion batteries, J. Mater. Chem. A. 3 (2015) 22–42, https://doi.org/10.1039/C4TA04428B.
[180] J. Jornè, C.W. Tobias, Electrodeposition of the alkali metals from propylene carbonate, J. Appl. Electrochem. 5 (1975) 279–290.
[181] F. Klein, R. Pinedo, P. Hering, A. Polity, J. Janek, P. Adelhelm, Reaction mechanism and surface film formation of conversion materials for lithium- and sodium-ion batteries: an XPS case study on sputtered copper oxide (CuO) thin film model electrodes, J. Phys. Chem. C 120 (2016) 1400–1414, https://doi.org/10.1021/acs.jpcc.5b10642.
[182] K. Kubota, S. Komaba, Review—practical issues and future perspective for Na-ion batteries, J. Electrochem. Soc. 162 (2015) A2538–A2550, https://doi.org/10.1149/2.0151514jes.
[183] G. Yan, D. Alves-Dalla-Corte, W. Yin, N. Madern, G. Gachot, J.-M. Tarascon, Assessment of the electrochemical stability of carbonate-based electrolytes in Na-ion batteries, J. Electrochem. Soc. 165 (2018) A1222–A1230, https://doi.org/10.1149/2.0311807jes.
[184] S. Komaba, T. Ishikawa, N. Yabuuchi, W. Murata, A. Ito, Y. Ohsawa, Fluorinated ethylene carbonate as electrolyte additive for rechargeable Na batteries, ACS Appl. Mater. Interfaces 3 (2011) 4165–4168.
[185] B. Mortemard De Boisse, J.H. Cheng, D. Carlier, M. Guignard, C.J. Pan, S. Bordère, D. Filimonov, C. Drathen, E. Suard, B.J. Hwang, A. Wattiaux, C. Delmas, O3-NaxMn1/3Fe2/3O2 as a positive electrode material for Na-ion batteries: structural evolutions and redox mechanisms upon Na+ (de) intercalation, J. Mater. Chem. A. 3 (2015) 10976–10989, https://doi.org/10.1039/c4ta06688j.
[186] A. Darwiche, C. Marino, M.T. Sougrati, B. Fraisse, L. Stievano, L. Monconduit, Better cycling performances of bulk sb in na-ion batteries compared to li-ion systems: an unexpected electrochemical mechanism, J. Am. Chem. Soc. 134 (2012) 20805–20811, https://doi.org/10.1021/ja310347x.
[187] M. Zarrabeitia, M. Muñoz-Márquez, F. Nobili, T. Rojo, M. Casas-Cabanas, Influence of using metallic Na on the interfacial and transport properties of Na-ion batteries, Batteries 3 (2017) 16, https://doi.org/10.3390/batteries3020016.
[188] G.G. Eshetu, S. Grugeon, H. Kim, S. Jeong, L. Wu, G. Gachot, S. Laruelle, M. Armand, S. Passerini, Comprehensive insights into the reactivity of electrolytes based on sodium ions, ChemSusChem 9 (2016) 462–471.
[189] R. Dugas, A. Ponrouch, G. Gachot, R. David, M.R. Palacin, J.M. Tarascon, Na reactivity toward carbonate-based electrolytes: the effect of FEC as additive, J. Electrochem. Soc. 163 (2016) A2333–A2339, https://doi.org/10.1149/2.0981610jes.
[190] G. Yan, K. Reeves, D. Foix, Z. Li, C. Cometto, S. Mariyappan, M. Salanne, J. Tarascon, A new electrolyte formulation for securing high temperature cycling and storage performances of Na-ion batteries, Adv. Energy Mater. 9 (2019) 1901431, https://doi.org/10.1002/aenm.201901431.
[191] M. Goktas, C. Bolli, J. Buchheim, E.J. Berg, P. Novák, F. Bonilla, T. Rojo, S. Komaba, K. Kubota, P. Adelhelm, Stable and unstable diglyme-based electrolytes for batteries with sodium or graphite as electrode, ACS Appl. Mater. Interfaces 11 (2019) 32844–32855, https://doi.org/10.1021/acsami.9b06760.
[192] Z.W. Seh, J. Sun, Y. Sun, Y. Cui, A highly reversible room-temperature sodium metal anode, ACS Cent. Sci. 1 (2015) 449–455, https://doi.org/10.1021/acscentsci.5b00328.
[193] J. Li, D. Yan, T. Lu, W. Qin, Y. Yao, L. Pan, Significantly improved sodium-ion storage performance of cus nanosheets anchored into reduced graphene oxide with ether-based electrolyte, ACS Appl. Mater. Interfaces 9 (2017) 2309–2316, https://doi.org/10.1021/acsami.6b12529.
[194] C. Wang, L. Wang, F. Li, F. Cheng, J. Chen, Bulk bismuth as a high-capacity and ultralong cycle-life anode for sodium-ion batteries by coupling with glyme-based electrolytes, Adv. Mater. 29 (2017) 1–7, https://doi.org/10.1002/adma.201702212.
[195] T. Palaniselvam, M. Goktas, B. Anothumakkool, Y. Sun, R. Schmuch, L. Zhao, B. Han, M. Winter, P. Adelhelm, Sodium storage and electrode dynamics of

tin–carbon composite electrodes from bulk precursors for sodium-ion batteries, Adv. Funct. Mater. 29 (2019) 1900790, https://doi.org/10.1002/adfm.201900790.
[196] B. Zhang, G. Rousse, D. Foix, R. Dugas, D.A.D. Corte, J.M. Tarascon, Microsized Sn as advanced anodes in glyme-based electrolyte for Na-ion batteries, Adv. Mater. 28 (2016) 9824–9830, https://doi.org/10.1002/adma.201603212.
[197] K. Li, J. Zhang, D. Lin, D.W. Wang, B. Li, W. Lv, S. Sun, Y.B. He, F. Kang, Q. H. Yang, L. Zhou, T.Y. Zhang, Evolution of the electrochemical interface in sodium ion batteries with ether electrolytes, Nat. Commun. 10 (2019) 1–10, https://doi.org/10.1038/s41467-019-08506-5.
[198] K. Westman, R. Dugas, P. Jankowski, W. Wieczorek, G. Gachot, M. Morcrette, E. Irisarri, A. Ponrouch, M.R. Palacín, J.M. Tarascon, P. Johansson, Diglyme based electrolytes for sodium-ion batteries, ACS Appl. Energy Mater. 1 (2018) 2671–2680, https://doi.org/10.1021/acsaem.8b00360.
[199] W. Brehm, J.R. Buchheim, P. Adelhelm, Reactive and nonreactive ball milling of tin-antimony (Sn-Sb) composites and their use as electrodes for sodium-ion batteries with glyme electrolyte, Energy Technol. 7 (2019) 1900389, https://doi.org/10.1002/ente.201900389.
[200] G.A. Giffin, Ionic liquid-based electrolytes for "beyond lithium" battery technologies, J. Mater. Chem. A. 4 (2016) 13378–13389, https://doi.org/10.1039/C6TA05260F.
[201] R.D. Rogers, K.R. Seddon, Ionic liquids- solvent of the future? Science 84 302 (2003) 792–793.
[202] H. Zhang, I. Hasa, D. Buchholz, B. Qin, D. Geiger, S. Jeong, U. Kaiser, S. Passerini, Exploring the Ni redox activity in polyanionic compounds as conceivable high potential cathodes for Na rechargeable batteries, NPG Asia Mater. 9 (2017), e370.
[203] L.G. Chagas, D. Buchholz, L. Wu, B. Vortmann, S. Passerini, Unexpected performance of layered sodium-ion cathode material in ionic liquid-based electrolyte, J. Power Sources 247 (2014) 377–383.
[204] L.G. Chagas, S. Jeong, I. Hasa, S. Passerini, Ionic liquid-based electrolytes for sodium-ion batteries: tuning properties to enhance the electrochemical performance of manganese-based layered oxide cathode, ACS Appl. Mater. Interfaces 11 (2019) 22278–22289, https://doi.org/10.1021/acsami.9b03813.
[205] M. Zarrabeitia, L. Gomes Chagas, M. Kuenzel, E. Gonzalo, T. Rojo, S. Passerini, M.Á. Muñoz-Márquez, Toward stable electrode/electrolyte interface of P2-layered oxide for rechargeable Na-ion batteries, ACS Appl. Mater. Interfaces 11 (2019) 28885–28893, https://doi.org/10.1021/acsami.9b07963.
[206] M. Hilder, P.C. Howlett, D. Saurel, H. Anne, M. Casas-Cabanas, M. Armand, T. Rojo, D.R. MacFarlane, M. Forsyth, Stable cycling of NaFePO4 cathodes in high salt concentration ionic liquid electrolytes, J. Power Sources 406 (2018) 70–80, https://doi.org/10.1016/j.jpowsour.2018.09.102.
[207] C. Ding, T. Nohira, R. Hagiwara, A. Fukunaga, S. Sakai, K. Nitta, Electrochemical performance of hard carbon negative electrodes for ionic liquid-based sodium ion batteries over a wide temperature range, Electrochim. Acta 176 (2015) 344–349, https://doi.org/10.1016/j.electacta.2015.07.024.
[208] I. Hasa, S. Passerini, J. Hassoun, Characteristics of an ionic liquid electrolyte for sodium-ion batteries, in: J. Power Sources, 2016, pp. 203–207.
[209] L. Wu, A. Moretti, D. Buchholz, S. Passerini, D. Bresser, Combining ionic liquid-based electrolytes and nanostructured anatase TiO2 anodes for intrinsically safer sodium-ion batteries, Electrochim. Acta 203 (2016) 109–116, https://doi.org/10.1016/j.electacta.2016.03.124.
[210] M. De Francesco, E. Simonetti, G. Gorgi, G. Appetecchi, About the purification route of ionic liquid precursors, Challenges 8 (2017) 11, https://doi.org/10.3390/challe8010011.
[211] X. Wang, E. Yasukawa, S. Kasuya, Nonflammable trimethyl phosphate solvent-containing electrolytes for lithium-ion batteries: I. Fundamental properties, J. Electrochem. Soc. 148 (2001) A1058, https://doi.org/10.1149/1.1397773.
[212] X. Zheng, Z. Gu, X. Liu, Z. Wang, J. Wen, X. Wu, W. Luo, Y. Huang, Bridging the immiscibility of an all-fluoride fire extinguishant with highly-fluorinated electrolytes toward safe sodium metal batteries, Energy Environ. Sci. 13 (2020) 1788–1798, https://doi.org/10.1039/d0ee00694g.
[213] J. Wang, Y. Yamada, K. Sodeyama, E. Watanabe, K. Takada, Y. Tateyama, A. Yamada, Fire-extinguishing organic electrolytes for safe batteries, Nat. Energy. 3 (2018) 22–29, https://doi.org/10.1038/s41560-017-0033-8.
[214] J. Wu, J. Liu, Z. Lu, K. Lin, Y.Q. Lyu, B. Li, F. Ciucci, J.K. Kim, Non-flammable electrolyte for dendrite-free sodium-sulfur battery, Energy Storage Mater 23 (2019) 8–16, https://doi.org/10.1016/j.ensm.2019.05.045.
[215] D. Bin, F. Wang, A.G. Tamirat, L. Suo, Y. Wang, C. Wang, Y. Xia, Progress in aqueous rechargeable sodium-ion batteries, Adv. Energy Mater. 8 (2018) 1–31, https://doi.org/10.1002/aenm.201703008.
[216] R. Demir-Cakan, M.R. Palacin, L. Croguennec, Rechargeable aqueous electrolyte batteries: from univalent to multivalent cation chemistry, J. Mater. Chem. A. 7 (2019) 20519–20539, https://doi.org/10.1039/c9ta04735b.
[217] J.Y. Luo, W.J. Cui, P. He, Y.Y. Xia, Raising the cycling stability of aqueous lithium-ion batteries by eliminating oxygen in the electrolyte, Nat. Chem. 2 (2010) 760–765, https://doi.org/10.1038/nchem.763.
[218] A.J. Fernández-Ropero, M.J. Piernas-Muñoz, E. Castillo-Martínez, T. Rojo, M. Casas-Cabanas, Electrochemical characterization of NaFe2(CN)6 Prussian Blue as positive electrode for aqueous sodium-ion batteries, Electrochim. Acta 210 (2016) 352–357, https://doi.org/10.1016/j.electacta.2016.05.176.
[219] Z. Li, D. Young, K. Xiang, W.C. Carter, Y.-M. Chiang, Towards high power high energy aqueous sodium-ion batteries: the NaTi 2 (PO 4) 3/Na 0.44 MnO 2 system, Adv. Energy Mater. 3 (2013) 290–294, https://doi.org/10.1002/aenm.201200598.
[220] L. Suo, O. Borodin, T. Gao, M. Olguin, J. Ho, X. Fan, C. Luo, C. Wang, K. Xu, "Water-in-salt" electrolyte enables high-voltage aqueous lithium-ion chemistries, Science 350 (2015) 938–943, https://doi.org/10.1126/science.aab1595.
[221] H. Zhang, X. Liu, H. Li, I. Hasa, S. Passerini, Challenges and strategies for high-energy aqueous electrolyte rechargeable batteries, Angew. Chem. Int. Ed. (2020), https://doi.org/10.1002/anie.202004433.
[222] H. Zhang, S. Jeong, B. Qin, D. Vieira Carvalho, D. Buchholz, S. Passerini, Towards high-performance aqueous sodium-ion batteries: stabilizing the solid/liquid interface for NASICON-type Na2VTi(PO4)3 using concentrated electrolytes, ChemSusChem 11 (2018) 1382–1389, https://doi.org/10.1002/cssc.201800194.
[223] A. Ponrouch, E. Marchante, M. Courty, J.-M. Tarascon, M.R. Palacín, In search of an optimized electrolyte for Na-ion batteries, Energy Environ. Sci. 5 (2012) 8572–8583.
[224] A. Bhide, J. Hofmann, A.K. Dürr, J. Janek, P. Adelhelm, Electrochemical stability of non-aqueous electrolytes for sodium-ion batteries and their compatibility with Na(0.7)CoO2, Phys. Chem. Chem. Phys. 16 (2014) 1987–1998.
[225] C.-H. Wang, Y.-W. Yeh, N. Wongittharom, Y.-C. Wang, C.-J. Tseng, S.-W. Lee, W.-S. Chang, J.-K. Chang, Rechargeable Na/Na0.44MnO2 cells with ionic liquid electrolytes containing various sodium solutes, J. Power Sources 274 (2015) 1016–1023.
[226] W. Wu, S. Shabhag, J. Chang, A. Rutt, J.F. Whitacre, Relating electrolyte concentration to performance and stability for NaTi 2 (PO 4) 3/Na 0.44 MnO 2 aqueous sodium-ion batteries, J. Electrochem. Soc. 162 (2015) A803–A808, https://doi.org/10.1149/2.0121506jes.
[227] H. Zhang, B. Qin, J. Han, S. Passerini, Aqueous/Nonaqueous hybrid electrolyte for sodium-ion batteries, ACS Energy Lett 3 (2018) 1769–1770, https://doi.org/10.1021/acsenergylett.8b00919.
[228] R.S. Kühnel, D. Reber, C. Battaglia, A high-voltage aqueous electrolyte for sodium-ion batteries, ACS Energy Lett 2 (2017) 2005–2006, https://doi.org/10.1021/acsenergylett.7b00623.
[229] J. Janek, W.G. Zeier, A solid future for battery development, Nat. Energy. 1 (2016), https://doi.org/10.1038/nenergy.2016.141.
[230] W.Z.S. Ohno, A. Bamnik, Materials design of ionic conductors for solid state batteries, Prog. Energy. 2 (2020).
[231] Q. Zhao, S. Stalin, C.-Z. Zhao, L.A. Archer, Designing solid-state electrolytes for safe, energy-dense batteries, Nat. Rev. Mater. 5 (2020) 229–252, https://doi.org/10.1038/s41578-019-0165-5.
[232] Z. Zhang, Y. Shao, B. Lotsch, Y.S. Hu, H. Li, J. Janek, L.F. Nazar, C.W. Nan, J. Maier, M. Armand, L. Chen, New horizons for inorganic solid state ion conductors, Energy Environ. Sci. 11 (2018), https://doi.org/10.1039/c8ee01053f.
[233] C. Zhao, L. Liu, X. Qi, Y. Lu, F. Wu, J. Zhao, Y. Yu, Y. Hu, L. Chen, Solid-State Sodium Batteries (1703012) (2018) 14–16, https://doi.org/10.1002/aenm.201703012.
[234] Y. Wang, S. Song, C. Xu, N. Hu, J. Molenda, L. Lu, Development of solid-state electrolytes for sodium-ion battery–A short review, Nano Mater. Sci. 1 (2019) 91–100, https://doi.org/10.1016/j.nanoms.2019.02.007.
[235] L. Qiao, X. Judez, M. Armand, H. Zhang, Review-polymer electrolytes for sodium batteries, J. Electrochem. Soc. 167 (2020), 070534, https://doi.org/10.1149/1945-7111/ab7aa0.
[236] K. West, A rechargeable all-solid-state sodium cell with polymer electrolyte, J. Electrochem. Soc. 132 (1985) 3061, https://doi.org/10.1149/1.2113725.
[237] G. Yamaguchi, K. Suzuki, On the structures of alkali polyaluminates, Bull. Chem. Soc. Jpn. 41 (1968) 93–99, https://doi.org/10.1246/bcsj.41.93.
[238] J.T. Kummer, W. Neill, Battery Having a Molten Alkali Metal Anode and a Molten Sulfur Cathode, 1968.
[239] K.B. Hueso, M. Armand, T. Rojo, High Temperature Sodium Batteries: Status, Challenges and Future Trends, The Royal Society of Chemistry, 2013, https://doi.org/10.1039/c3ee24086j.
[240] T. Famprikis, P. Canepa, J.A. Dawson, M.S. Islam, C. Masquelier, Fundamentals of inorganic solid-state electrolytes for batteries, Nat. Mater. (2019), https://doi.org/10.1038/s41563-019-0431-3.
[241] J.B. Goodenough, H.Y.P. Hong, J.A. Kafalas, Fast Na+ - Ion Transport in Skeleton Structures 11 (1976) 203–220.
[242] H.Y.P. Hong, Crystal structures and crystal chemistry in the system Na1+ xZr2SixP3-xO12, Mater. Res. Bull. 11 (1976) 173–182, https://doi.org/10.1016/0025-5408(76)90073-8.
[243] Y. Deng, C. Eames, L.H.B. Nguyen, O. Pecher, K.J. Griffith, M. Courty, B. Fleutot, J.-N. Chotard, C.P. Grey, M.S. Islam, C. Masquelier, Crystal structures, local atomic environments and ion diffusion mechanisms of scandium-substituted NASICON solid electrolytes, Chem. Mater. 30 (2018) 2618–2630, https://doi.org/10.1021/acs.chemmater.7b05237.
[244] S. Lunghammer, D. Prutsch, S. Breuer, D. Rettenwander, I. Hanzu, Q. Ma, F. Tietz, Fast Na ion transport triggered by rapid ion exchange on local length scales, Sci. Rep. (2018) 1–8, https://doi.org/10.1038/s41598-018-30478-7.
[245] Z. Zhang, Z. Zou, K. Kaup, R. Xiao, S. Shi, M. Avdeev, Y. Hu, D. Wang, B. He, H. Li, Correlated migration invokes higher Na+-Ion conductivity in NaSICON-type solid electrolytes, Adv. Energy Mater. 9 (2019) 1902373.
[246] Y. Shao, G. Zhong, Y. Lu, L. Liu, C. Zhao, Q. Zhang, Y.-S. Hu, Y. Yang, L. Chen, A novel NASICON-based glass-ceramic composite electrolyte with enhanced Na-ion conductivity, Energy Storage Mater 23 (2019) 514–521.
[247] F. Lalère, J.B. Leriche, M. Courty, S. Boulineau, V. Viallet, C. Masquelier, V. Seznec, An all-solid state NASICON sodium battery operating at 200 °C, J. Power Sources 247 (2014) 975–980, https://doi.org/10.1016/j.jpowsour.2013.09.051.

[248] Y. Noguchi, E. Kobayashi, L.S. Plashnitsa, S. Okada, J.I. Yamaki, Fabrication and performances of all solid-state symmetric sodium battery based on NASICON-related compounds, Electrochim. Acta 101 (2013) 59–65, https://doi.org/10.1016/j.electacta.2012.11.038.

[249] M. Jansen, U. Henseler, Synthesis, structure determination, and ionic conductivity of sodium tetrathiophosphate, J. Solid State Chem. 99 (1992) 110–119, https://doi.org/10.1016/0022-4596(92)90295-7.

[250] A. Hayashi, K. Noi, A. Sakuda, M. Tatsumisago, Superionic glass-ceramic electrolytes for room-temperature rechargeable sodium batteries, Nat. Commun. 3 (2012) 856, https://doi.org/10.1038/ncomms1843.

[251] N. Tanibata, K. Noi, A. Hayashi, N. Kitamura, Y. Idemoto, M. Tatsumisago, X-ray crystal structure analysis of sodium-ion conductivity in 94 Na_3PS_4·6 Na_4SiS_4 glass-ceramic electrolytes, ChemElectroChem 1 (2014) 1130–1132, https://doi.org/10.1002/celc.201402016.

[252] H. Wang, Y. Chen, Z.D. Hood, G. Sahu, A.S. Pandian, J.K. Keum, K. An, C. Liang, An air-stable Na3SbS4 superionic conductor prepared by a rapid and economic synthetic procedure, Angew. Chem. Int. Ed. 55 (2016) 8551–8555.

[253] W.D. Richards, T. Tsujimura, L.J. Miara, Y. Wang, J.C. Kim, S.P. Ong, I. Uechi, N. Suzuki, G. Ceder, Design and synthesis of the superionic conductor Na10SnP2S12, Nat. Commun. 7 (2016) 11009, https://doi.org/10.1038/ncomms11009.

[254] Z. Zhang, E. Ramos, F. Lalère, A. Assoud, K. Kaup, P. Hartman, L.F. Nazar, $Na_{11}Sn_2PS_{12}$: a new solid state sodium superionic conductor, Energy Environ. Sci. 11 (2018) 87–93, https://doi.org/10.1039/C7EE03083E.

[255] E.P. Ramos, Z. Zhang, A. Assoud, K. Kaup, F. Lalere, L.F. Nazar, Correlating ion mobility and single crystal structure in sodium-ion chalcogenide-based solid state fast ion conductors: Na11Sn2PnS12 (Pn= Sb, P), Chem. Mater. 12 (2018) 8b02077, https://doi.org/10.1021/acs.chemmater.8b02077, acs.chemmater.

[256] M. Duchardt, U. Ruschewitz, S. Adams, S. Dehnen, B. Roling, Vacancy-controlled Na+ superion conduction in Na11Sn2PS12, Angew. Chem. Int. Ed. 57 (2018), https://doi.org/10.1002/anie.201712769.

[257] A. Hayashi, N. Masuzawa, S. Yubuchi, F. Tsuji, C. Hotehama, A. Sakuda, M. Tatsumisago, A sodium-ion sulfide solid electrolyte with unprecedented conductivity at room temperature, Nat. Commun. 10 (2019) 5266, https://doi.org/10.1038/s41467-019-13178-2.

[258] A.L. Santhosha, L. Medenbach, T. Palaniselvam, P. Adelhelm, Sodium-storage behavior of exfoliated MoS 2 as an electrode material for solid-state batteries with Na 3 PS 4 as the solid electrolyte, J. Phys. Chem. C 124 (2020) 10298–10305, https://doi.org/10.1021/acs.jpcc.0c00387.

[259] S. Takeuchi, K. Suzuki, M. Hirayama, R. Kanno, Sodium superionic conduction in tetragonal Na_3PS_4, J. Solid State Chem. 265 (2018) 353–358, https://doi.org/10.1016/j.jssc.2018.06.023.

[260] T. Famprikis, J.A. Dawson, F. Fauth, O. Clemens, E. Suard, B. Fleutot, M. Courty, J.-N. Chotard, M.S. Islam, C. Masquelier, A new superionic plastic polymorph of the Na^+ conductor Na_3PS_4, ACS Mater. Lett. 1 (2019) 641–646, https://doi.org/10.1021/acsmaterialslett.9b00322.

[261] N.J.J. De Klerk, M. Wagemaker, Diffusion mechanism of the sodium-ion solid electrolyte Na_3PS_4 and potential improvements of halogen doping, Chem. Mater. 28 (2016) 3122–3130, https://doi.org/10.1021/acs.chemmater.6b00698.

[262] S.-H. Bo, Y. Wang, G. Ceder, Structural and Na-ion conduction characteristics of $Na_3PS_xSe_{4-x}$, J. Mater. Chem. A. 4 (2016) 9044–9053, https://doi.org/10.1039/C6TA03027K.

[263] T. Krauskopf, S. Muy, S.P. Culver, S. Ohno, O. Delaire, Y. Shao-Horn, W.G. Zeier, Comparing the descriptors for investigating the influence of lattice dynamics on ionic transport using the superionic conductor Na_3PS_{4-x} se_x, J. Am. Chem. Soc. 140 (2018) 14464–14473, https://doi.org/10.1021/jacs.8b09340.

[264] A. Banerjee, K.H. Park, J.W. Heo, Y.J. Nam, C.K. Moon, S.M. Oh, S. Hong, Y. S. Jung, Na3SbS4: a solution processable sodium superionic conductor for all-solid-state sodium-ion batteries, Angew. Chem. Int. Ed. 55 (2016) 9634–9638.

[265] M. Uematsu, S. Yubuchi, F. Tsuji, A. Sakuda, A. Hayashi, M. Tatsumisago, Suspension synthesis of Na3-PS4-Cl solid electrolytes, J. Power Sources 428 (2019) 131–135, https://doi.org/10.1016/j.jpowsour.2019.04.069.

[266] T. Krauskopf, S.P. Culver, W.G. Zeier, Local tetragonal structure of the cubic superionic conductor Na 3 PS 4, Inorg. Chem. 57 (2018) 4739–4744, https://doi.org/10.1021/acs.inorgchem.8b00458.

[267] N. Kamaya, K. Homma, Y. Yamakawa, M. Hirayama, R. Kanno, M. Yonemura, T. Kamiyama, Y. Kato, S. Hama, K. Kawamoto, A. Mitsui, A lithium superionic conductor, Nat. Mater. 10 (2011) 682–686, https://doi.org/10.1038/nmat3066.

[268] Z. Zhang, P.-N. Roy, H. Li, M. Avdeev, L.F. Nazar, Coupled cation–anion dynamics enhances cation mobility in room-temperature superionic solid-state electrolytes, J. Am. Chem. Soc. 141 (2019) 19360–19372, https://doi.org/10.1021/jacs.9b09343.

[269] K. Oh, D. Chang, I. Park, K. Yoon, K. Kang, First-Principles investigations on sodium superionic conductor Na11Sn2PS12, Chem. Mater. 31 (2019) 6066–6075, https://doi.org/10.1021/acs.chemmater.8b04965.

[270] A. Sorkin, S. Adams, First-principles study of superionic Na 9+ x Sn x M 3-x S 12 (M= P, Sb), Mater. Adv. (2020).

[271] A. Remhof, Z. Łodziana, F. Buchter, P. Martelli, F. Pendolino, O. Friedrichs, A. Züttel, J.P. Embs, Rotational diffusion in NaBH4, J. Phys. Chem. C 113 (2009) 16834–16837, https://doi.org/10.1021/jp906174e.

[272] T.J. Udovic, M. Matsuo, A. Unemoto, N. Verdal, V. Stavila, A.V. Skripov, J. J. Rush, H. Takamura, S.I. Orimo, Sodium superionic conduction in Na2B12H12, Chem. Commun. 50 (2014) 3750–3752, https://doi.org/10.1039/c3cc49805k.

[273] M. Matsuo, H. Oguchi, T. Sato, H. Takamura, E. Tsuchida, T. Ikeshoji, S. Orimo, Sodium and magnesium ionic conduction in complex hydrides, J. Alloys Compd. 580 (2013) S98–S101.

[274] Y. Sadikin, P. Schouwink, M. Brighi, Z. Łodziana, R. Černý, Modified anion packing of $Na_2B_{12}H_{12}$ in close to room temperature superionic conductors, Inorg. Chem. 56 (2017) 5006–5016, https://doi.org/10.1021/acs.inorgchem.7b00013.

[275] A. Unemoto, M. Matsuo, S.I. Orimo, Complex hydrides for electrochemical energy storage, Adv. Funct. Mater. 24 (2014) 2267–2279, https://doi.org/10.1002/adfm.201303147.

[276] W.S. Tang, A. Unemoto, W. Zhou, V. Stavila, M. Matsuo, H. Wu, S.I. Orimo, T. J. Udovic, Unparalleled lithium and sodium superionic conduction in solid electrolytes with large monovalent cage-like anions, Energy Environ. Sci. 8 (2015) 3637–3645, https://doi.org/10.1039/c5ee02941d.

[277] L. Duchene, R.-S. Kuhnel, D. Rentsch, A. Remhof, H. Hagemann, C. Battaglia, A highly stable sodium solid-state electrolyte based on a dodeca/deca-borate equimolar mixture, Chem. Commun. 1 (2017), https://doi.org/10.1039/C7CC00794A.

[278] K. Yoshida, T. Sato, A. Unemoto, M. Matsuo, T. Ikeshoji, T.J. Udovic, S. Orimo, Fast sodium ionic conduction in $Na_2B_{10}H_{10}$-$Na_2B_{12}H_{12}$ pseudo-binary complex hydride and application to a bulk-type all-solid-state battery, Appl. Phys. Lett. 110 (2017) 103901, https://doi.org/10.1063/1.4977885.

[279] L. Duchêne, S. Lunghammer, T. Burankova, W.-C. Liao, J.P. Embs, C. Copéret, H. M.R. Wilkening, A. Remhof, H. Hagemann, C. Battaglia, Ionic conduction mechanism in the $Na_2(B_{12}H_{12})_{0.5}$ $(B_{10}H_{10})_{0.5}$ closo -borate solid-state electrolyte: interplay of disorder and ion–ion interactions, Chem. Mater. 31 (2019) 3449–3460, https://doi.org/10.1021/acs.chemmater.9b00610.

[280] L. Duchêne, R.S. Kühnel, E. Stilp, E. Cuervo Reyes, A. Remhof, H. Hagemann, C. Battaglia, A stable 3 v all-solid-state sodium-ion battery based on a closo-borate electrolyte, Energy Environ. Sci. 10 (2017) 2609–2615, https://doi.org/10.1039/c7ee02420g.

[281] F. Murgia, M. Brighi, R. Černý, Room-temperature-operating Na solid-state battery with complex hydride as electrolyte, Electrochem. Commun. 106 (2019) 106534, https://doi.org/10.1016/j.elecom.2019.106534.

[282] Y. Sun, Y. Wang, X. Liang, Y. Xia, L. Peng, H. Jia, H. Li, L. Bai, J. Feng, H. Jiang, J. Xie, Rotational cluster Anion enabling superionic conductivity in sodium-rich antiperovskite Na3OBH4, J. Am. Chem. Soc. 141 (2019) 5640–5644, https://doi.org/10.1021/jacs.9b01746.

[283] E. Ahiavi, J.A. Dawson, U. Kudu, M. Courty, M.S. Islam, O. Clemens, C. Masquelier, T. Famprikis, Mechanochemical synthesis and ion transport properties of Na3OX (X = Cl, Br, I and BH4) antiperovskite solid electrolytes, J. Power Sources 471 (2020) 228489, https://doi.org/10.1016/j.jpowsour.2020.228489.

[284] P. Adelhelm, P. Hartmann, C.L. Bender, M. Busche, C. Eufinger, J. Janek, From lithium to sodium: cell chemistry of room temperature sodium-air and sodium-sulfur batteries, Beilstein J. Nanotechnol. 6 (2015) 1016–1055, https://doi.org/10.3762/bjnano.6.105.

[285] K.W. Semkow, A lithium oxygen secondary battery, J. Electrochem. Soc. 134 (1987) 2084, https://doi.org/10.1149/1.2100826.

[286] K.M. Abraham, A polymer electrolyte-based rechargeable lithium/oxygen battery, J. Electrochem. Soc. 143 (1996) 1, https://doi.org/10.1149/1.1836378.

[287] E. Peled, D. Golodnitsky, H. Mazor, M. Goor, S. Avshalomov, Parameter analysis of a practical lithium- and sodium-air electric vehicle battery, J. Power Sources 196 (2011) 6835–6840, https://doi.org/10.1016/j.jpowsour.2010.09.104.

[288] Q. Sun, Y. Yang, Z.W. Fu, Electrochemical properties of room temperature sodium-air batteries with non-aqueous electrolyte, Electrochem. Commun. 16 (2012) 22–25, https://doi.org/10.1016/j.elecom.2011.12.019.

[289] P. Hartmann, C.L. Bender, M. Vračar, A.K. Dürr, A. Garsuch, J. Janek, P. Adelhelm, A rechargeable room-temperature sodium superoxide (NaO2) battery, Nat. Mater. 12 (2013) 228–232, https://doi.org/10.1038/nmat3486.

[290] R.E. Williford, J.G. Zhang, Air electrode design for sustained high power operation of Li/air batteries, J. Power Sources 194 (2009) 1164–1170, https://doi.org/10.1016/j.jpowsour.2009.06.005.

[291] K.G. Gallagher, S. Goebel, T. Greszler, M. Mathias, W. Oelerich, D. Eroglu, V. Srinivasan, Quantifying the promise of lithium-air batteries for electric vehicles, Energy Environ. Sci. 7 (2014) 1555–1563, https://doi.org/10.1039/c3ee43870h.

[292] S.A. Freunberger, True performance metrics in beyond-intercalation batteries, Nat. Energy. 2 (2017) 1–4, https://doi.org/10.1038/nenergy.2017.91.

[293] B.D. McCloskey, D.S. Bethune, R.M. Shelby, G. Girishkumar, A.C. Luntz, Solvents critical role in nonaqueous Lithium-Oxygen battery electrochemistry, J. Phys. Chem. Lett. 2 (2011) 1161–1166, https://doi.org/10.1021/jz200352v.

[294] R. Pinedo, D.A. Weber, B. Bergner, D. Schröder, P. Adelhelm, J. Janek, Insights into the chemical nature and formation mechanisms of discharge products in Na-O2 batteries by means of operando X-ray diffraction, J. Phys. Chem. C 120 (2016) 8472–8481, https://doi.org/10.1021/acs.jpcc.6b00903.

[295] C. Liu, M. Carboni, W.R. Brant, R. Pan, J. Hedman, J. Zhu, T. Gustafsson, R. Younesi, On the stability of NaO2 in Na-O2 batteries, ACS Appl. Mater. Interfaces 10 (2018) 13534–13541, https://doi.org/10.1021/acsami.8b01516.

[296] J. Kim, H. Park, B. Lee, W.M. Seong, H.D. Lim, Y. Bae, H. Kim, W.K. Kim, K. H. Ryu, K. Kang, Dissolution and ionization of sodium superoxide in sodium-oxygen batteries, Nat. Commun. 7 (2016) 1–9, https://doi.org/10.1038/ncomms10670.

[297] D. Aurbach, B.D. McCloskey, L.F. Nazar, P.G. Bruce, Advances in understanding mechanisms underpinning lithium-air batteries, Nat. Energy. 1 (2016) 1–11, https://doi.org/10.1038/nenergy.2016.128.

[298] I.M. Aldous, L.J. Hardwick, Solvent-Mediated control of the electrochemical discharge products of non-aqueous sodium-oxygen electrochemistry, Angew. Chem. Int. Ed. 55 (2016) 8254–8257, https://doi.org/10.1002/anie.201601615.

[299] V.S. Dilimon, C. Hwang, Y.G. Cho, J. Yang, H.D. Lim, K. Kang, S.J. Kang, H. K. Song, Superoxide stability for reversible Na-O2 electrochemistry, Sci. Rep. 7 (2017) 1–10, https://doi.org/10.1038/s41598-017-17745-9.
[300] L. Lutz, W. Yin, A. Grimaud, D. Alves Dalla Corte, M. Tang, L. Johnson, E. Azaceta, V. Sarou-Kanian, A.J. Naylor, S. Hamad, J.A. Anta, E. Salager, R. Tena-Zaera, P.G. Bruce, J.M. Tarascon, High capacity Na-O2 batteries: key parameters for solution-mediated discharge, J. Phys. Chem. C 120 (2016) 20068–20076, https://doi.org/10.1021/acs.jpcc.6b07659.
[301] L. Schafzahl, N. Mahne, B. Schafzahl, M. Wilkening, C. Slugovc, S.M. Borisov, S. A. Freunberger, Singlet oxygen during cycling of the aprotic sodium-O $_2$ battery, Angew. Chem. Int. Ed. 56 (2017) 15728–15732, https://doi.org/10.1002/anie.201709351.
[302] J. Wandt, P. Jakes, J. Granwehr, H.A. Gasteiger, R.-A. Eichel, Singlet oxygen formation during the charging process of an aprotic lithium–oxygen battery, Angew. Chem. Int. Ed. 55 (2016) 6892–6895, https://doi.org/10.1002/anie.201602142.
[303] W.J. Kwak, S.A. Freunberger, H. Kim, J. Park, T.T. Nguyen, H.G. Jung, H.R. Byon, Y.K. Sun, Mutual conservation of redox mediator and singlet oxygen quencher in lithium-oxygen batteries, ACS Catal. 9 (2019) 9914–9922, https://doi.org/10.1021/acscatal.9b01337.
[304] X. Zhang, Y. Yang, Z. Zhou, Towards practical lithium-metal anodes, Chem. Soc. Rev. 49 (2020) 3040–3071, https://doi.org/10.1039/c9cs00838a.
[305] K. Doi, Y. Yamada, M. Okoshi, J. Ono, C. Chou, H. Nakai, A. Yamada, Reversible sodium metal electrodes: is fluorine an essential interphasial component? Angew. Chem. Int. Ed. 58 (2019) 8024–8028, https://doi.org/10.1002/anie.201901573.
[306] Kummer, N. Weber, A sodium-sulfur secondary battery, SAE Pap. (1967) 670179.
[307] G. Nikiforidis, M.C.M. van de Sanden, M.N. Tsampas, M.C.M. de Sanden, M. N. Tsampas, High and intermediate temperature sodium-sulfur batteries for energy storage: development, challenges and perspectives, RSC Adv. 9 (2019) 5649–5673, https://doi.org/10.1039/c8ra08658c.
[308] L. Medenbach, P. Adelhelm, Cell concepts of metal–sulfur batteries (metal = Li, Na, K, Mg): strategies for using sulfur in energy storage applications, Top. Curr. Chem. 375 (2017), https://doi.org/10.1007/s41061-017-0168-x.
[309] K.B. Hueso, V. Palomares, M. Armand, T. Rojo, Challenges and perspectives on high and intermediate-temperature sodium batteries, Nano Res 10 (2017) 4082–4114, https://doi.org/10.1007/s12274-017-1602-7.
[310] S.-H. Chung, A. Manthiram, Current status and future prospects of metal–sulfur batteries, Adv. Mater. 31 (2019) 1901125, https://doi.org/10.1002/adma.201901125.
[311] K. Zhu, C. Wang, Z. Chi, F. Ke, Y. Yang, A. Wang, W. Wang, L. Miao, How far away are lithium-sulfur batteries from commercialization? Front. Energy Res. 7 (2019) https://doi.org/10.3389/fenrg.2019.00123.
[312] S. Dörfler, H. Althues, P. Härtel, T. Abendroth, B. Schumm, S. Kaskel, Challenges and key parameters of lithium-sulfur batteries on pouch cell level, Joule 4 (2020) 539–554, https://doi.org/10.1016/j.joule.2020.02.006.
[313] T. Cleaver, P. Kovacik, M. Marinescu, T. Zhang, G. Offer, Commercializing lithium sulfur batteries: are we doing the right research? J. Electrochem. Soc. 165 (2018) A6029–A6033, https://doi.org/10.1149/2.0071801jes.
[314] Y. V Mikhaylik, J.R. Akridge, Polysulfide shuttle study in the Li/S battery system, J. Electrochem. Soc. 151 (2004) A1969–A1976, https://doi.org/10.1149/1.1806394.
[315] S. Xin, Y.X. Yin, Y.G. Guo, L.J. Wan, A high-energy room-temperature sodium-sulfur battery, Adv. Mater. 26 (2014) 1261–1265, https://doi.org/10.1002/adma.201304126.
[316] S. Wenzel, H. Metelmann, C. Raiß, A.K. Dürr, J. Janek, P. Adelhelm, Thermodynamics and cell chemistry of room temperature sodium/sulfur cells with liquid and liquid/solid electrolyte, J. Power Sources 243 (2013) 758–765, https://doi.org/10.1016/j.jpowsour.2013.05.194.
[317] I. Bauer, M. Kohl, H. Althues, S. Kaskel, Shuttle suppression in room temperature sodium-sulfur batteries using ion selective polymer membranes, Chem. Commun. 50 (2014) 3208–3210, https://doi.org/10.1039/c4cc00161c.
[318] X. Yu, A. Manthiram, Performance enhancement and mechanistic studies of room-temperature sodium-sulfur batteries with a carbon-coated functional nafion separator and a Na_2S/activated carbon nanofiber cathode, Chem. Mater. 28 (2016) 896–905, https://doi.org/10.1021/acs.chemmater.5b04588.
[319] E. Ceylan Cengiz, Z. Erdol, B. Sakar, A. Aslan, A. Ata, O. Ozturk, R. Demir-Cakan, Investigation of the effect of using Al2O3–nafion barrier on room-temperature Na–S batteries, J. Phys. Chem. C 121 (2017) 15120–15126, https://doi.org/10.1021/acs.jpcc.7b04711.
[320] M. Kohl, F. Borrmann, H. Althues, S. Kaskel, Hard carbon anodes and novel electrolytes for long-cycle-life room temperature sodium-sulfur full cell batteries, Adv. Energy Mater. 6 (2016), https://doi.org/10.1002/aenm.201502185.
[321] S. Wei, S. Xu, A. Agrawral, S. Choudhury, Y. Lu, Z. Tu, L. Ma, L.A. Archer, A stable room-temperature sodium–sulfur battery, Nat. Commun. 7 (2016) 11722, https://doi.org/10.1038/ncomms11722.
[322] X. Xu, D. Zhou, X. Qin, K. Lin, F. Kang, B. Li, D. Shanmukaraj, T. Rojo, M. Armand, G. Wang, A room-temperature sodium–sulfur battery with high capacity and stable cycling performance, Nat. Commun. 9 (2018) 3870, https://doi.org/10.1038/s41467-018-06443-3.
[323] X. Lu, B.W. Kirby, W. Xu, G. Li, J.Y. Kim, J.P. Lemmon, V.L. Sprenkle, Z. Yang, Advanced intermediate-temperature Na–S battery, Energy Environ. Sci. 6 (2013) 299–306, https://doi.org/10.1039/C2EE23606K.
[324] L. Medenbach, P. Hartmann, J. Janek, T. Stettner, A. Balducci, C. Dirksen, M. Schulz, M. Stelter, P. Adelhelm, A sodium polysulfide battery with liquid/solid electrolyte: improving sulfur utilization using P2S5 as additive and tetramethylurea as catholyte solvent, Energy Technol. 8 (2020) 1901200, https://doi.org/10.1002/ente.201901200.
[325] F. Yang, S.M.A. Mousavie, T.K. Oh, T. Yang, Y. Lu, C. Farley, R.J. Bodnar, L. Niu, R. Qiao, Z. Li, Sodium–Sulfur flow battery for low-cost electrical storage, Adv. Energy Mater. 8 (2018) 1701991, https://doi.org/10.1002/aenm.201701991.
[326] N. Tanibata, M. Deguchi, A. Hayashi, M. Tatsumisago, All-solid-state Na/S batteries with a Na3PS4 electrolyte operating at room temperature, Chem. Mater. 29 (2017) 5232–5238, https://doi.org/10.1021/acs.chemmater.7b01116.
[327] X. Fan, J. Yue, F. Han, J. Chen, T. Deng, X. Zhou, S. Hou, C. Wang, High-performance all-solid-state Na–S battery enabled by casting–annealing technology, ACS Nano 12 (2018) 3360–3368, https://doi.org/10.1021/acsnano.7b08856.
[328] T. Ando, A. Sakuda, M. Tatsumisago, A. Hayashi, All-solid-state sodium-sulfur battery showing full capacity with activated carbon MSP20-sulfur-Na3SbS4 composite, Electrochem. Commun. 116 (2020) 106741, https://doi.org/10.1016/j.elecom.2020.106741.
[329] H. Okamoto, The Li-S (lithium-sulfur) system, J. Phase Equil. 16 (1995) 94–97, https://doi.org/10.1007/BF02646258.
[330] J. Sangster, A.D. Pelton, The Na-S (Sodium-Sulfur) system, J. Phase Equil. 18 (1997) 89–96, https://doi.org/10.1007/BF02646762.
[331] J. Pampel, S. Dörfler, H. Althues, S. Kaskel, Designing room temperature sodium sulfur batteries with long cycle-life at pouch cell level, Energy Storage Mater 21 (2019) 41–49, https://doi.org/10.1016/j.ensm.2019.05.035.
[332] Lain, Brandon, Kendrick, Design strategies for high power vs. High energy lithium ion cells, Batteries 5 (2019) 64, https://doi.org/10.3390/batteries5040064.
[333] No Title), (n.d.). https://setis.ec.europa.eu/system/files/integrated_set-plan/action7_declaration_of_intent_0.pdf (accessed May 31, 2020).
[334] M. Wentker, M. Greenwood, J. Leker, A bottom-up approach to lithium-ion battery cost modeling with a focus on cathode active materials, Energies 12 (2019) 504, https://doi.org/10.3390/en12030504.
[335] BatPaC model software | Argonne National Laboratory, (n.d.). https://www.anl.gov/cse/batpac-model-software (accessed June 10, 2020).
[336] Y. Nishi, Past, present and future of lithium-ion batteries, in: Lithium-Ion Batter, Elsevier, 2014, pp. 21–39, https://doi.org/10.1016/B978-0-444-59513-3.00002-9.
[337] J. Peters, D. Buchholz, S. Passerini, M. Weil, Life cycle assessment of sodium-ion batteries, Energy Environ. Sci. 9 (2016) 1744–1751, https://doi.org/10.1039/c6ee00640j.
[338] S.F. Schneider, C. Bauer, P. Novák, E.J. Berg, A modeling framework to assess specific energy, costs and environmental impacts of Li-ion and Na-ion batteries, Sustain. Energy Fuels 3 (2019) 3061–3070, https://doi.org/10.1039/c9se00427k.